



10 CFR 52.79

December 23, 2009
NRC3-09-0051

U. S. Nuclear Regulatory Commission
Attention: Document Control Desk
Washington, DC 20555-0001

References: 1) Fermi 3 Docket No. 52-033
2) Letter from Ilka Berrios (USNRC) to Jack M. Davis (Detroit Edison),
"Request for Additional Information Letter No. 16, Related to the SRP
Sections 2.5.1, 2.5.2, 2.5.3, 2.5.4, and 2.5.5 for the Fermi 3 Combined License
Application, dated November 13, 2009

Subject: Detroit Edison Company Response to NRC Request for Additional Information
Letter No. 16, Part I

In the referenced letter, the NRC requested additional information to support the review of certain portions of the Fermi 3 Combined License Application (COLA). Detroit Edison has divided its response to Letter 16 into three parts: Part I which comprises RAIs whose response is due within 45 days of the date of this letter; Part II which comprises RAIs whose response is due within 60 days of the date of this letter; and Part III which comprises RAIs whose response is due within 90 days of the date of this letter. This letter provides the DTE response to all Part I RAIs.

If you have any questions, or need additional information, please contact me at (313) 235-3341.

D095
NRC

I state under penalty of perjury that the foregoing is true and correct. Executed on the 23rd day of December, 2009.

Sincerely,



Peter W. Smith
Director, Nuclear Development
Licensing and Engineering
Detroit Edison Company

- Attachments:
- 1) Response to RAI Letter No. 16 (Question No. 02.05.01-1)
 - 2) Response to RAI Letter No. 16 (Question No. 02.05.01-5)
 - 3) Response to RAI Letter No. 16 (Question No. 02.05.01-8)
 - 4) Response to RAI Letter No. 16 (Question No. 02.05.01-19)
 - 5) Response to RAI Letter No. 16 (Question No. 02.05.01-25)
 - 6) Response to RAI Letter No. 16 (Question No. 02.05.01-27)
 - 7) Response to RAI Letter No. 16 (Question No. 02.05.02-7)
 - 8) Response to RAI Letter No. 16 (Question No. 02.05.03-1)
 - 9) Response to RAI Letter No. 16 (Question No. 02.05.03-8)
 - 10) Response to RAI Letter No. 16 (Question No. 02.05.04-2)
 - 11) Response to RAI Letter No. 16 (Question No. 02.05.04-3)
 - 12) Response to RAI Letter No. 16 (Question No. 02.05.04-5)
 - 13) Response to RAI Letter No. 16 (Question No. 02.05.04-6)
 - 14) Response to RAI Letter No. 16 (Question No. 02.05.04-8)
 - 15) Response to RAI Letter No. 16 (Question No. 02.05.04-10)
 - 16) Response to RAI Letter No. 16 (Question No. 02.05.04-11)
 - 17) Response to RAI Letter No. 16 (Question No. 02.05.04-12)
 - 18) Response to RAI Letter No. 16 (Question No. 02.05.04-23)

cc: Jerry Hale, NRC Fermi 3 Project Manager (w/o attachments)
Ilka T. Berrios, NRC Fermi 3 Project Manager (w/o attachments)
Bruce Olsen, NRC Fermi 3 Environmental Project Manager (w/o attachments)
Fermi 2 Resident Inspector (w/o attachments)
NRC Region III Regional Administrator (w/o attachments)
NRC Region II Regional Administrator (w/o attachments)
Supervisor, Electric Operators, Michigan Public Service Commission
(w/o attachments)
Michigan Department of Environmental Quality
Radiological Protection and Medical Waste Section (w/o attachments)

Attachment 1
NRC3-09-0051

Response to RAI Letter No. 16
(eRAI Tracking No. 3913)

RAI Question No. 02.05.01-1

RAI 02.05.01-1

FSAR Section 2.5.1.1.1.2 states that the local relief of the Southern New York section is up to 320 m (200 ft). The same paragraph states that the Southern New York section has a lower local relief than the Kanawha section, which has local relief up to 244 m (800 ft). Please clarify these statements given that 320 meters is not equivalent to 200 feet as suggested in regards to the Southern New York section.

Response

Brockman (1998, FSAR Reference 2.5.1-219) states that the Southern New York section (or Glaciated Allegheny Plateau) has very low (10 feet) to moderate (200 feet) relief in the 5 subsections that make up the section. The highest relief is then 200 feet. Dividing this value by the standard conversion factor (3.281 feet/meter) and rounding the result to two significant figures yields a relief value of 61 meters. The value in meters in FSAR 2.5.1.1.1.2 will be changed to 61 meters.

Proposed COLA Revision

A proposed markup to revise FSAR Section 2.5.1.1.1.2 is attached.

Markup of Detroit Edison COLA
(following 1 page)

The following markup represents how Detroit Edison intends to reflect this RAI response in the next appropriate update of the Fermi 3 COLA. However, the same COLA content may be impacted by revisions to the ESBWR DCD, responses to other COLA RAIs, other COLA changes, plant design changes, editorial or typographical corrections, etc. As a result, the final COLA content that appears in a future submittal may be different than presented here.

Mississippian age and younger. Layers of limestone and sandstone that are more resistant to erosion create the topographic highs. The Central Lowlands physiographic province has less local relief, thicker glacial deposits, and fewer exposures than the Kanawha section (Reference 2.5.1-219).

61

The Southern New York section is the glaciated portion of the Appalachian Plateaus physiographic province. The section is characterized by gently rolling to hilly topography with local relief up to 320-m (200 ft) and glacial landforms including end moraines, ground moraines, kames, eskers, kettles, outwash plains, and lacustrine deposits. Local ridges and hills expose bedrock and residual soils. The local relief is the greatest and elevation is the highest in the southeast bordering the Kanawha section and decreases to the north and west (Reference 2.5.1-219). The section is underlain by flat-lying to broadly folded Paleozoic sediments of Mississippian to Pennsylvanian age (Reference 2.5.1-220). Layers of limestone and sandstone that are more resistant to erosion create the topographic highs. Compared to the Kanawha section, the Southern New York section has a lower local relief and more glacial landforms and thicker glacial deposits. The Central Lowland physiographic province has a lower local relief and fewer bedrock exposures than the Southern New York section. (Reference 2.5.1-219)

2.5.1.1.1.3 **St. Lawrence Lowlands Physiographic Province**

The St. Lawrence Lowlands physiographic province in Canada extends to the east and northeast from Fermi 3 (Figure 2.5.1-202). This physiographic province is characterized by a low plain with distributed glacial landforms including moraines, outwash deposits, eskers, and drumlins along with beach and lacustrine landforms (Reference 2.5.1-222; Reference 2.5.1-223). The glacial deposits overlie relatively flat-lying Paleozoic sedimentary rocks of Silurian and Devonian age. Bedrock is locally exposed at the surface (Figure 2.5.1-204). The Niagara Escarpment, which extends from Niagara Falls to the southern part of Georgian Bay in the eastern portion of the site region, is a bedrock escarpment about 77-m (250-ft) high that was formed by differential erosion of Paleozoic sedimentary rocks (Reference 2.5.1-224).

**Attachment 2
NRC3-09-0051**

**Response to RAI Letter No. 16
(eRAI Tracking No. 3913)**

RAI Question No. 02.05.01-5

RAI 02.05.01-05

FSAR Section 2.5.1.1.4.1.1 states that the elevation of the Onondaga Limestone at Buffalo New York is now the main control on the level of Lake Erie. The FSAR states that that the elevation of the Onondaga is 25 km (8200 feet) upriver from Niagara Falls. Please clarify the elevation given that 25 km is not equivalent to 8200 feet.

Response

The conversion from kilometers to miles was incorrect in the FSAR Section 2.5.1.1.4.1.1. The value represents a distance from Niagara Falls and not an elevation. The text will be revised to include the correct distance in miles (25 km [16 mi.]).

Proposed COLA Revision

A proposed markup to revise the third paragraph of FSAR Section 2.5.1.1.4.1.1 is attached.

Markup of Detroit Edison COLA
(following 2 page(s))

The following markup represents how Detroit Edison intends to reflect this RAI response in the next appropriate update of the Fermi 3 COLA. However, the same COLA content may be impacted by revisions to the ESBWR DCD, responses to other COLA RAIs, other COLA changes, plant design changes, editorial or typographical corrections, etc. As a result, the final COLA content that appears in a future submittal may be different than presented here.

for Fermi 3. The following sections describe the region in terms of (1) the contemporary tectonic stress environment (Subsection 2.5.1.1.4.1); (2) regional geophysical data sets that have been used to evaluate basement geology and structures (Subsection 2.5.1.1.4.2); (3) primary structural provinces and tectonic features within the 320-km (200-mi) radius of the site (Subsection 2.5.1.1.4.3); and (4) significant seismic sources at distances greater than 320 km (200 mi) (Subsection 2.5.1.1.4.4). Historical seismicity is shown on Figure 2.5.1-207 described in Subsection 2.5.1.1.4 and discussed in more detail in Subsection 2.5.2.1.

2.5.1.1.4.1 Contemporary Tectonic Stress Environment

Fermi 3 lies within a compressive midplate stress province, characterized by a relatively uniform east-northeast compressive stress field that extends from the midcontinent east toward the Atlantic continental margin and possibly into the western Atlantic basin (Reference 2.5.1-287). Zoback and Zoback (Reference 2.5.1-287) note that although localized stresses may be important in places, the overall uniformity in the midplate stress pattern suggests a far-field source, and the range in orientations coincides with both absolute plate motion and ridge push directions for North America. Modeling of various tectonic processes using an elastic finite-element analysis has indicated that distributed ridge forces are capable of accounting for the dominant east-northeast trend of maximum compression throughout much of the North American plate east of the Rocky Mountains (Reference 2.5.1-288).

Based on analysis of well-constrained focal mechanisms of North American midplate earthquakes, Zoback (Reference 2.5.1-289) concludes that earthquakes in the CEUS occur primarily on strike-slip faults that dip between 43 and 80 degrees, primarily in the range of 60 to 75 degrees and primarily in response to a strike-slip stress regime. This is indicated by a more recent compilation of worldwide stress information that shows east-northeast-oriented maximum horizontal compression and strike-slip events within the study region (Reference 2.5.1-290) (Figure 2.5.1-219).

2.5.1.1.4.1.1 Glacial Isostatic Adjustments

Post-glacial rebound or glacial isostatic adjustment (GIA) is the response of the solid earth to changing surface loads brought on by the waxing and

waning of large-scale ice sheets and glaciers. Tilting of relic lake shorelines, changes to modern lake levels, and secular (persisting for a long time) changes to surface gravity observations are manifestations of land uplift and subsidence brought about by GIA (Reference 2.5.1-291). GIA is also suspected to be a cause of deformation within continental plates and may be a trigger of seismicity in eastern North America and other formerly glaciated regions (Reference 2.5.1-292; Reference 2.5.1-293).

The Port Huron shoreline (approximately 13,000 years BP) was uplifted approximately 60 m (197 ft) between 11,000 and 7,000 years BP (Reference 2.5.1-272), and shorelines dated between 10,500 and 4,700 years BP were upwarped, with more uplift occurring in the north (Reference 2.5.1-294). Early rebound concepts of immediate rebound north of a "hinge-line" were eventually replaced, and it is now recognized that there was continued uplift and rebound over the entire region through the Holocene (Reference 2.5.1-295). Rebound information is most easily conveyed in plots of the elevation of a given shoreline across a distance (Reference 2.5.1-296).

Larsen (Reference 2.5.1-274) reviewed various historical measurements and concluded that uplift continues to the present. In Lake Erie the directional trend in uplift does not strictly correlate with those of proposed isostatic rebound, but is very small (less than 64 mm/century) (Reference 2.5.1-297). Minor climate fluctuations during the Holocene may have affected lake levels on the order of 1 to 2 m (3.3 to 6.6 ft), although this is difficult to prove (Reference 2.5.1-274). The main control on the level of Lake Erie now is the elevation of the Onondaga Limestone at Buffalo, New York (Reference 2.5.1-297), which is 25 km (16 mi) upriver from Niagara Falls and has experienced some uplift (Reference 2.5.1-296). The outflow through the Niagara appears to have been variable; retreat of the falls is estimated to have been 1.6 m (5.25 ft) per year since its inception 12,400 years ago and 1.1 m/yr (3.6 ft/yr) between 1670 and 1969 (Reference 2.5.1-297). The complexity of lake level history is not adequately accounted for in previous models, suggesting that neotectonics may influence lake level history (Reference 2.5.1-296).

located
16 mi

Recent observations of Glacial Isostatic Adjustment (GIA) from Global Positioning System (GPS) velocity field data indicate that the hinge line marking the approximate boundary between regions of vertical rebound

**Attachment 3
NRC3-09-0051**

**Response to RAI Letter No. 16
(eRAI Tracking No. 3913)**

RAI Question No. 02.05.01-8

RAI 02.05.01-08

In FSAR Section 2.5.1.1.4.3.2.12, the Royal Center fault is described as "a steeply southeastdipping, down-to-the-southwest normal fault on the north flank of the Kankakee arch." It is unclear how the fault can be dipping to the southeast with a down-to-the-southwest sense of slip. Please correct, or clarify, this statement.

Response

The sense of displacement was incorrectly stated as down-to-the-southwest, and will be corrected in a revision to the FSAR to read down-to-the-southeast. The same error occurred in FSAR Table 2.5.1-201 and this error has also been corrected.

Proposed COLA Revision

Proposed markups to revise FSAR Section 2.5.1.1.4.3.2.12 and Table 2.5.1-201 are attached:

Markup of Detroit Edison COLA
(following 3 pages)

The following markup represents how Detroit Edison intends to reflect this RAI response in the next appropriate update of the Fermi 3 COLA. However, the same COLA content may be impacted by revisions to the ESBWR DCD, responses to other COLA RAIs, other COLA changes, plant design changes, editorial or typographical corrections, etc. As a result, the final COLA content that appears in a future submittal may be different than presented here.

2.5.1.1.4.3.2.12 **Royal Center Fault**

The Royal Center fault is a northeast-southwest trending fault in the subsurface of Cass, Fulton, and Kosciusko Counties in Indiana, and is about 77 km (48 mi) long. At its closest, the Royal Center fault is approximately 223 km (138 mi) southwest of Fermi 3 (Figure 2.5.1-203). The fault is a steeply southeast-dipping, down-to-the-southwest normal fault on the north flank of the Kankakee arch. The fault offsets the top of the Precambrian surface and the top of the Middle Silurian Salamonie Dolomite, but not the top of the Middle Devonian Muscatatuck group. (Reference 2.5.1-338)

southeast

2.5.1.1.4.3.2.13 **Sharpsville Fault**

The Sharpsville fault is a northeast-southwest-trending, vertical normal fault in the subsurface of Tipton and Howard Counties of central Indiana. The fault is approximately 21 km (13 mi) long and offsets the top of the Middle Ordovician Trenton Formation down-to-the-southeast on the crest of the Kankakee arch. (Reference 2.5.1-339)

2.5.1.1.4.3.2.14 **Transylvania Fault Extension**

The Transylvania fault extension is the extension of faulting identified in Pennsylvania into Ohio. The Transylvania fault is a major zone of east-west-trending, near-vertical faults in the subsurface in Pennsylvania recognized from boring and geophysical data. The westernmost of these faults, the Middleburg fault, is approximately 186 km (115 mi) southeast of Fermi 3 at its closest distance (Figure 2.5.1-203). The fault originated in the Precambrian and was reactivated during the Middle Ordovician Taconic orogeny, during the terminal Paleozoic Alleghenian orogeny, and during the Early Jurassic faulting of the rift basins along the margin of the continent (Reference 2.5.1-342). Transylvania fault zone has been extended northwest from the Ohio-Pennsylvania border to Cuyahoga County near Lake Erie in northeast Ohio. The zone is defined by six high-angle (>80 degrees), normal, southwest-dipping, down-to-the-southwest faults: the Pittsburg-Washington cross-strike structural discontinuity, the Highlandtown fault, the Smith Township fault, the Suffield fault system, the Akron fault, and the Middleburg fault (Figure 2.5.1-203). These faults are mapped on the structure contour map of the Precambrian unconformity surface (Reference 2.5.1-237), and on structure maps on the top of the latest Early Mississippian Berea

Table 2.0-201 Evaluation of Site/Design Parameters and Characteristics (Sheet 9 of 28)

[EF3 COL 2.0-1-A]

Subject ⁽¹⁶⁾	DCD Site Parameter Value ⁽¹⁾ / ₍₁₆₎	Fermi 3 Site Characteristic	Evaluation
Soil Properties (continued)			
Minimum Dynamic Bearing Capacity (continued)			
Minimum Shear Wave Velocity ⁽⁸⁾	300 m/s (1000 ft/s)	Value for each Seismic Category I structure: 1,768 m/s (5,800 ft/sec) for the reactor building/fuel building 1,219 m/s (4,000 ft/sec) for the control building 1,524 m/s (5,000 ft/sec) for the FWSC	The Fermi 3 site characteristic value for each Seismic Category I structure is based on the equivalent uniform shear wave velocity over the entire soil column calculated using the formula in Note (8). The value for each structure falls within (is greater than) the DCD site parameter minimum value. As shown in Figure 2.5.4-220 through Figure 2.5.4-225, the FB/RB, CB, and FWSC foundations are founded on uniform material. Therefore, the ratio of the largest to the smallest shear wave velocity over each mat foundation level does not exceed 1.7.
Liquefaction Potential			
Seismic Category I structures	None under footprint of Seismic Category I structures resulting from site-specific SSE	None at site-specific SSE under Seismic Category I structures	The Fermi 3 Category I structures are founded on bedrock or lean concrete and there is no potential for liquefaction under Fermi 3 Seismic Category I structures at the site-specific SSE ground motion.
Other than Seismic Category I structures	See Note (14)	See Evaluation column	Note (14) in DCD Table 2.0-1 identifies a requirement to address liquefaction potential under other than Seismic Category I structures. Subsection 2.5.4.8 provides the results of the analysis for the glacial till at the Fermi 3 site and addresses potential liquefaction under other than Seismic Category I structures. Based on the analysis provided, the glacial till is not susceptible to liquefaction.
Angle of Internal Friction	≥ 30 degrees	≥ 30 degrees	The Fermi 3 site characteristic value for angle of internal friction is provided in Subsection 2.5.4.10 and falls within (is the same as) the DCD site parameter value.
<div style="border: 1px solid black; padding: 2px; display: inline-block;">Insert 1 Here</div>			

Insert 1

Subject	DCD Parameter Value	Fermi 3 Site Characteristic	Evaluation
Backfill on sides of and underneath Seismic Category I structures (not applicable if the fill material is concrete)		See Evaluation Column	The Fermi 3 site characteristic values for the backfill on the sides of Category I structures are specified in Subsection 2.5.4.5.4.2 and fall within (is the same as) the DCD site parameter value. For Fermi 3, the fill material used underneath Seismic Category I structures is concrete.
i. Product of peak ground acceleration α (in g), Poisson's ratio ν and density γ	$\alpha(0.95\nu + 0.65)\gamma$: 1220 kg/m ³ (76 lbf/ft ³) maximum		
ii. Product of at-rest pressure coefficient k_0 and density:	$k_0\gamma$: 750 kg/m ³ (47 lbf/ft ³) minimum		
iii. At-rest pressure coefficient:	k_0 : 0.36 minimum		
iv. Soil density	γ : 1900 kg/m ³ (119 lbf/ft ³) minimum		

**Attachment 4
NRC3-09-0051**

**Response to RAI Letter No. 16
(eRAI Tracking No. 3913)**

RAI Question No. 02.05.01-19

RAI 02.05.01-19

In FSAR Section 2.5.1.2.4.1, there are numerous incorrect figure references. For example, the discussion of Structures Within the Site Vicinity refers to FSAR Figure 2.5.1-234 ("Maps Showing Late Wisconsinan Ice Margins and Proglacial Lake Shorelines") when discussing the Bowling Green fault and the Howell anticline. When discussing the Bowling Green fault, the FSAR incorrectly refers to FSAR Figure 2.5.1-231 and to FSAR Figure 2.5.1-246. Please make the appropriate corrections.

Response

The reference to Figure 2.5.1-234 in the fifth paragraph of Section 2.5.1.2.4.1 is incorrect; the correct figure is Figure 2.5.1-223.

The reference to Figure 2.5.1-234 in the seventh paragraph of Section 2.5.1.2.4.1 is incorrect; the figure reference was determined to be unneeded and was removed.

The Bowling Green and Maumee faults shown on Figure 2.5.1-230 will be added to Figure 2.5.1-246.

Section 2.5.1.2.4.1 has been reviewed for figure references and revised to correct figure references.

The Stony Island anticline will be labeled on 2.5.1-247.

Proposed COLA Revision

Proposed markups to revise FSAR Section 2.5.1.2.4.1 and Figures 2.5.1-246 and 2.5.1-247 are attached.

Markup of Detroit Edison COLA
(following 7 pages)

The following markup represents how Detroit Edison intends to reflect this RAI response in the next appropriate update of the Fermi 3 COLA. However, the same COLA content may be impacted by revisions to the ESBWR DCD, responses to other COLA RAIs, other COLA changes, plant design changes, editorial or typographical corrections, etc. As a result, the final COLA content that appears in a future submittal may be different than presented here.

The following discussion of structures within the site vicinity was based on a review of published literature, discussions with geologists from the Ohio Geological Survey and Michigan Geological Survey, interpretation of high-altitude imagery and aerial photographs, and field and helicopter reconnaissance conducted during August 2007. Identification and characterization of structures at the site is based on subsurface information developed as part of previous studies conducted for Fermi 2 and results of more recent drilling completed as part of the Fermi 3 subsurface investigations.

2.5.1.2.4.1 Structures Within the Site Vicinity

Major Precambrian structures in the site vicinity include the GFTZ and the MRS, which intersect in the site vicinity (Figure 2.5.1-203). These structures, which are buried beneath a thick (approximately 1100-m [3600-ft] section of Paleozoic sediments, are interpreted from potential field and seismic data as discussed in detail in Subsection 2.5.1.1.2.2.4.

The structure of Paleozoic rocks in the subsurface in the site vicinity has been interpreted from boring and geophysical data obtained primarily from oil and gas exploration (Reference 2.5.1-406; Reference 2.5.1-407; Reference 2.5.1-408; Reference 2.5.1-333).

The surface of the Precambrian basement unconformity is regular with a gentle gradient ranging from about 0.3 degree (5.9 m/km [31 ft/mi]) to locally about 1 degree [Chatham Sag] (16 m/km [85 ft/mi]) on the northwest flank of the Findlay arch northwest into the Michigan basin and about 1 degree (6 m/km [32 ft/mi]) southeast into the Appalachian basin (Reference 2.5.1-325). Dips on Paleozoic units through the lower Middle Devonian Detroit River Group are similar (Reference 2.5.1-325) and define the pattern of Paleozoic rocks in the site vicinity (Reference 2.5.1-325) (Figure 2.5.1-241). The youngest Paleozoic rocks at Fermi 3 are the Upper Silurian Bass Islands Group. Younger Paleozoic rocks were either deposited and eroded or not deposited on the crest of the positive Findlay arch.

No Quaternary faults are known within the site vicinity. The Bowling Green fault and the Maumee fault are bedrock faults mapped within 40 km (25 mi) of the site (Figure 2.5.1-246). The Howell anticline and associated fault, which is mapped to within 45 km (28 mi) of the site, are discussed in Subsection 2.5.1.1.4.3.2. A series of folds are recognized in subsurface bedrock units along the southeastern projected trend of the

Howell anticline/fault structure (Reference 2.5.1-341). Two possible fault trends associated with the small New Boston and Sumpter oil and gas pools in Huron Township and Sumpter Township, Wayne County, Michigan, respectively, are mapped along the southwestern flank of this series of folds (Reference 2.5.1-406). Additional shorter faults are mapped in southwestern Ontario, including two subparallel unnamed faults, one of which is associated with the Colchester oil and gas field (Reference 2.5.1-409). Structures within the site vicinity (40-km [25-mi] radius) are described in more detail below.

The central and northern segments of the Bowling Green fault are located approximately 40 km (25 mi) from the site (Figure 2.5.1-234; Subsection 2.5.1.1.4.3.2). The Bowling Green fault displaces the Precambrian unconformity surface down to the west (Reference 2.5.1-237) and has approximately 122 m (400 ft), down to the west displacement on the top of the Middle Silurian Lockport Dolomite (Reference 2.5.1-332). The Bowling Green fault has had at least six episodes of displacement through the Middle Silurian (Reference 2.5.1-332; Figure 2.5.1-234). Onasch and Kahle (Reference 2.5.1-332) speculate that fault-parallel, east-dipping thrust faults with maximum displacements of less than 5 m (16 ft), generally on the east side of the fault, may represent younger deformation (post-Middle Silurian to Cenozoic). The youngest unit displaced by the Bowling Green fault is the latest Silurian Bass Islands Group; no younger units except for unfaulted Pleistocene glacial deposits occur along the fault (Reference 2.5.1-332).

The northeast-southwest-trending Maumee fault is coincident with the Maumee River in northwest Ohio, and extends to the shore of Lake Erie (Figure 2.5.1-203; Subsection 2.5.1.1.4.3.2). The Maumee fault is a normal fault that trends northeast-southwest and is expressed on the Precambrian unconformity surface (Figure 2.5.1-203) (Reference 2.5.1-237). The Maumee fault is offset in an apparent left-lateral sense about 2 km (1.2 mi) by the Bowling Green fault. No geomorphic expression of the Maumee fault was identified in aerial photographs or during the helicopter reconnaissance (August 2007) along the mapped trace of the fault where it is overlain by late Pleistocene glacial lacustrine deposits.

The southeast end of the Howell anticline/fault extends into the northwest corner of Wayne County, 45 km (28 mi) north of the site (Figure 2.5.1-234

230

223

230

and Figure 2.5.1-230). As discussed in Subsection 2.5.1.1.4.3.2 the Howell anticline is interpreted as a steep, asymmetrical, northwest-southeast trending, northwest-plunging, faulted anticline, having maximum relief of approximately 300 m (1000 ft) on the top of the Middle Ordovician Trenton Formation (Reference 2.5.1-325). The Howell fault offsets the base but not the top of the lower Middle Devonian Detroit River Group (Reference 2.5.1-340). In detail, this second order structure, which is superimposed on the flanks of the first order Findley arch, is probably more complex, consisting of several en-echelon folds and associated faults, as expressed in the structure contour maps on the top of lower Middle Devonian Dundee Formation, Middle Devonian Traverse Formation, and Early Mississippian Sunbury Shale (Figure 2.5.1-225). Overall, the Howell fault trends northwest-southeast and is normal, steeply dipping to vertical, and down-to-the-southwest.

To gain an understanding of the bedrock structure in the site vicinity, available structure contour maps were reviewed. No available structure contour map covered the entire site vicinity sufficiently to provide a complete interpretation; therefore, structure contour maps for the following have been combined on Figure 2.5.1-247:

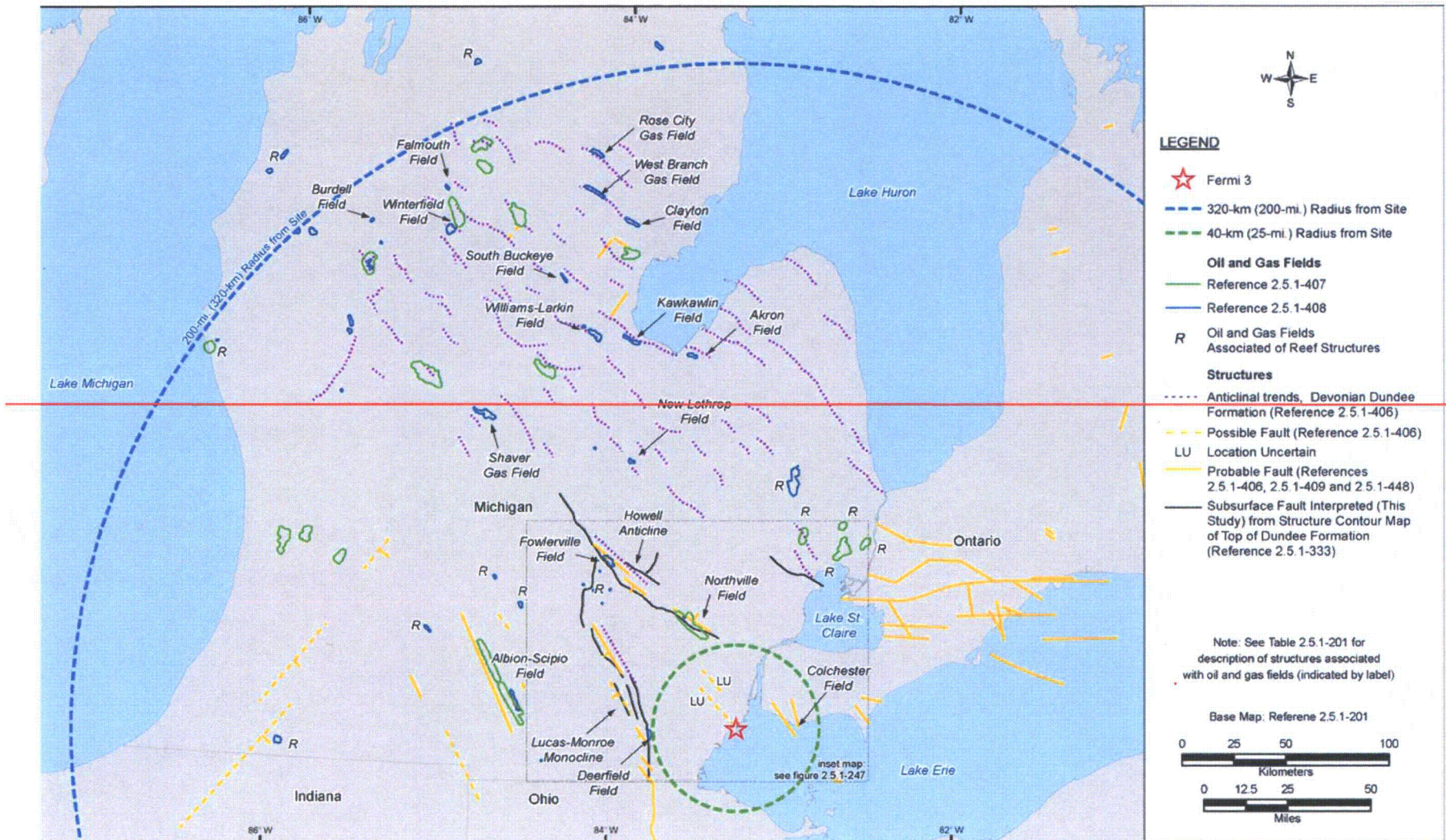
- Structure contours of the top of the Devonian Dundee Limestone (Reference 2.5.1-333),
- Structure contours of the top of the Devonian Sylvania Sandstone (Reference 2.5.1-341), and
- Structure contours of the top of the Ordovician Trenton Formation (Reference 2.5.1-341).

The structure contours on the top of the Trenton Formation in Figure 2.5.1-247 define a number of folds in the site vicinity. A subsequent map of structure contours on the top of the Trenton Formation covering the site vicinity (Reference 2.5.1-352) (Figure 2.5.1-248a) does not show these folds. The discussion presented below uses a conservative approach that assumes the folds defined by the structure contours from Reference 2.5.1-341 presented in Figure 2.5.1-247 exist.

A series of north to northwest-southeast trending, southeast plunging synclines and intervening anticlines are expressed in structure contour maps on the top of the Ordovician Trenton Formation along the southeastern projected trend of the Howell anticline in Wayne and northeast Monroe Counties (Reference 2.5.1-341) (Figure 2.5.1-247).

Figure 2.5.1-246 Tectonic Structures in the Fermi 3 Site Vicinity

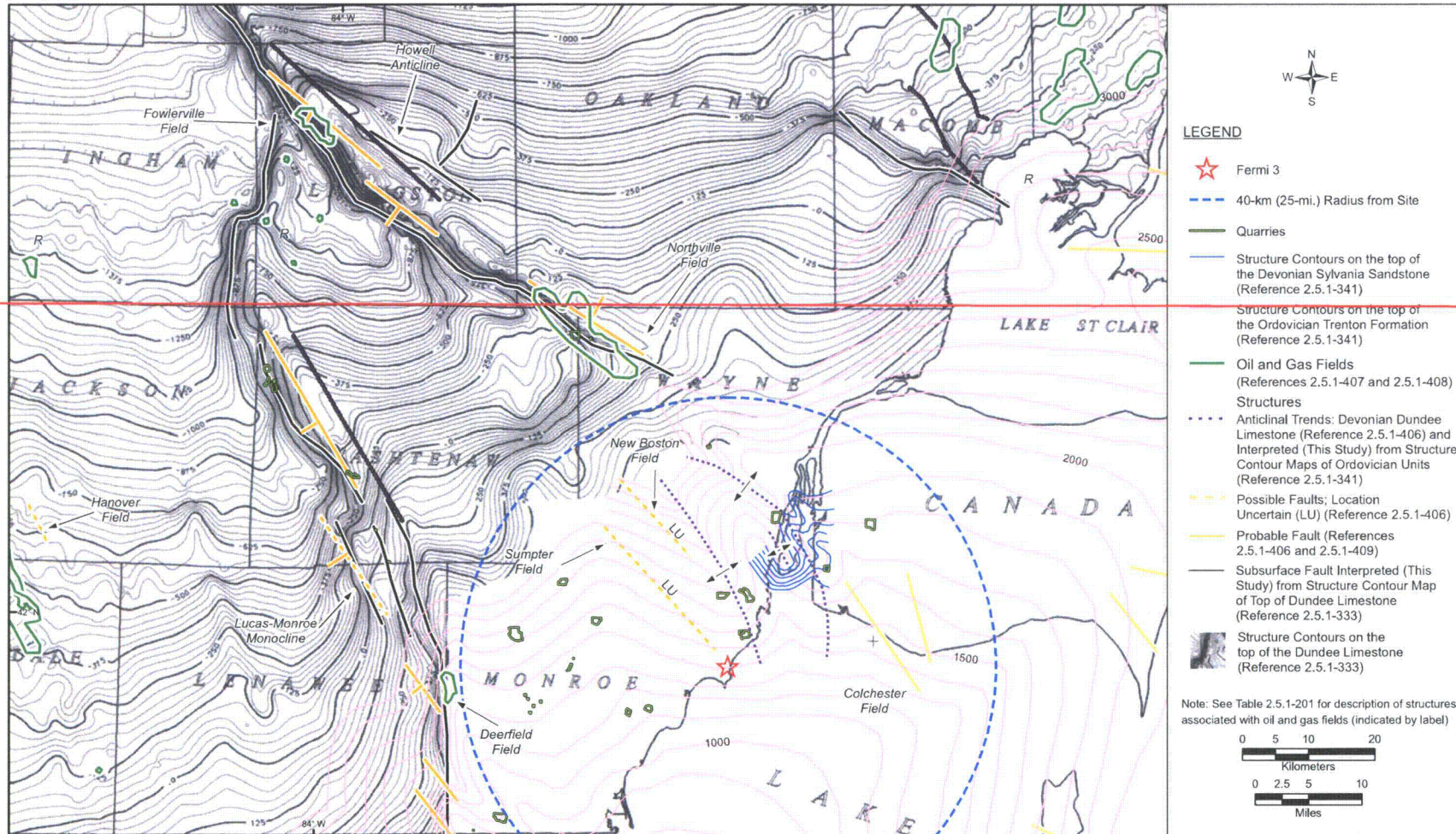
[EF3 COL 2.0-26-A]



Insert 1

Figure 2.5.1-247 Structure Contour Maps from Monroe County, Michigan

[EF3 COL 2.0-26-A]

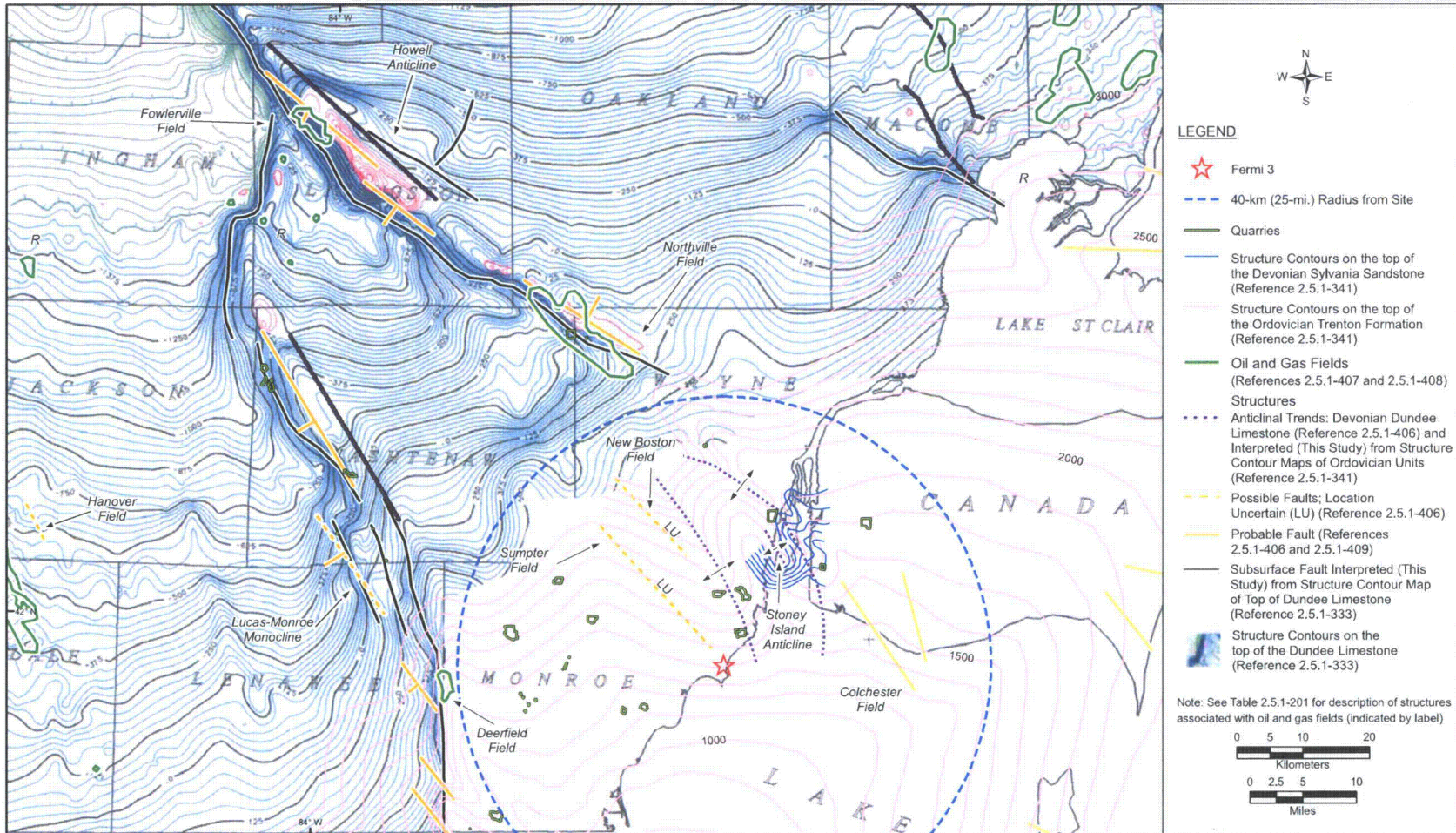


Insert 2

Insert 1



Insert 2



**Attachment 5
NRC3-09-0051**

**Response to RAI Letter No. 16
(eRAI Tracking No. 3913)**

RAI Question No. 02.05.01-25

RAI 02.05.01-25

FSAR Figure 2.5.1-236 shows an enlargement of the site exploration plan with geologic cross section locations. The cross section labels (A-A', B-B', etc.) are obscured and difficult to read. Please provide an updated figure with clear labels in order to identify each of the geologic cross sections described in the FSAR.

Response

Figures 2.5.1-235 and 2.5.1-236 were upgraded in Fermi 3 FSAR Revision 1, submitted to the NRC in March, 2009. These figures no longer contain obscured references to cross section labels.

Proposed COLA Revision

None

**Attachment 6
NRC3-09-0051**

**Response to RAI Letter No. 16
(eRAI Tracking No. 3913)**

RAI Question No. 02.05.01-27

RAI 02.05.01-27

Please provide the following text and figural corrections:

- a. FSAR Section 2.5.1.1.4.2.1 discusses the gravity and magnetic data and states "Figure 2.5.2-219 illustrates the boundary interpreted by Van Schumus." This figure number is incorrect; it should be FSAR Figure 2.5.1-220.*
- b. FSAR Section 2.5.1.1.4.3.3 introduces and describes the Northeast Ohio and Anna seismic zones. Although these zones are shown in FSAR Figure 2.5.1-207 (Sheets 1 through 3), this figure is not cited in this FSAR section. Please include the appropriate figure citations.*
- c. The two references to "FSAR Subsection 2.5.1.1.4.4" in FSAR Section 2.5.1.1.4.3 should read "Subsection 2.5.1.1.4.3.3".*

Response

The following text and figure corrections will be made:

- a) The reference to Figure 2.5.2-219 will be changed to 2.5.1-220 in FSAR Section 2.5.1.1.4.2.1 as shown in the attached markups.
- b) The figure citations to Figure 2.5.1-207 will be added to FSAR Section 2.5.1.1.4.3.3 as shown in the attached markups.
- c) The references to "FSAR Subsection 2.5.1.1.4.4" will be changed to "FSAR Subsection 2.5.1.1.4.3.3" in FSAR Section 2.5.1.1.4.3 as shown in the attached markups.

Proposed COLA Revision

Proposed markups to revise the eighth paragraph of FSAR Section 2.5.1.1.4.2.1, FSAR Section 2.5.1.1.4.3, and FSAR Section 2.5.1.1.4.3.3 are attached.

Markup of Detroit Edison COLA
(following 10 page(s))

The following markup represents how Detroit Edison intends to reflect this RAI response in the next appropriate update of the Fermi 3 COLA. However, the same COLA content may be impacted by revisions to the ESBWR DCD, responses to other COLA RAIs, other COLA changes, plant design changes, editorial or typographical corrections, etc. As a result, the final COLA content that appears in a future submittal may be different than presented here.

to the north and subsidence to the south lies close to the northern margin of the site region. The site lies at the southern margin of the region affected by GIA. The residual velocity field indicates subsidence (1 – 2 mm/yr) throughout most of the site region with possible minor uplift near the western end of Lake Erie (Reference 2.5.1-291). Data from water level gauges along the Great Lakes show subsidence along the southern shores of the Great Lakes (Reference 2.5.1-298).

2.5.1.1.4.2 Regional Geophysical Data

Regional gravity and magnetic survey maps are important data sets that in conjunction with borehole data and regional seismic profile surveys have been used to decipher major structural and rheological boundaries within the basement underlying the site region.

2.5.1.1.4.2.1 Gravity and Magnetic Survey Data and Maps

Regional gravity and magnetic survey data and derivative maps are used to study the basement geology of the midcontinent region, including the lithology and depth of basement rocks and the location and origin of basement structures. Patterns and lineaments on gravity maps are used to infer faults, structure boundaries, and the boundaries between basement provinces. Strong magnetic anomalies are used to infer basalt and related mafic igneous rock which are often associated with basement rifts.

Portions of the Gravity Anomaly Map of North America (Reference 2.5.1-299) and the Magnetic Anomaly Map of North America (Reference 2.5.1-300) covering the site region are reproduced as Figure 2.5.1-220 and Figure 2.5.1-221, respectively. Several prominent gravity anomalies are shown on Figure 2.5.1-220, including the Mid-Michigan Gravity Anomaly (MGA), the East Continent Gravity High (ECGH), the Anorthosite Complex Anomaly (ACA), the Seneca anomaly, and the Butler anomaly (Reference 2.5.1-301; Reference 2.5.1-302; Reference 2.5.1-227; Reference 2.5.1-303).

The MGA, located in the southern peninsula of Michigan, is associated with the midcontinent gravity anomaly, which extends southwestward from Lake Superior. Both anomalies are associated with the midcontinent rift system (MRS) and are characterized by a strong, curvilinear gravity high flanked by gravity lows, and both are associated with magnetic highs (Reference 2.5.1-301).

The ECGH is a chain of positive gravity anomalies from southwestern Michigan to north-central Tennessee (Reference 2.5.1-227). It is associated with the East Continent Rift System (ECRS), which may be related to the MRS, as discussed in Subsection 2.5.1.1.2.2.4.

The Anorthosite Complex anomaly of southern Ohio was described by Lucius and von Frese (Reference 2.5.1-302) as an oblong gravity and magnetic maximum that, based on modeling, was interpreted as an anorthosite body at intermediate crustal depths. Subsequent modeling by Harbi supports this hypothesis and suggests that the anorthosite body dips 8 degrees to the east at midcrustal depths (Reference 2.5.1-303).

The Seneca anomaly, located in northeastern Ohio, is visible on Figure 2.5.1-220 and Figure 2.5.1-221 as a circular magnetic and gravity high. Based on gravity and magnetic modeling, Lucius and von Frese (Reference 2.5.1-302) interpreted the Seneca anomaly as a shallow gabbroic intrusion surrounded by a large, homogeneous granitic body. This model was later confirmed by the presence of gabbro in a core drilled by the Ohio Department of Natural Resources (Reference 2.5.1-303).

The Butler anomaly of southwestern Ohio is visible on Figure 2.5.1-220 as a large, positive circular gravity and magnetic maximum. It was first modeled by Lucius and von Frese (Reference 2.5.1-302) as a crystallized magma chamber that extends to intermediate crustal depths. Harbi (Reference 2.5.1-303) interpreted it as a cylindrical mafic batholith.

Regional gravity and magnetic data sets are used to identify crustal boundaries and lineaments (Reference 2.5.1-301; Reference 2.5.1-228; Reference 2.5.1-304; Reference 2.5.1-305). Hinze et al. (Reference 2.5.1-301) interpreted the boundary between the Penokean and Granite-Rhyolite provinces to lie between 43 and 44 degrees latitude based on the east-southeast-trending anomalies in the Penokean province and the broad positive gravity anomaly with local positive magnetic anomalies in the Granite-Rhyolite province. Atekwana (Reference 2.5.1-228) noted that the Penokean province is characterized by high-frequency, high-amplitude gravity and magnetic anomalies, whereas the Eastern Granite-Rhyolite province is characterized by northwest-southeast-trending lower-frequency and lower-amplitude anomalies. Atekwana (Reference 2.5.1-228) identified a lineament separating these two provinces based on regional data sets and their derivative maps. The boundary between the Penokean and

Granite-Rhyolite provinces is a transition zone and is not well constrained (Reference 2.5.1-301). ~~Figure 2.5.1-219~~ illustrates the boundary interpreted by Van Schmus (Reference 2.5.1-210).

The location of the Grenville Front Tectonic Zone (GFTZ) has been placed in several locations. In Michigan, Hinze et al. (Reference 2.5.1-301) interpreted areas of positive, northeast-southwest-trending gravity and magnetic anomalies as characteristic of the Grenville province consistent with the trend of anomalies of exposed Grenville province rocks in Ontario. Lucius and von Frese (Reference 2.5.1-302) placed the GFTZ west of the anorthosite anomaly based on their model that the Anorthosite Complex anomaly was uplifted during the Grenville orogeny after forming in the deep crust. Atekwana (Reference 2.5.1-228) characterized the Grenville province as having higher-amplitude and higher-frequency magnetic anomalies that trend northwest to north in Kentucky, Ohio, and southeastern Michigan, and north-northeast in southwestern Ontario. Easton and Carter (Reference 2.5.1-306) interpreted the location of the GFTZ by incorporating these results with deep seismic profiles and borehole data, as described in the following section (Subsection 2.5.1.1.4.2.2).

In the western third of Ohio, the gravity and magnetic models of Lucius and von Frese (Reference 2.5.1-302) indicate high-density, low-magnetization intrusions into lower and middle crustal depths associated with the MRS. Drahovzal et al. (Reference 2.5.1-227) later postulated that these anomalies are associated with the East Continent Rift Basin (ECRB) and were overprinted by the GFTZ.

Within the Grenville province, Carter et al. (Reference 2.5.1-304) correlated regional west-northwest- to northeast-trending magnetic anomalies with deformed, magnetite-bearing plutons in southwestern Ontario, Canada, and concluded that the trends are associated with the strikes of gneissic layering and fold axes. Boyce and Morris (Reference 2.5.1-305) identified northeast-trending lineaments that parallel the Central Metasedimentary Belt Boundary Zone (CMBBZ), northwest-trending lineaments that parallel Georgian Bay and Lake Huron, and east-west geophysical anomalies that parallel Lakes Erie and Ontario.

characterized by west-dipping, mid- to deep-crustal reflectors (Reference 2.5.1-238) (Figure 2.5.1-221). Culotta and Pratt (Reference 2.5.1-234) later synthesized these results (Figure 2.5.1-222) and interpreted the GFTZ as a 50-km (30-mi) wide, 25- to 30-degree east-dipping zone penetrating to 25 km (15 mi) deep, attributing the west-dipping reflectors to the CMB. Easton and Carter (Reference 2.5.1-306) combined this data with results of drill data in southwestern Ontario and interpreted the location of the GFTZ (Figure 2.5.1-203, Figure 2.5.1-220, and Figure 2.5.1-221).

GLIMPCE line H, which transects Lake Michigan, images structures and basement terrane boundaries associated with the Penokean orogeny as illustrated on Figure 2.5.1-210 and Figure 2.5.1-213 (Reference 2.5.1-213; Reference 2.5.1-300) (see Subsection 2.5.1.1.2.2.1).

2.5.1.1.4.3 **Regional Tectonic Structures (within 320-km [200-Mi] Radius)**

The Fermi 3 site is located in the stable continental region of the North American Craton, which is characterized by low earthquake activity and low stress (Reference 2.5.1-311; Reference 2.5.1-312; Reference 2.5.1-313; Reference 2.5.1-314) (Figure 2.5.1-207). The site lies within the Central Stable Region tectonic province of the North American continent (Reference 2.5.1-212). This tectonic province is characterized by a thick sequence of sedimentary strata overlying the Precambrian basement. The Precambrian basement is exposed in Wisconsin, Minnesota, the upper peninsula of Michigan, and Ontario, Canada. As described in Subsection 2.5.1.1.4.1, regional geophysical data have been used to infer the major structural and rheological boundaries within subsurface basement in the site region.

The (320-km [200-mi] radius) site region lies within a transition zone between the central Appalachian foreland and the Illinois and Michigan interior cratonic basins; this transition zone contains a variety of structural features that were intermittently active throughout the entire Paleozoic. Basement faults in this zone were initiated, in part, by Precambrian plate convergent episodes at the margin of Laurentia and were reactivated throughout the Paleozoic, principally as growth faults of modest displacement. Deformational loads that accumulated at the Laurentian plate margin during the Taconic and Alleghenian orogenies in the central Appalachians created arches in the site region. (Reference 2.5.1-213)

There is no evidence to indicate that reactivation of structures in the Mesozoic, such as occurred in the New Madrid seismic zone to the southwest, occurred within the site region.

The Fermi 2 UFSAR (Reference 2.5.1-221) concluded that there were no capable tectonic faults within the Fermi 2 site region. Recent reviews of suspected Quaternary tectonic features in the CEUS by Crone and Wheeler (Reference 2.5.1-316) and Wheeler (Reference 2.5.1-317) did not identify any Class A Quaternary tectonic faults or Class B tectonic features in the site region. Crone and Wheeler (Reference 2.5.1-316) define Class A features as those where geologic evidence demonstrates the existence of a Quaternary fault of tectonic origin. Class B features are those where the fault may not extend deeply enough to be a potential source of significant earthquakes, or where the currently available geologic evidence is not definitive enough to assign the feature to Class C or to Class A. Class C features are those for which geologic evidence is insufficient to demonstrate the existence of a tectonic fault, Quaternary slip, or deformation associated with the feature. Crone and Wheeler (Reference 2.5.1-316) identify two Class C seismic zones in the site region that are described below in Subsection ~~2.5.1.1.4.4~~ 2.5.1.1.4.3.3

A description of major basins and arches in the site region is provided in Subsection 2.5.1.1.4.3.1; specific tectonic features and structures are described in Subsection 2.5.1.1.4.3.2; and seismic zones in the site region are described in Subsection ~~2.5.1.1.4.4~~ 2.5.1.1.4.3.3

2.5.1.1.4.3.1 **Basins and Arches**

Intracratonic basins and bounding arches developed in the (200 mi-radius) site region during the Paleozoic (570 – 250 Ma) and include the Michigan, Illinois, and Appalachian basins, and the Cincinnati, Kankakee, Findlay, and Algonquin arches (Figure 2.5.1-208 and Figure 2.5.1-218). The most significant with respect to the site are the Michigan basin and the Findlay and Algonquin arches. In addition to these structures, the now outdated name “Washtenaw Anticlinorium” was proposed by Ells (Reference 2.5.1-318) to describe a broad northwest plunging structure in southeast Michigan and was discussed in the Fermi 2 UFSAR (Reference 2.5.1-221). As defined, local structures included within this broad structural feature are the Bowling Green (Lucas-Monroe) fault/anticline (northern segment) and the Howell (Howell-Northville) anticline/fault described in Subsection 2.5.1.1.4.3.2.

Sandstone, Devonian Onondaga Limestone, and top of the Silurian Packer Shell horizon (Reference 2.5.1-342).

The geometry of the Akron-Suffield-Smith Township faults suggest that they originated as en-echelon, synthetic faults produced by right-lateral wrenching, with inferred minimum displacement of 21 km (13 mi) and subsequent normal displacements on the faults (Reference 2.5.1-342). Displacement on the Precambrian unconformity surface is 60 – 120 m (200 – 400 ft), while maximum vertical displacement of the Devonian Onondaga Limestone across the Akron-Suffield faults is 60 m (200 ft) and across the Highlandtown fault it is 72 m (240 ft) (Reference 2.5.1-342). Hook and Ferm (Reference 2.5.1-343) postulate that deposition of the Linton channel deposits below the Middle Pennsylvanian (Westphalian D) Upper Freeport coal may have been controlled by movement on the Transylvania fault extension (Pittsburgh-Washington cross-strike structural discontinuity). Post-Lower Pennsylvanian faulting cannot be assessed because of the absence of younger units. The northeast-southwest-trending Akron magnetic boundary crosses between the Middleburg and Akron faults.

2.5.1.1.4.3.3 Seismic Zones

Earthquakes in the site region are generally shallow events associated with reactivated Precambrian faults favorably oriented in the modern northeast-southwest compressive stress regime (Reference 2.5.1-344). None of these events has associated surface rupture, and no faults in the site region exhibit evidence of movement since the Paleozoic (Reference 2.5.1-344). Two seismic zones in the study region, the Anna seismic zone and the northeast Ohio seismic are designated as Class C features in the USGS Quaternary fault and fold database (Reference 2.5.1-316).

(Figure 2.5.1-207)

2.5.1.1.4.3.3.1 Northeast Ohio Seismic Zone

The Northeast Ohio seismic zone, also called the Ohio-Pennsylvania seismic zone, defines an approximately 50-km (30.5-mi) long, northeast-southwest-trending zone of earthquakes south of Lake Erie on the Ohio-Pennsylvania border (Reference 2.5.1-328). The largest historic event in this zone was the January 31, 1986, magnitude (m_b) 5.0 event located about 40 km (24.4 mi) east of Cleveland in southern Lake County, Ohio, and about 17 km (10.4 mi) south of the Perry Nuclear Power Plant (Reference 2.5.1-345). The earthquake produced Modified Mercalli

(Figure 2.5.1-207)

intensity (MMI) VI to VII at distances of 15 km (9 mi) from the epicenter and short-duration high accelerations of 0.18 g at the Perry Plant (Reference 2.5.1-345). Thirteen aftershocks were detected by April 15, 1986, with magnitudes ranging from 0.5 to 2.5 and focal depths ranging from 2 to 6 km (1.2 to 3.7 mi) (Reference 2.5.1-345). The aftershocks occurred in a tight cluster about 1 km wide and oriented north-northeast, and focal mechanisms of the aftershocks represent predominantly oblique, right-slip motion on nearly vertical planes oriented N15° to 45°E, with a nearly horizontal *P* (maximum compressive stress) axis (Reference 2.5.1-345), consistent with the modern stress regime. This earthquake and the aftershocks were within 12 km (7.3 mi) of deep waste disposal injection wells, and this earthquake sequence may be due to injection activities at the well reactivating favorably oriented, pre-existing fractures (Reference 2.5.1-346; Reference 2.5.1-345). However, the relative distance to the earthquake cluster (12 km [7.3 mi]), as well as the lack of large numbers of earthquakes typical of induced sequences, a history of small to moderate earthquakes in the region prior to well activities, and the attenuation of the pressure field with distance from the wells all argue for a natural origin for the earthquakes (Reference 2.5.1-345).

In 1987, the first in a series of earthquakes continuing to 2001 occurred within the Northeast Ohio seismic zone near Ashtabula in Ashtabula County Ohio, northeast of the 1986 earthquakes (Reference 2.5.1-347). The initial magnitude 3.8 event occurred on July 13, 1987, followed by a magnitude 2.6 event on January 19, 2001, a foreshock to a magnitude 4.5 event on January 25, 2001, which had a MMI of VI, followed by a magnitude 3.2 event on June 3, 2001, and a magnitude 2.3 event on June 5, 2001 (Reference 2.5.1-347). The July 13, 1987, main shock was close to a deep Class I injection well pumping fluids into the Mount Simon Sandstone, the basal Paleozoic unit overlying Precambrian crystalline basement, at a depth of about 1.8 km (1.1 mi), and a number of portable seismographs were deployed to study the aftershocks (Reference 2.5.1-347). The 1987 aftershocks (36) were all within 1 km (0.6 mi) of the injection well, and defined a 1.5-km (1-mi) long by 0.25-km (0.15-mi) wide area at a depth of about 2 km (1.2 mi), with left-lateral strike-slip movement on an east-west-striking fault (Reference 2.5.1-345). The Ohio Seismic Network was installed in 1999 and precisely recorded the 2001 earthquakes (Reference 2.5.1-347). The sequence of earthquakes near Ashtabula beginning in 1987 is likely due

to fluid injection causing failure along favorably oriented, pre-existing fractures (Reference 2.5.1-347; Reference 2.5.1-346). Seeber and Armbruster (Reference 2.5.1-346) speculate that a single-event rupture of a 5 to 10 km (3 to 6 mi) long fault could generate a magnitude 5 to 6 earthquake.

Nicholson et al. (Reference 2.5.1-345) observe that the 1986 cluster is coincident with a N40°E trending gravity and magnetic anomaly (Akron magnetic boundary). Seeber and Armbruster (Reference 2.5.1-346) and Dineva et al. (Reference 2.5.1-328) also associate the Northeast Ohio seismic zone with the Akron magnetic boundary, which is also called the Akron magnetic anomaly or lineament. Seeber and Armbruster (Reference 2.5.1-346) speculate that the Akron magnetic boundary may be associated with the Niagara-Pickering magnetic lineament/Central Metasedimentary Belt boundary zone as a continental-scale Grenville-age structure.

The Northeast Ohio seismic zone was included in alternative smaller seismic source zones by two of the EPRI-SOG earth science teams (EST), the Rondout and Woodward-Clyde Consultants teams, and was partly incorporated into a smaller zone by a third team (Bechtel team) (see Subsection 2.5.2).

2.5.1.1.4.3.3.2 Anna Seismic Zone

(Figure 2.5.1-207)

The Anna seismic zone, also called the Western Ohio seismic zone, coincides with northwest-southeast-trending basement faults associated with the Fort Wayne rift in Shelby, Auglaize, and nearby counties (Reference 2.5.1-344). Ruff et al. (Reference 2.5.1-348) attribute seismicity to the Anna-Champaign, Logan, and Auglaize faults. This zone has produced at least 40 felt earthquakes since 1875, including events in 1875, 1930, 1931, 1937, 1977, and 1986 that caused minor to moderate damage (Reference 2.5.1-344). The July 12, 1986, event near the town of St. Marys in Auglaize County was the largest earthquake to occur in the zone since 1937 (Reference 2.5.1-344). Schwartz and Christensen (Reference 2.5.1-349) determined a hypocenter of 5 km (3 mi) for the magnitude (m_b) 4.5 event and a focal mechanism (strike = 25°, dip = 90°, rake = 175°) representing mostly strike-slip with a small oblique component approximately parallel to the Anna-Champaign fault and a nearly horizontal P axis oriented east-northeast. The earthquake produced an MMI V1 event (Reference 2.5.1-349). Hansen

(Reference 2.5.1-344) concluded that the historic record indicates a maximum magnitude of 5, but suggested that this zone was capable of producing a magnitude 6.0 to 7.0 event. Obermeier (Reference 2.5.1-350) investigated stream banks in the vicinity of Anna, Ohio, and portions of the Auglaize, Great Miami, Stillwater, and St. Marys rivers and found no evidence of paleoliquifaction features indicative of a magnitude 7 event in the past several thousand years. Crone and Wheeler (Reference 2.5.1-316) designated the Anna seismic zone as a Class C feature based on the occurrence of significant historical earthquakes and the lack of paleoseismic evidence. With the exception of one team (Law Engineering), the EPRI-SOG ESTs included smaller source zones to account for the concentration of seismicity in the Anna seismic zone (Subsection 2.5.2).

2.5.1.1.4.4 **Significant Seismic Sources at Distance Greater than 320 Km (200 Mi)**

More distant sources of large-magnitude earthquakes are the New Madrid seismic zone (NMSZ) and the Wabash Valley seismic zone (WVSZ), which are approximately 800 km (500 mi) and 500 km (300 mi) southwest, respectively, from Fermi 3 (Figure 2.5.1-207). The results of the 1989 EPRI study (Reference 2.5.1-351) indicated that neither the NMSZ nor the WVSZ sources contributed to 99 percent of the hazard at Fermi 2. New information developed since the EPRI-SOG study, however, indicates changes in the frequency or magnitude of large-magnitude events that are expected to occur within these seismic zones, and this information is considered in updating the EPRI hazard model for this study (Subsection 2.5.2). Recent evaluations and new information used to update the source characterizations are described below.

2.5.1.1.4.4.1 **New Madrid Seismic Zone**

The New Madrid seismic zone (NMSZ) lies within the Reelfoot rift and is defined by Post-Eocene to Quaternary faulting, and historical seismicity (Reference 2.5.1-316). The NMSZ, which is approximately 200 km (124 mi) long and 40 km (25 mi) wide, extends from southeastern Missouri to northeastern Arkansas and northwestern Tennessee (Figure 2.5.1-207). Research conducted since 1986 shows that a distinct fault system is embedded within this source zone. The fault system consists of three distinct segments (Figure 2.5.1-203). These three segments include a

southern northeast-trending dextral slip fault referred to as the Cottonwood Grove fault and Blytheville arch, a middle northwest-trending reverse fault referred to as the Reelfoot fault, and a northern northeast-trending dextral strike-slip fault referred to as the New Madrid North fault (Reference 2.5.1-352; Reference 2.5.1-353; Reference 2.5.1-354; Reference 2.5.1-355; Reference 2.5.1-316; Reference 2.5.1-356). In the current east-northeast to west-southwest directed regional stress field, Precambrian and Late Cretaceous-age extensional structures of the Reelfoot rift have been reactivated as right-lateral strike-slip and reverse faults.

Forte et al. (Reference 2.5.1-357) present viscous flow models for North America based on high-resolution seismic tomography that suggest a possible driving mechanism for the intraplate seismicity in the New Madrid region. From analysis of these flow models it is postulated that the descent of the ancient Farallon slab into the deep mantle beneath central North America induces a highly localized flow and stresses directly below the NMSZ. This localization arises because of structural variability in the Farallon slab and the low viscosity of the sublithospheric upper mantle. It is hypothesized that the mantle-flow-induced surface depression and associated local focusing of bending stresses in the upper crust may operate analogously to previous crustal loading scenarios, with the difference being that the slab-related loads reside in the mantle. (Reference 2.5.1-357)

The NMSZ produced three large-magnitude earthquakes (estimates range from M_w 7.1 to 8.4) between December 1811 and February 1812. The actual size of these pre-instrumental events is not known with certainty and is based primarily on various estimates of damage intensity and amount and pattern of liquefaction. (Reference 2.5.1-358; Reference 2.5.1-359; Reference 2.5.1-360; Reference 2.5.1-361)

The December 16, 1811, earthquake is inferred to be associated with strike-slip displacement along the southern portion of the NMSZ (Reference 2.5.1-361; Reference 2.5.1-356). Johnston (Reference 2.5.1-361) estimated the December event to have a magnitude of M_w 8.1 ± 0.31 . Hough et al. (Reference 2.5.1-360) later re-evaluated the intensity data for the region and concluded that the event had a magnitude of M_w 7.2 to 7.3. Bakun and Hopper (Reference 2.5.1-358) also re-evaluated the intensity data and derived a preferred magnitude of M_w 7.6 for the December 1811 event.

**Attachment 7
NRC3-09-0051**

**Response to RAI Letter No. 16
(eRAI Tracking No. 3918)**

RAI Question No. 02.05.02-7

RAI 02.05.02-07

FSAR Figures 2.5.2-236 through 2.5.2-241 display the effects of various factors (seismic sources, ground motion models, model uncertainties, etc.) on the calculated seismic hazard at the Fermi site. However, these figures alternate between comparing mean and median ground motion. Please verify the content of the “mean” and “median” in those figures.

Response

FSAR Figure 2.5.2-236 compares the contributions to total hazard from EPRI-SOG, New Madrid, and Wabash Valley sources. The total hazard curve is the mean hazard curve and is correctly labeled.

FSAR Figures 2.5.2-237 and 2.5.2-238 present the sensitivity of the mean hazard to the choice of median ground motion model. In Figures 2.5.2-237 and 2.5.2-238 the mean hazard curve is incorrectly label as the median hazard. The labeling is as shown in the attached markup to the FSAR.

FSAR Figure 2.5.2-239 illustrates the effect of magnitude conversions on the hazard results, with one curve correctly presented as the mean hazard. Figure 2.5.2-240 illustrates the contribution of all expert teams to the hazard calculations and correctly presents the mean hazard.

Proposed COLA Revision

A proposed markup to the FSAR, Figures 2.5.2-237 and 2.5.2-238, is attached to revise “mean” instead of “median” in the legend.

Markup of Detroit Edison COLA
(following 4 pages)

The following markup represents how Detroit Edison intends to reflect this RAI response in the next appropriate update of the Fermi 3 COLA. However, the same COLA content may be impacted by revisions to the ESBWR DCD, responses to other COLA RAIs, other COLA changes, plant design changes, editorial or typographical corrections, etc. As a result, the final COLA content that appears in a future submittal may be different than presented here.

Figure 2.5.2-237 Effect of Alternative EPRI (2004) Ground Motion Cluster Median Models on the Hazard Computed for the Fermi 3 Site [EF3 COL 2.0-27-A]

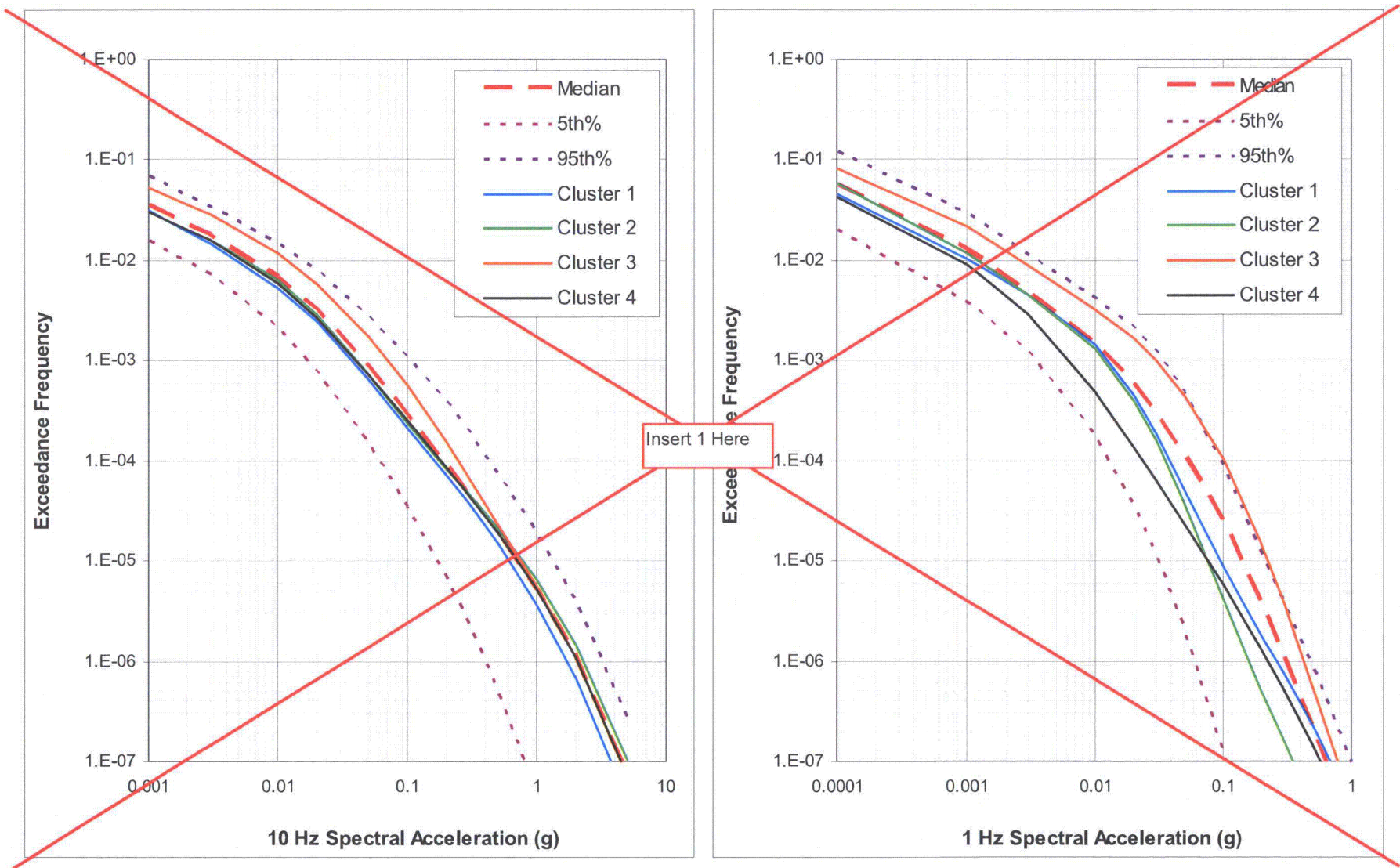
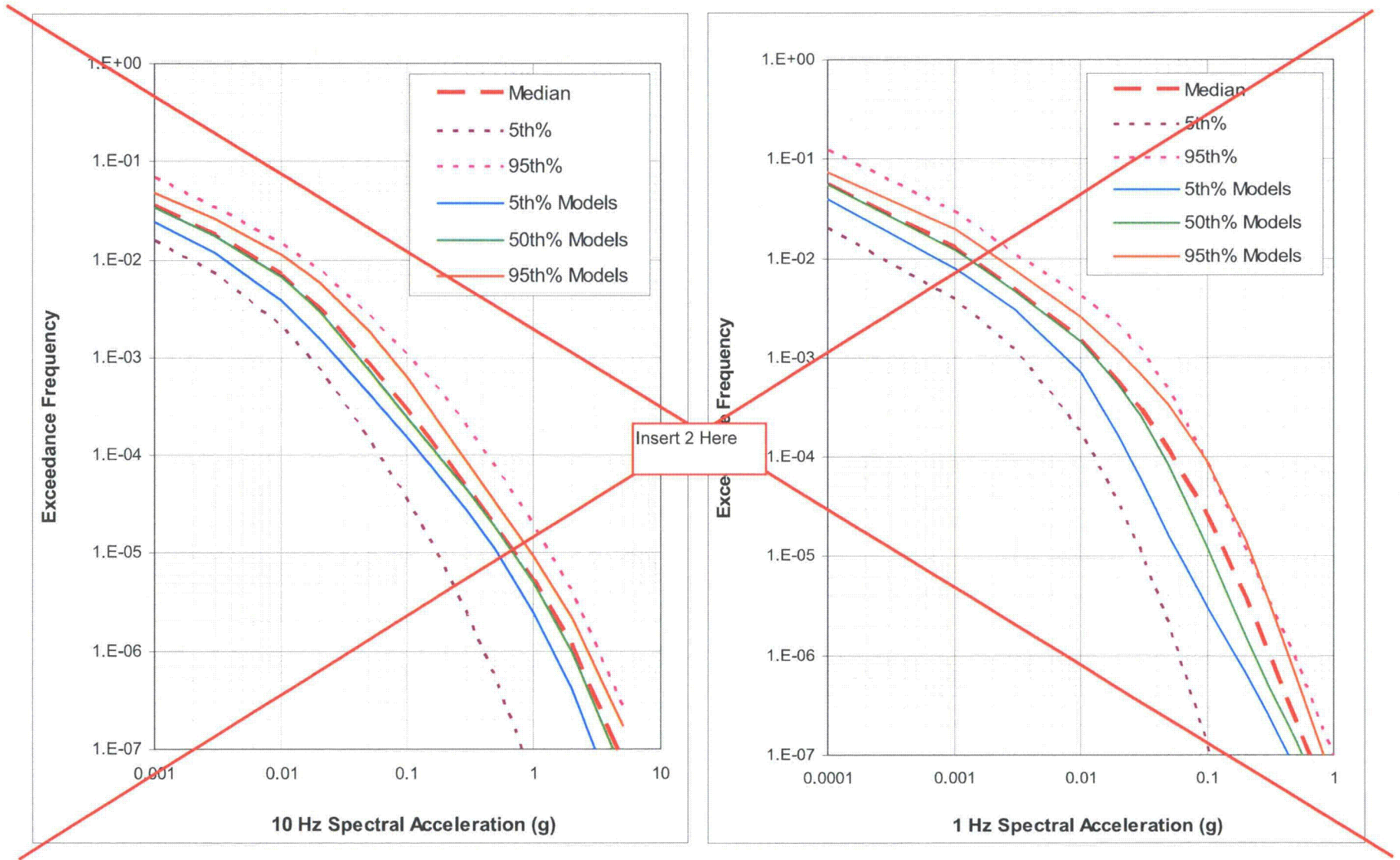
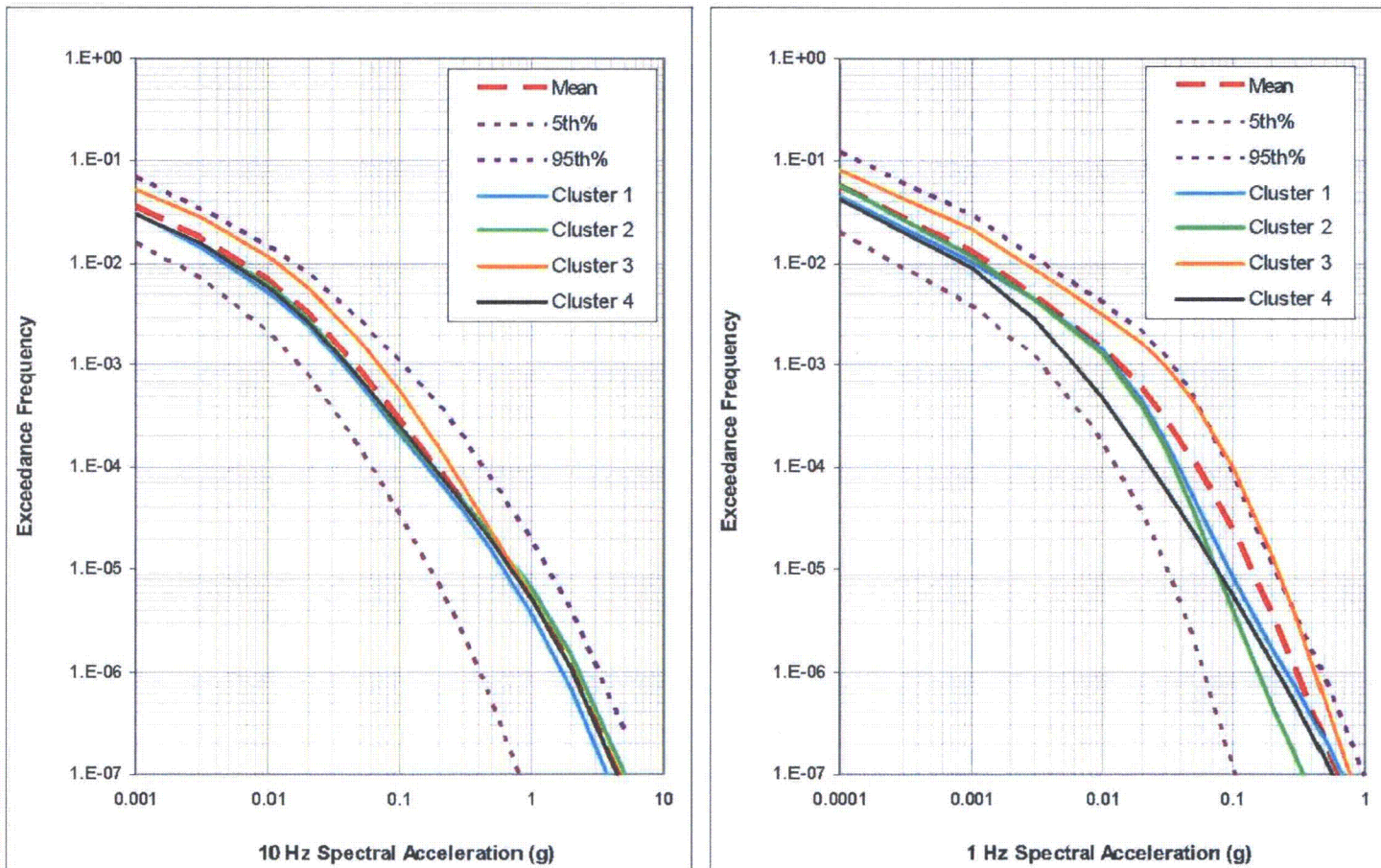


Figure 2.5.2-238 Effect of Uncertainty in the EPRI (2004) Ground Motion Cluster Median Models on the Hazard Computed for the Fermi 3 Site [EF3 COL 2.0-27-A]



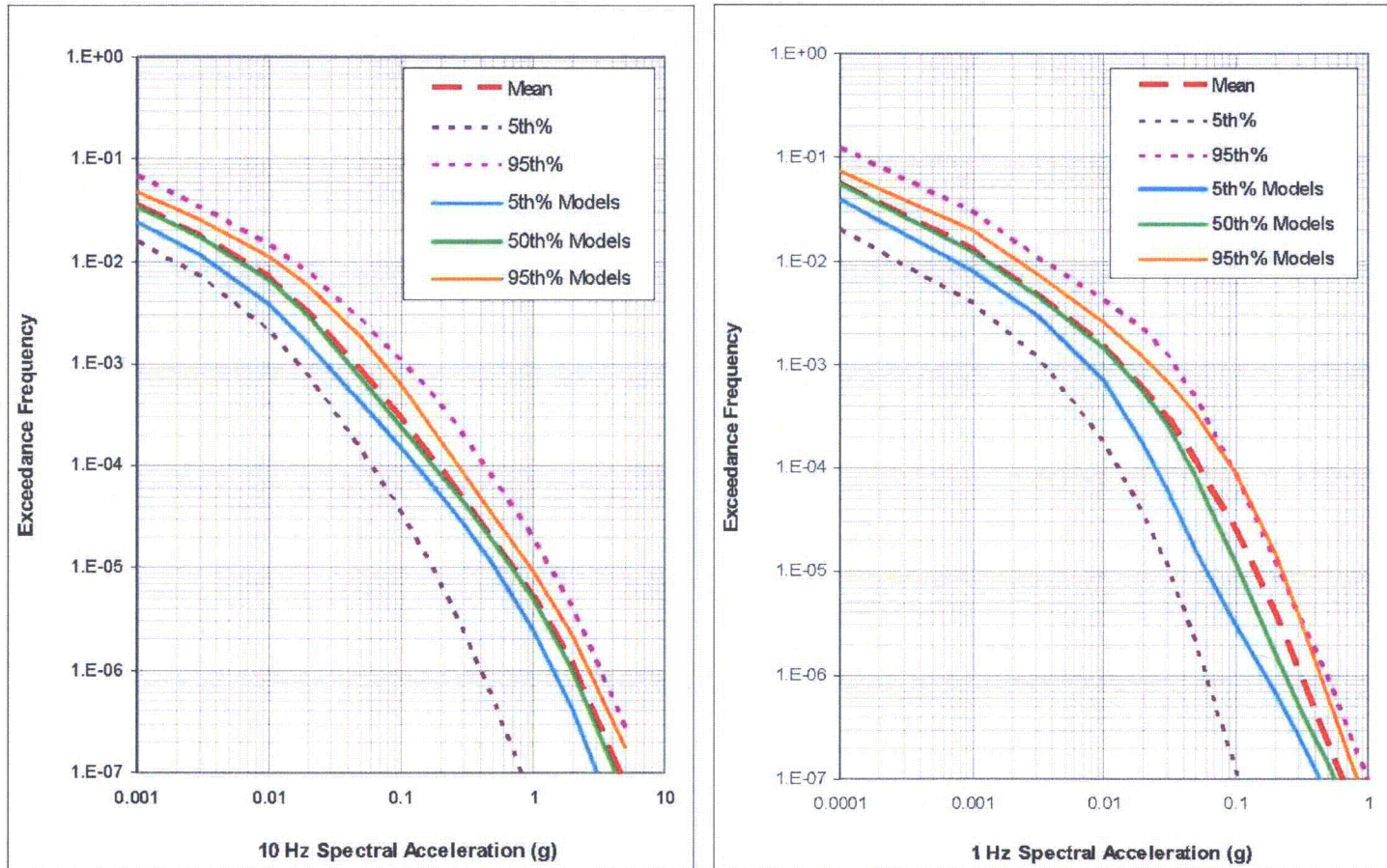
Insert 1

Figure 2.5.2-237



Insert 2

Figure 2.5.2-238



**Attachment 8
NRC3-09-0051**

**Response to RAI Letter No. 16
(eRAI Tracking No. 3917)**

RAI Question No. 02.05.03-1

RAI 02.05.03-01

FSAR Section 2.5.3.2.1 states that "only one possible fault, the fault trend associated with the New Boston pool" may extend into the site area. However, Figures 2.5.3-202 and 2.5.3-203 show the possible Sumpter pool fault, and not the New Boston pool fault, extending into the site area. In addition, FSAR Section 2.5.1.2.4.1 suggests that the Sumpter pool fault is the only fault that extends into the site area. Please reconcile the inconsistency between the FSAR statements and FSAR Figures 2.5.3-202 and 2.5.3-203.

Response

The reference to the New Boston pool in FSAR Section 2.5.3.2.1 will be corrected to reference the Sumpter Pool fault. Figures 2.5.3-202 and 2.5.3-203 correctly show that the Sumpter Pool fault is the only fault that extends into the site area.

Proposed COLA Revision

A proposed markup to revise the third paragraph in FSAR Section 2.5.3.2.1 as follows is attached.

Markup of Detroit Edison COLA
(following 2 pages)

The following markup represents how Detroit Edison intends to reflect this RAI response in the next appropriate update of the Fermi 3 COLA. However, the same COLA content may be impacted by revisions to the ESBWR DCD, responses to other COLA RAIs, other COLA changes, plant design changes, editorial or typographical corrections, etc. As a result, the final COLA content that appears in a future submittal may be different than presented here.

2.5.3.2 Geological Evidence, or Absence of Evidence, for Surface Deformation

2.5.3.2.1 Tectonic Deformation

Based on a review of published literature and maps and field reconnaissance in the site area, there are no faults at or near the ground surface in Quaternary glacial or lacustrine sediments within 40-km (25-mi) of the site. The Fermi 2 UFSAR also concluded, based on a review of available literature, conferences with geological organizations, and onsite investigations, that no known faults exist within 40-km (25-mi) of the Fermi 2 site and that there are no capable faults within 320-km (200-mi) of the site.

No Quaternary faults are known within the site vicinity based on review of more recent publications and data, interpretation of remote sensing imagery (10-m DEM and 1:20,000 aerial photographs) and observations from field and aerial reconnaissance. Review of available data and published interpretations of boring and geophysical data obtained primarily from oil and gas exploration indicates, however, that faults are present within Paleozoic rocks in the subsurface in the site vicinity. The location of known and postulated structures within the site vicinity is shown on Figure 2.5.3-201 and discussed in Subsection 2.5.1.2.4. The Bowling Green fault and the Maumee fault are subsurface bedrock faults mapped within 40-km (25-mi) of the site (Figure 2.5.1-246). The Howell anticline and associated fault, is mapped to within 45-km (28-mi) of the site. A series of folds are recognized in subsurface bedrock units along the southeastern projected trend of the Howell anticline/fault structure. Two poorly documented possible fault trends, associated with the New Boston and Sumpter oil and gas pools, are postulated along the southwestern flank of this series of folds (Figure 2.5.1-203, Figure 2.5.1-230). Additional shorter faults are mapped in southwestern Ontario, including two subparallel unnamed faults, one of which is associated with the Colchester oil and gas field. A summary of the evidence for the location, timing, and displacement on these structures is provided in Subsection 2.5.1.2.4.1 and Table 2.5.1-201.

identified in a 1948 publication by Cohee (Reference 2.5.1-410) and subsequently postulated as a fault

Sumpter

Only one possible fault, the fault trend associated with the New Boston pool as mapped in a 1962 publication by Ells (Reference 2.5.3-202), extends within the site area (8-km [5-mi] radius). However, as discussed in Subsection 2.5.1.2.4.1, there is no documentation supporting the existence of this postulated structure; the location is known only from a

small scale map (approximately one inch = 60 miles) (Reference 2.5.3-202). The folds, which are defined based on structure contours on the top of the Ordovician Trenton Formation (Figure 2.5.1-247), have gently dipping limbs (less than 0.9 degrees) and there is nothing in the character of the folds that suggests the folds are fault-cored. The folds are not well expressed in the structure contours on the Trenton Group as illustrated on Figure 2.5.1-248a. Ells does not show these postulated fault trends along the New Boston and Sumpter oil pools on his more recent compilation of fault or fold structures (Reference 2.5.3-203).

The shallow-dipping northwest-southeast-trending synclinal fold identified based on subsurface investigations for the Fermi 2 site (Reference 2.5.3-201) and confirmed by additional Fermi 3 borings (Figure 2.5.1-237 and Figure 2.5.1-249) has a similar orientation to the other fold trends observed in Devonian bedrock units to the north of the site (Figure 2.5.1-247). These minor folds may be third-order structures that are structurally related to the distal end of the Howell anticline/fault structure as it dies out to the southeast. These minor folds and postulated faults are assumed to be comparable in age to the Howell anticline/fault structure, which is older than late Mississippian (Subsection 2.5.1.1.4.3.2.9).

Faults were not identified within the basement rocks or overlying sedimentary strata at the Fermi 2 site (Reference 2.5.3-201). As noted in the Fermi 2 UFSAR, competent bedrock strata were shown to underlie the site and there are no major solution cavities or zones of solution weathering in the site area. Subsequent to blasting operations during excavation of the Fermi 2 site, the exposed foundation bedrock was sluiced with high-pressure water jets and carefully examined by a qualified geologist to ensure that no excessive natural fracturing or blasting back-break existed that might be unsuitable for foundation support (Reference 2.5.3-201).

2.5.3.2.2 Nontectonic Deformation

Various glacial and periglacial processes may create geomorphic features that mimic surface tectonic fault rupture. The various types of faults observed in glaciated regions are classified into the following categories: (Reference 2.5.3-204)

**Attachment 9
NRC3-09-0051**

**Response to RAI Letter No. 16
(eRAI Tracking No. 3917)**

RAI Question No. 02.05.03-8

RAI 02.05.03-08

FSAR Section 2.5.3.2.3 discusses the results of lineament analyses and implies that the postulated Sumpter Pool fault may line up with a mapped lineament. Please clarify which topographic lineament/s could be possible continuations of the postulated Sumpter Pool fault.

Response

Figure 2.5.3-203 shows lineaments interpreted from the 10-m DEM hillshade model in relation to faults, folds, and possible faults. The text incorrectly stated that the Sumpter Pool fault may line up with a mapped lineament. The text will be as shown in the attached markup to show that New Boston Pool fault lines up with a mapped lineament (Figure 2.5.3-203).

Proposed COLA Revision

Proposed markups to revise the third paragraph of FSAR Section 2.5.3.2.3 are attached .

Markup of Detroit Edison COLA
(following 2 pages)

The following markup represents how Detroit Edison intends to reflect this RAI response in the next appropriate update of the Fermi 3 COLA. However, the same COLA content may be impacted by revisions to the ESBWR DCD, responses to other COLA RAIs, other COLA changes, plant design changes, editorial or typographical corrections, etc. As a result, the final COLA content that appears in a future submittal may be different than presented here.

described in Subsection 2.5.1.2.4.3. The dominant trends of joints in the Bass Islands Group are N45° to 60°W and N40° to 50°E and are nearly vertical in dip (Reference 2.5.3-201). Mapping of the excavation for the Fermi 2 reactor/auxiliary building indicated trends of N45° to 60°W and N60° to 50°E.

Many of the lineaments parallel the trend of the Howell Anticline, N40° to 60°W. The subsurface Sumpter Pool and New Boston Pool possible faults (Reference 2.5.3-202) located to the north and west of the site also trend approximately N40W. However, with the possible exception of the possible Sumpter Pool fault, none of the identified structures directly coincide with the identified lineaments and there is no geomorphic evidence of recent surface deformation along any of the identified or postulated structures. Paleo-shoreline features, beach ridges, cross the trend of the postulated Sumpter Pool and New Boston field possible fault trends with no apparent disruption (n_1 on Figure 2.5.3-201). The actual channels of the drainages are very sinuous and appear to follow both northwest- and northeast-trending fracture and joint trends observed in bedrock elsewhere in the site area. However, bedrock in the site area generally is mantled by several meters of Quaternary glacial and glacio-lacustrine sediments, and it is not clear that present drainage channels are controlled by bedrock structure. Glacial (subglacial meltwater channels) and post-glacial shoreline features also may have influenced present drainage patterns.

New Boston Pool

Add "Insert
1"

The site area lies east of a series of paleo shorelines that post-date the last glacial epoch. Therefore, the surficial deposits and geomorphic surfaces in the site area are younger than about 13,000 years. Given the low strain rates in the site region, the young surficial and near surface deposits are unsuitable for detecting long-term neotectonic strain deformation. Despite these limitations, the USDA 1:20,000-scale color stereo photographs were examined to assess whether or not any significant structural trends could be identified. As shown on Figure 2.5.3-205, there are several WNW- to NNW-trending lineaments in the site area. The lineaments generally consist of aligned linear features that include linear tonal contrasts, linear drainages, linear breaks in slope (e.g., the back edges of flood plains and alluvial terraces). The observed trends are consistent with the trends of the topographic lineaments identified in the site vicinity (Figure 2.5.3-203) and the lineaments are inferred to be the result of surficial erosional processes. The near-surface

Insert 1

Place Insert 1 in second paragraph under "Proposed COLA Revision"

The postulated Sumpter Pool fault is not coincident with a mapped lineament, although a short segment of Swan Creek approximately 2.4 km (1.3 mi) to the north does subparallel the postulated structure. A regional joint trend also subparallels the orientation of this segment of Swan Creek and segments of other streams in the site area. Thus, the orientation of this linear segment of Swan Creek may be controlled by a regional joint trend. There

Attachment 10
NRC3-09-0051

Response to RAI Letter No. 16
(eRAI Tracking No. 3936)

RAI Question No. 02.05.04-2

RAI 02.05.04-2

FSAR Section 2.5.4.2.1.2.1 "Bass Islands Group" states that: "Twelve rock direct shear tests were performed along sample discontinuities to provide the residual friction angle along the discontinuities presented in FSAR Table 2.5.4-206. The residual friction along discontinuities ranges between 33 and 74 degrees, with a mean of 52 degrees." Please provide information on how prevalent these discontinuities are and whether there are any preferential directions involved. Also please provide information on how representative are the discontinuities provided by the twelve rock direct shear tests.

Response

The discontinuities of the Bass Islands Group encountered during the Fermi 3 subsurface investigation are discussed in Fermi 3 FSAR, Revision 1, Section 2.5.1.2.4.3:

"During the Fermi 3 subsurface investigation jointing was observed throughout the Bass Islands Group and Salina Group Unit F. The joints encountered are opening-mode fractures. The joint density in the Bass Islands Group and Salina Group Unit F varies from isolated joints to groups of closely spaced joints referred to on the logs as highly fractured zones. The existence of joints and fracture zones is confirmed on the optical televiewer logs; however, the field boring logs have more joints and fracture zones possibly indicating mechanical breaking of the core during the drilling process. The orientations vary from horizontal to vertical with near horizontal and near vertical fractures dominating. The joint apertures were from tight or hairline up to several inches. Some joints were filled with anhydrite, calcite, or clay while others had no filling. A small percentage of joints have weathering along the joint walls or display minor dissolution (solutioning). Below Salina Group Unit F, the joint density decreases, and joints are rare in Salina Group Units C and B, but mineral (anhydrite) filled joints are present even in the deepest formations."

"Joint orientations vary from horizontal to vertical, with near horizontal and near vertical joints dominating. Optical televiewer logging completed for the Fermi 3 project determined the presence of low angle ($< 45^\circ$) bedding planes, low angle fractures ($< 45^\circ$), and high angle fractures ($> 45^\circ$). The dominant strike orientations of the bedding planes are north-northeast and west-northwest. The dominant strike orientations of all fracture planes are north-northwest and west-northwest. (Reference 2.5.1-418)"

Discontinuities in the Bass Islands Group at Borings TB-C5, RB-C8, CB-C3, and RB-C4 are shown on optical televiewer log images displayed in Figures 2.5.4-209 through 2.5.4-212 of the Fermi 3 FSAR, Revision 1. The boring logs in Appendix 2.5DD document individual discontinuities encountered during drilling in the Bass Islands Group dolomite. As indicated in the FSAR text, near horizontal and near vertical joints dominate, with joint density that varies from isolated joints to groups of closely spaced joints.

Pictures of the bedrock discontinuities samples selected for direct shear testing were taken prior to laboratory testing. Figures 1 through 12 below provide the photos of the core/discontinuity prior to laboratory testing and the optical televiewer log corresponding to the depth of the sample. The depths of the discontinuities were estimated using photographs of the bedrock core samples taken during the Fermi 3 subsurface investigation. Therefore, discontinuity depths are approximate and do not precisely match the actual depths on the optical televiewer log.

The orientation of the discontinuities tested is nearly horizontal, except the orientation of samples CB-C4 at 57.0 feet and RB-C3 at 46.9 feet, which were at inclined angles. The discontinuities of all tested samples matched the actual orientation of discontinuities observed in the ground as shown in the televiewer logs except for the discontinuity at 57.0 feet in CB-C4. As no discontinuity is observed in the televiewer log, the discontinuity in the CB-C4 core appears to be a mechanical break of a weak zone found between 56.0 and 57.0 feet in CB-C4.

The discontinuities tested were disturbed during coring of bedrock, this type of disturbance was unavoidable. Prior to testing the discontinuities of the bedrock were fitted together to bring them back to the in-situ condition.

The test results are considered representative of the discontinuities tested; however, due to discontinuity disturbance, the measured friction angles may be lower than the actual friction angle of the discontinuities. Therefore, it is concluded that the discontinuities tested and the results are representative of the discontinuities observed within the Bass Islands Group.

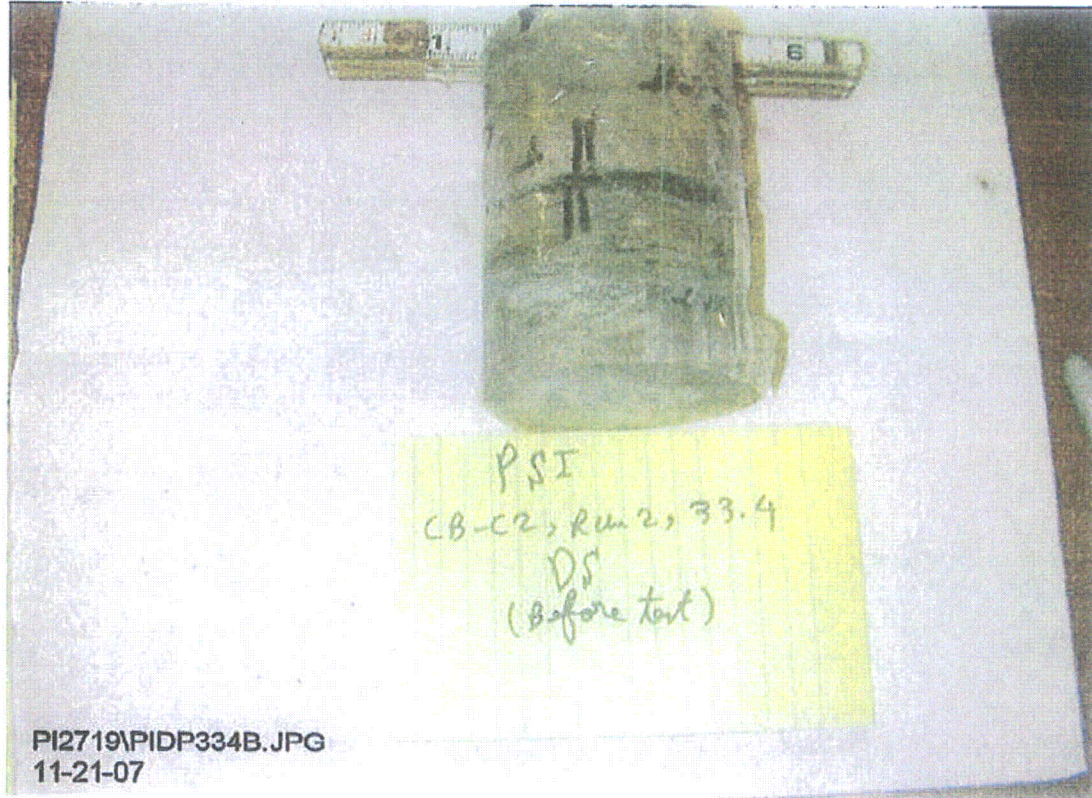


Figure 1A

Photo of discontinuity at approximately 33.4 feet in Boring CB-C2 taken prior to laboratory testing.

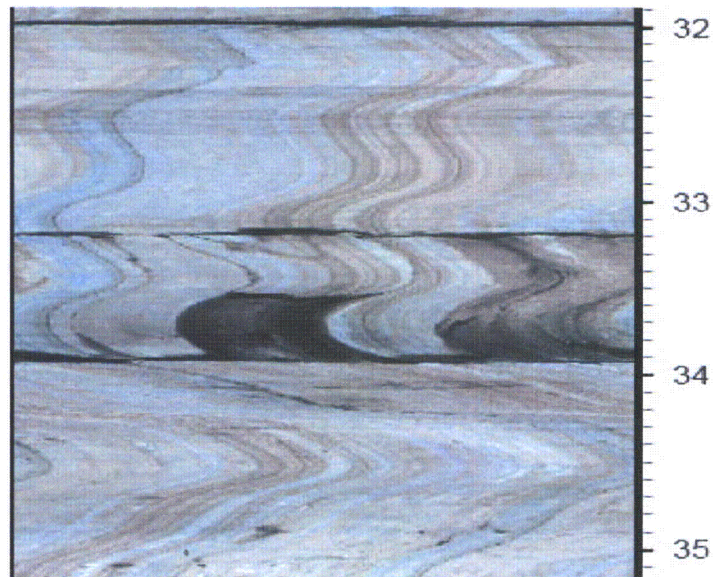


Figure 1B

Optical Televiewer Log in Boring CB-C2 from 32.0 to 35.2 feet.

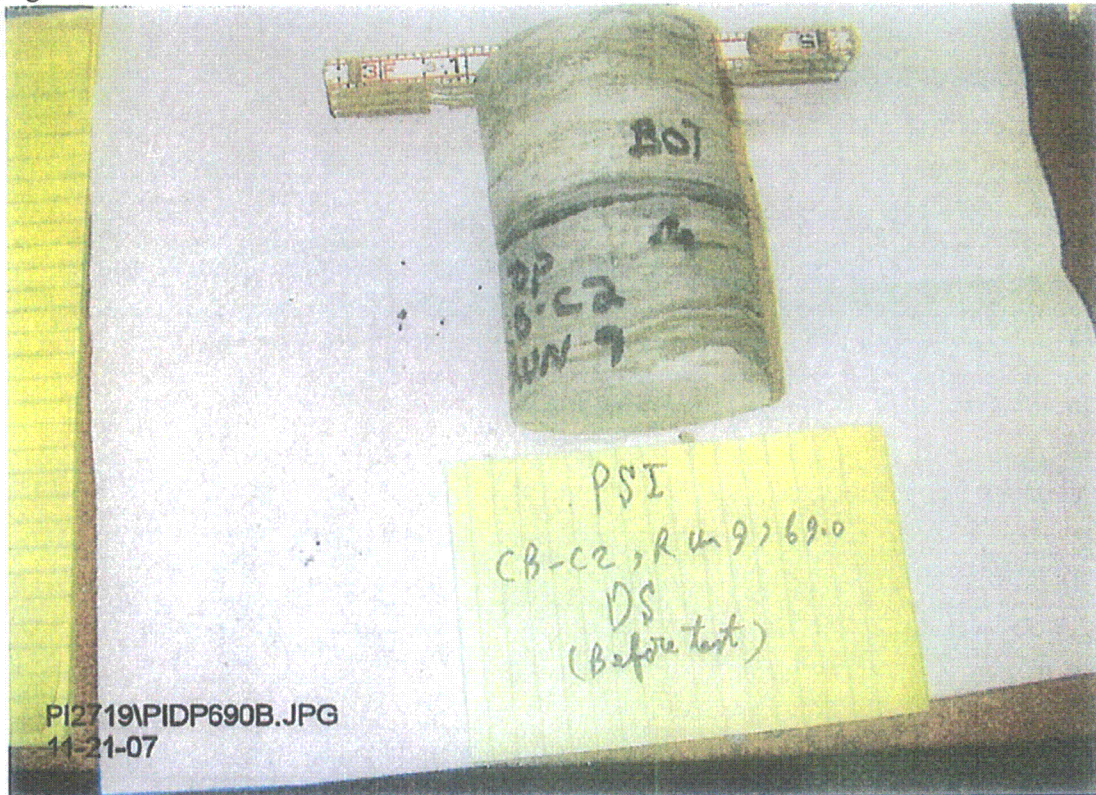


Figure 2A

Photo of discontinuity at approximately 69.0 feet in Boring CB-C2 taken prior to laboratory testing.

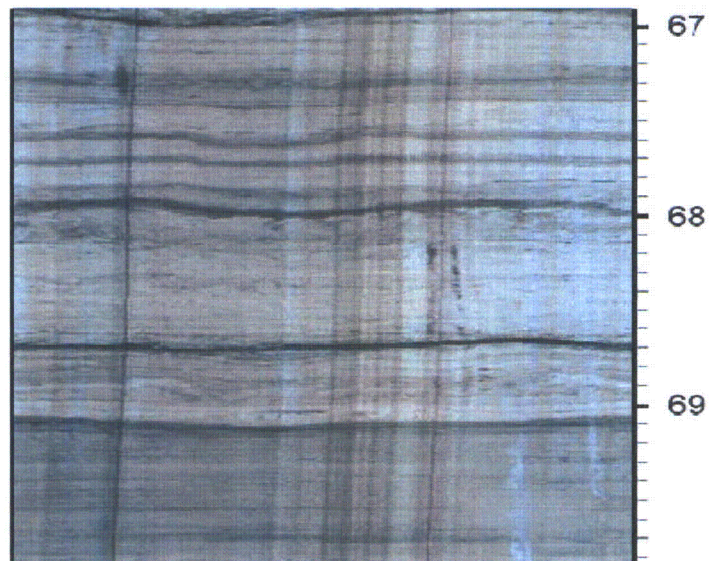


Figure 2B

Optical Televiewer Log in Boring CB-C2 from 67.0 to 69.8 feet.

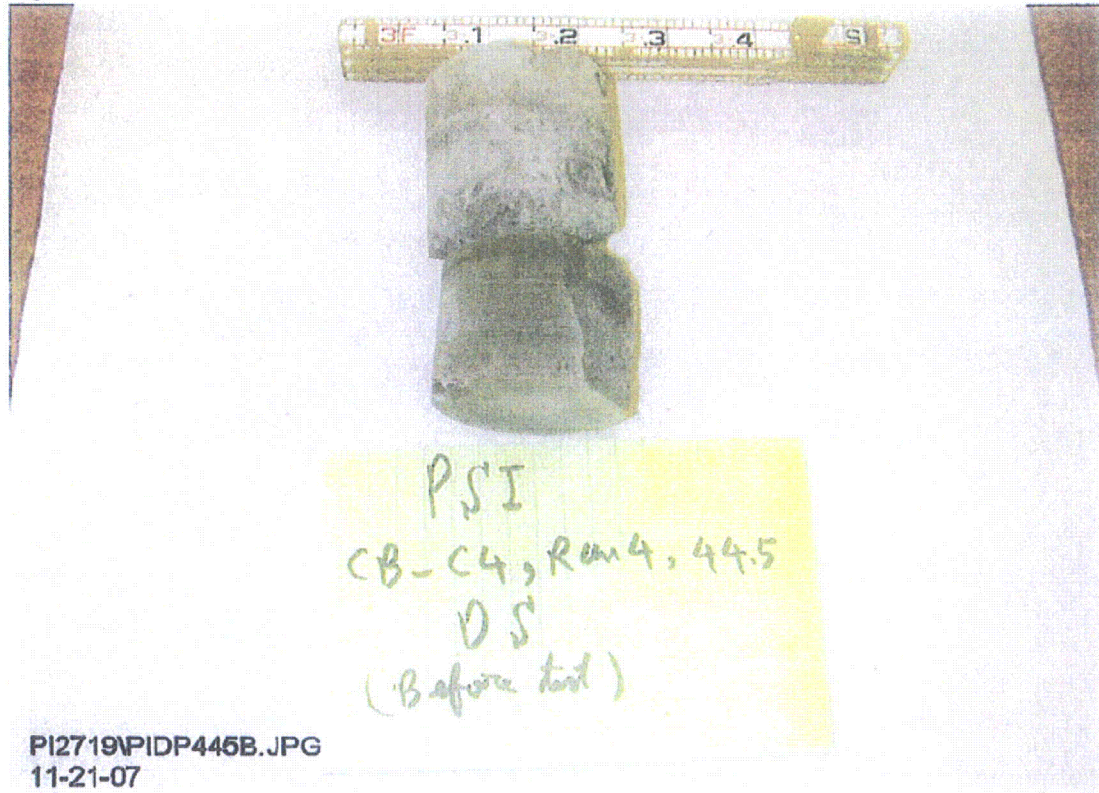


Figure 3A
Photo of discontinuity at approximately 44.5 feet in Boring CB-C4 taken prior to laboratory testing.

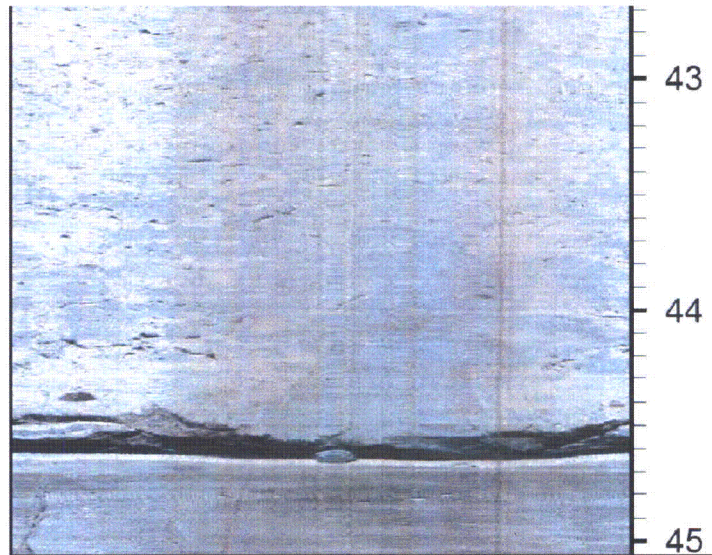
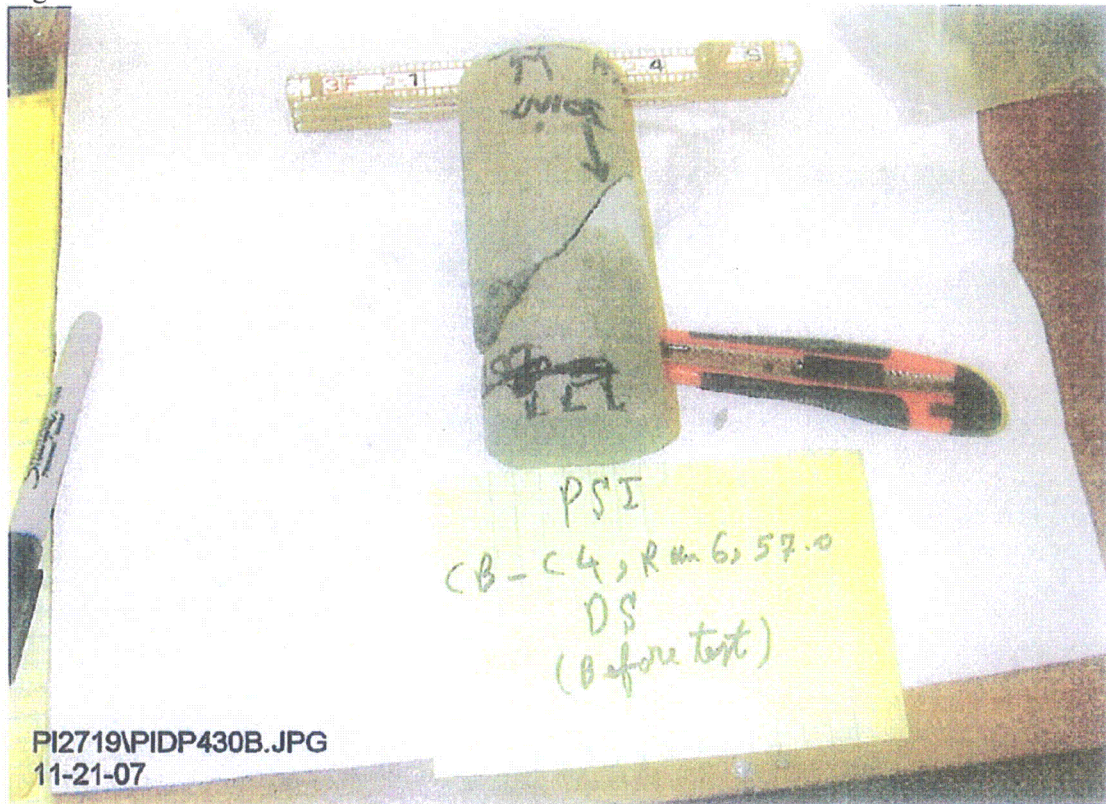


Figure 3B
Optical Televiewer Log in Boring CB-C4 from 42.7 to 45.1 feet.



PI2719\PIDP430B.JPG
11-21-07

Figure 4A

Photo of discontinuity at approximately 57.0 feet in Boring CB-C4 taken prior to laboratory testing.

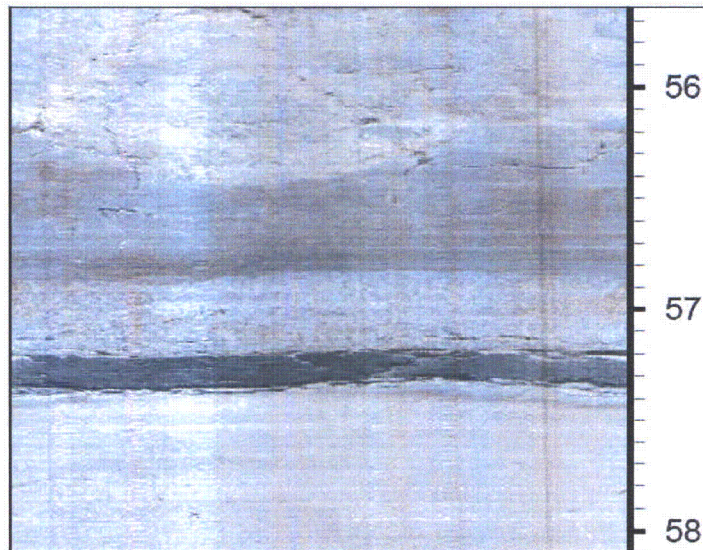


Figure 4B

Optical Televiewer Log in Boring CB-C4 from 55.6 to 58.1 feet.

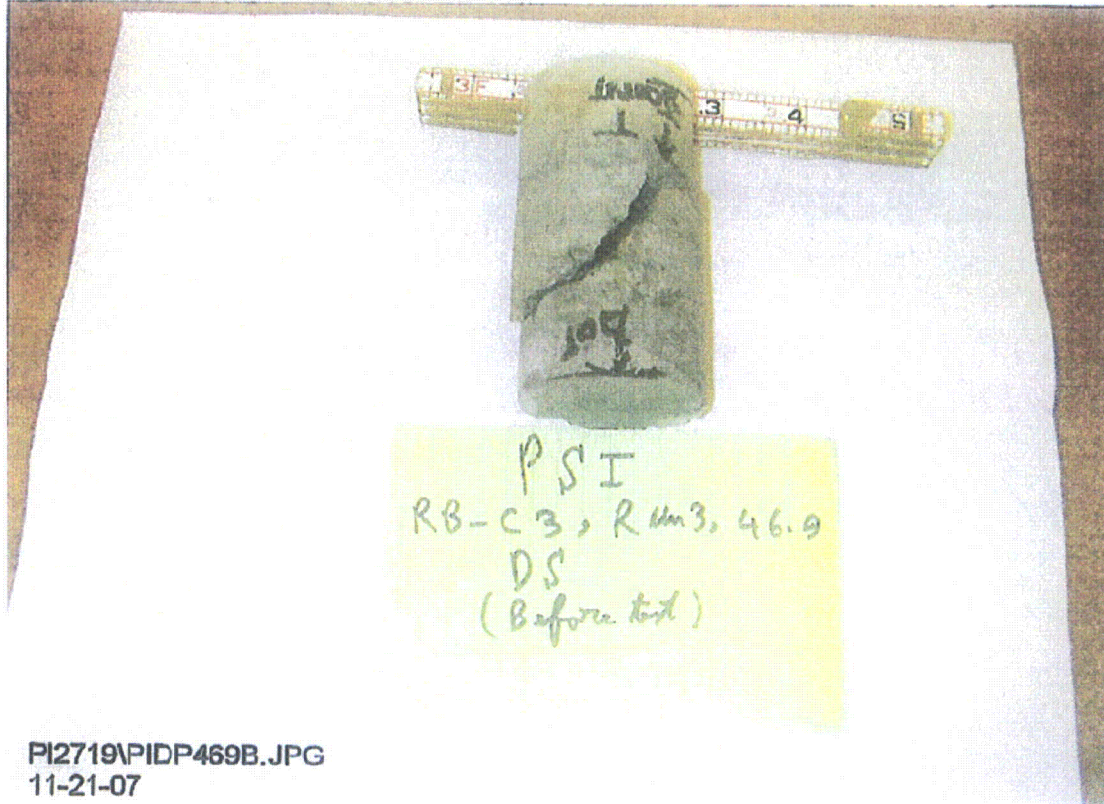


Figure 5A
Photo of discontinuity at approximately 46.9 feet in Boring RB-C3 taken prior to laboratory testing.

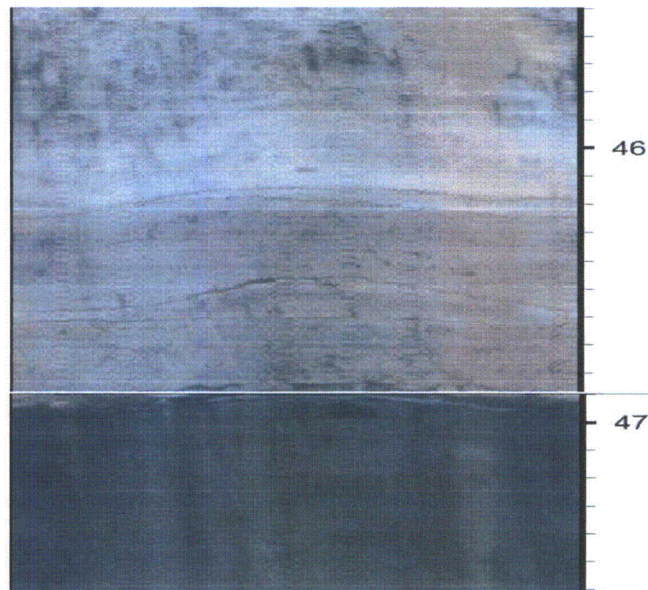


Figure 5B
Optical Televiewer Log in Boring RB-C3 from 45.5 to 47.6 feet.

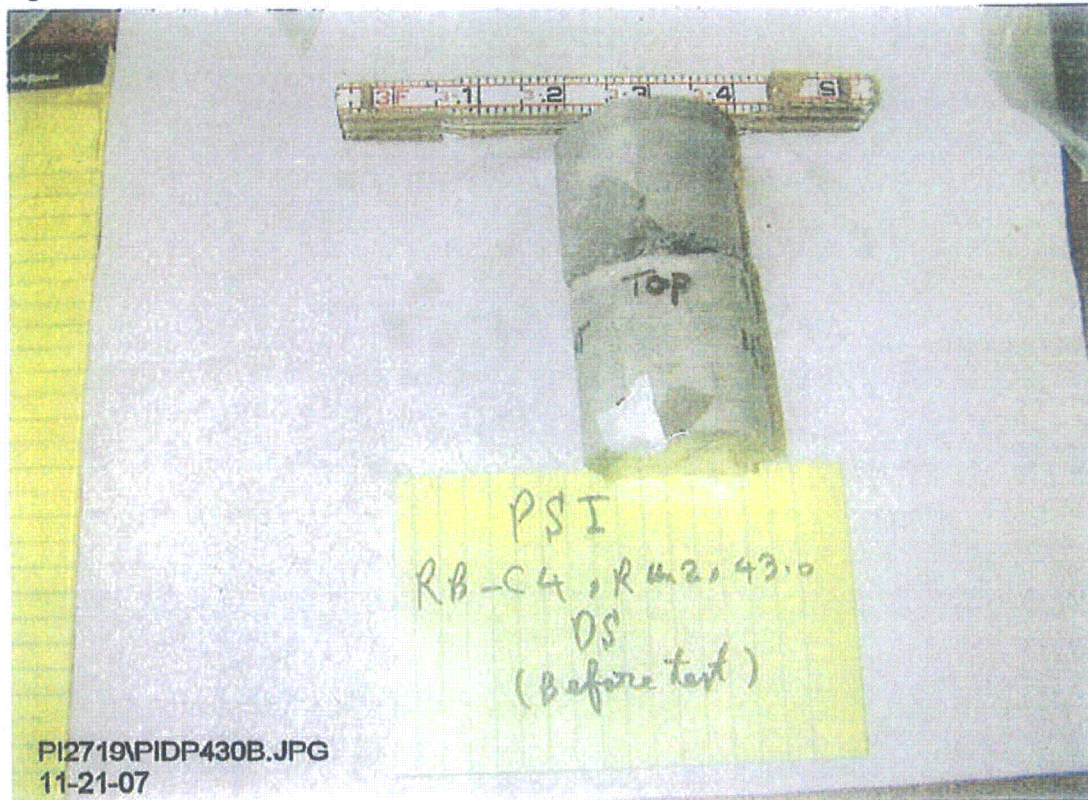


Figure 6A
Photo of discontinuity at approximately 43.0 feet in Boring RB-C4 taken prior to laboratory testing.

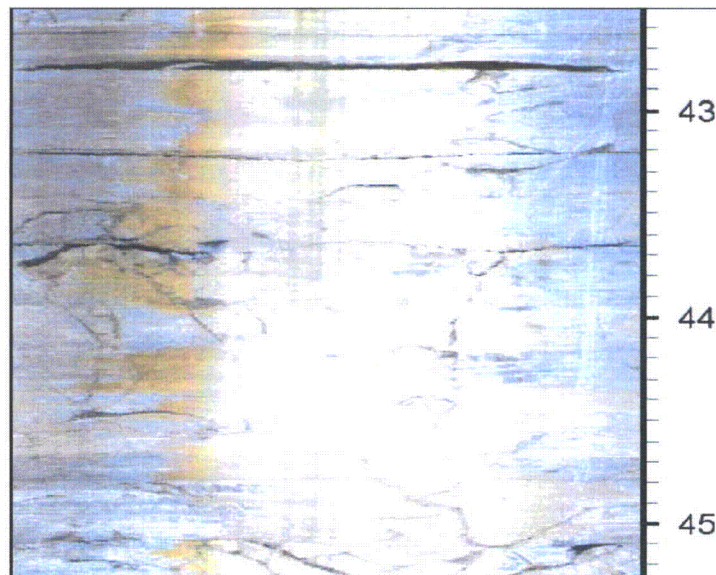


Figure 6B
Optical Televiewer Log in Boring RB-C4 from 42.5 to 45.3 feet.

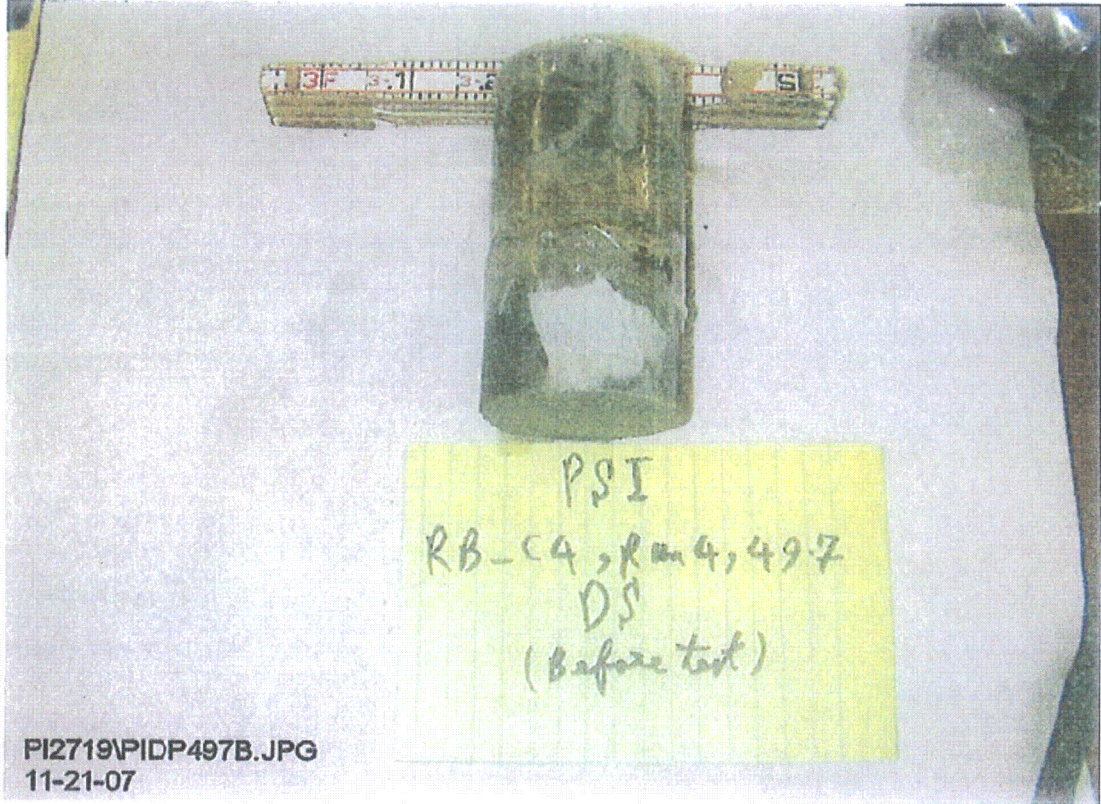


Figure 7A

Photo of discontinuity at approximately 49.7 feet in Boring RB-C4 taken prior to laboratory testing.

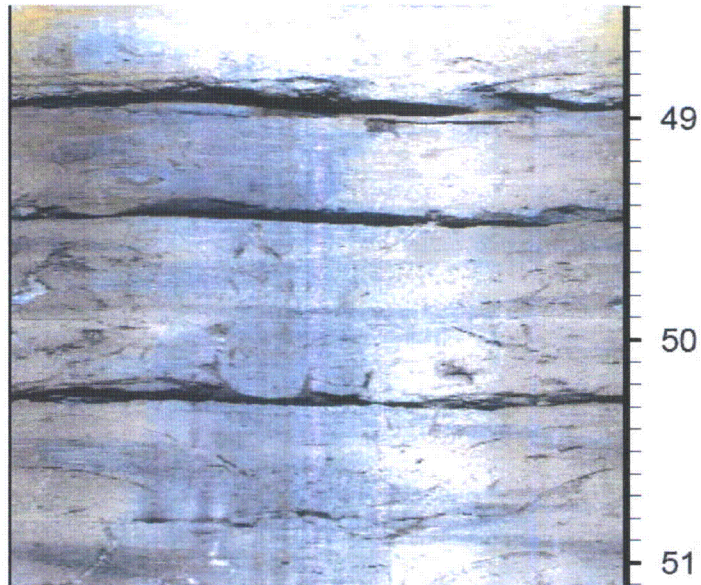


Figure 7B

Optical Televiewer Log in Boring RB-C4 from 48.5 to 51.1 feet.

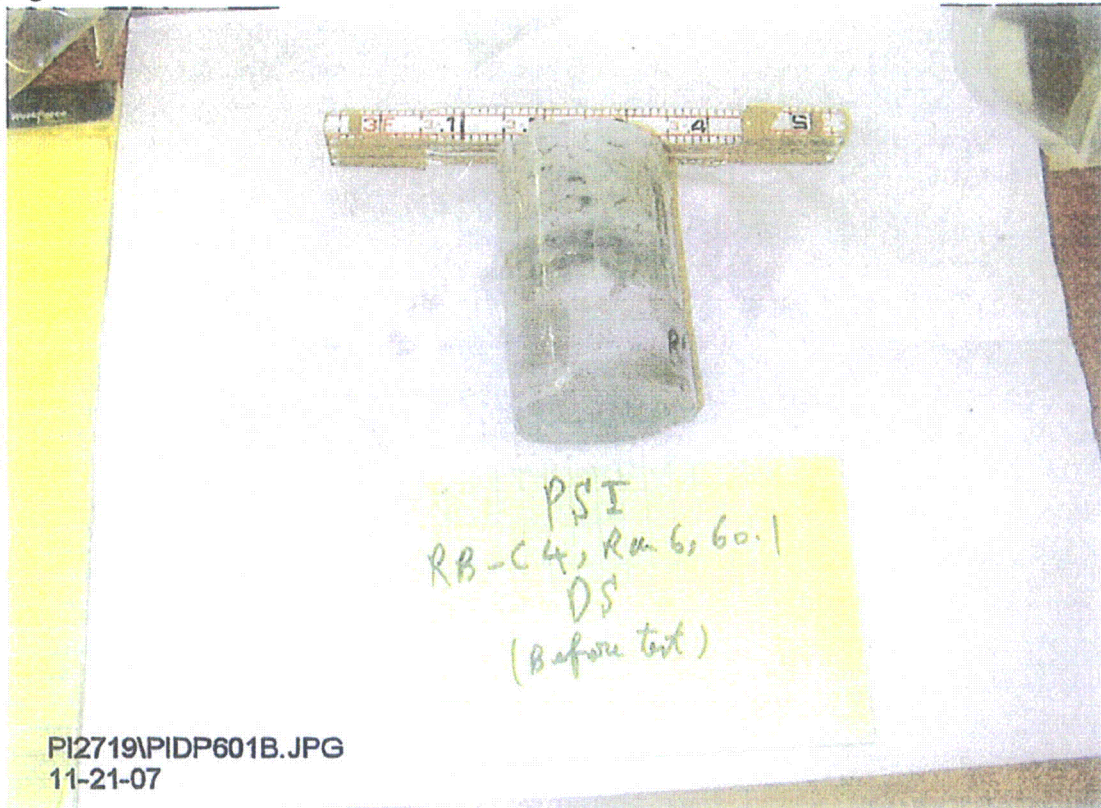


Figure 8A
Photo of discontinuity at approximately 60.1 feet in Boring RB-C4 taken prior to laboratory testing.

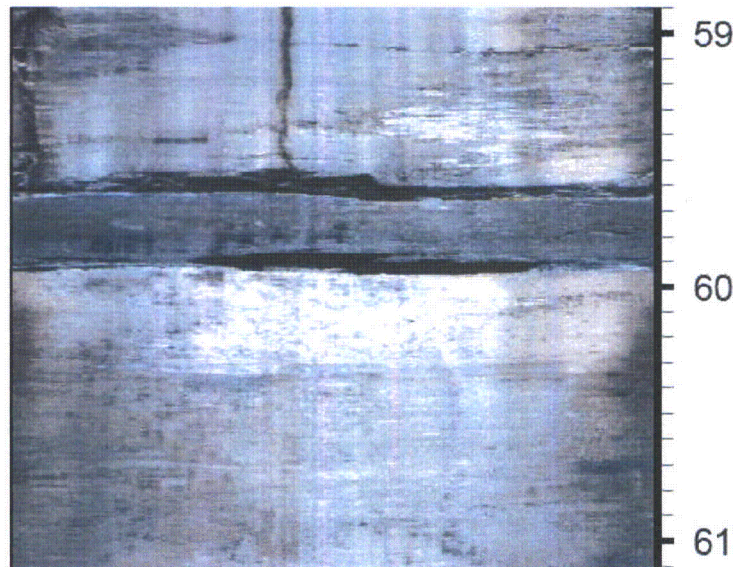


Figure 8A
Optical Televiewer Log in Boring RB-C4 from 58.9 to 61.1 feet.

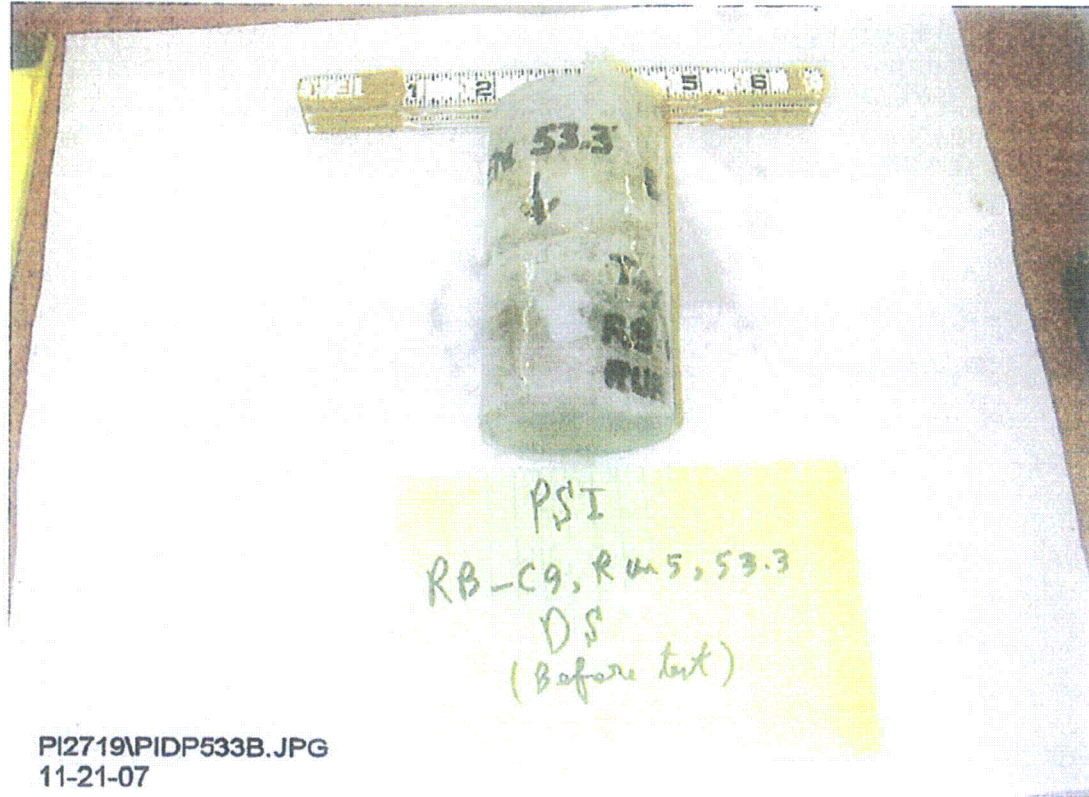


Figure 9A

Photo of discontinuity at approximately 53.3 feet in Boring RB-C9 taken prior to laboratory testing.

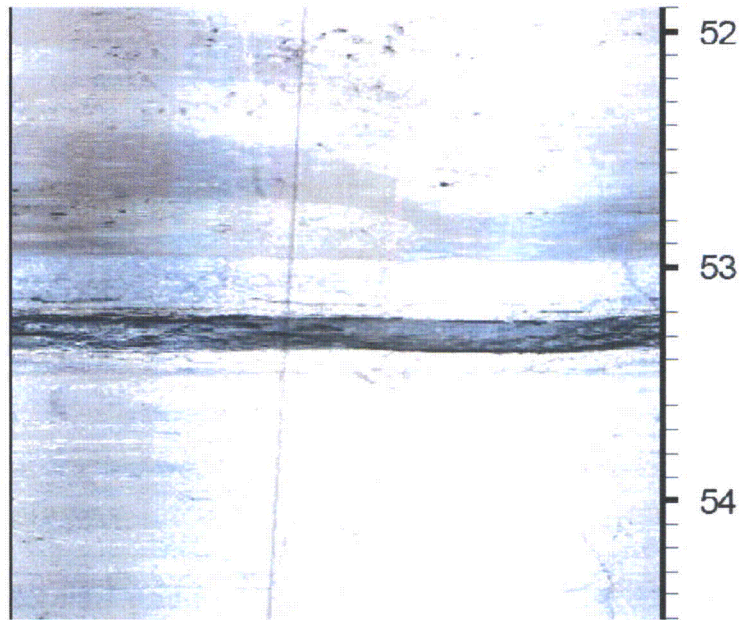


Figure 9B

Optical Televiewer Log in Boring RB-C9 from 51.9 to 54.5 feet.

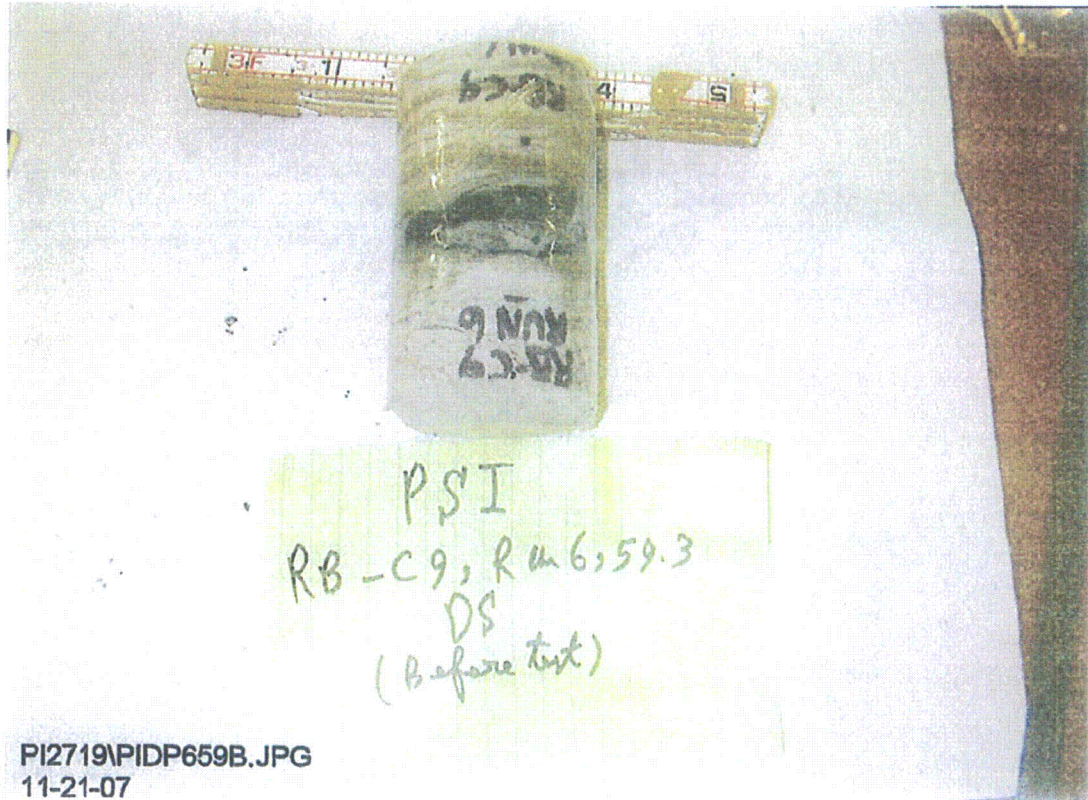


Figure 10A

Photo of discontinuity at approximately 59.3 feet in Boring RB-C9 taken prior to laboratory testing.

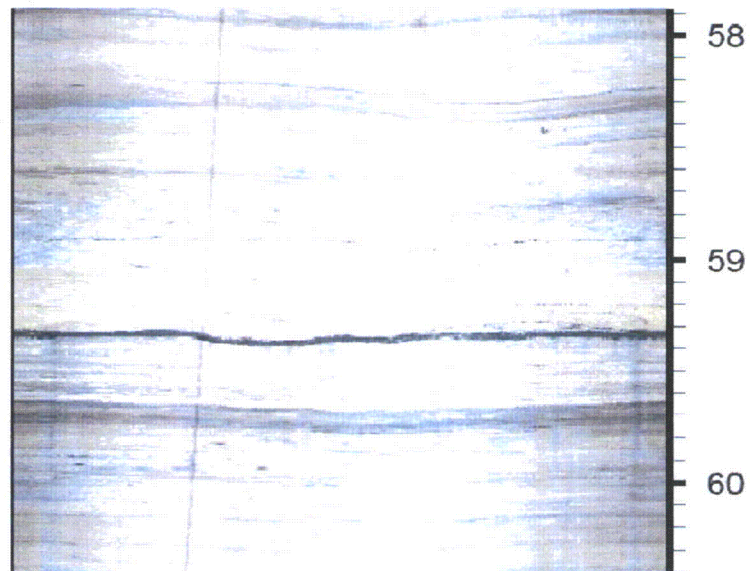


Figure 10B

Optical Televiewer Log in Boring RB-C9 from 57.9 to 60.4 feet.

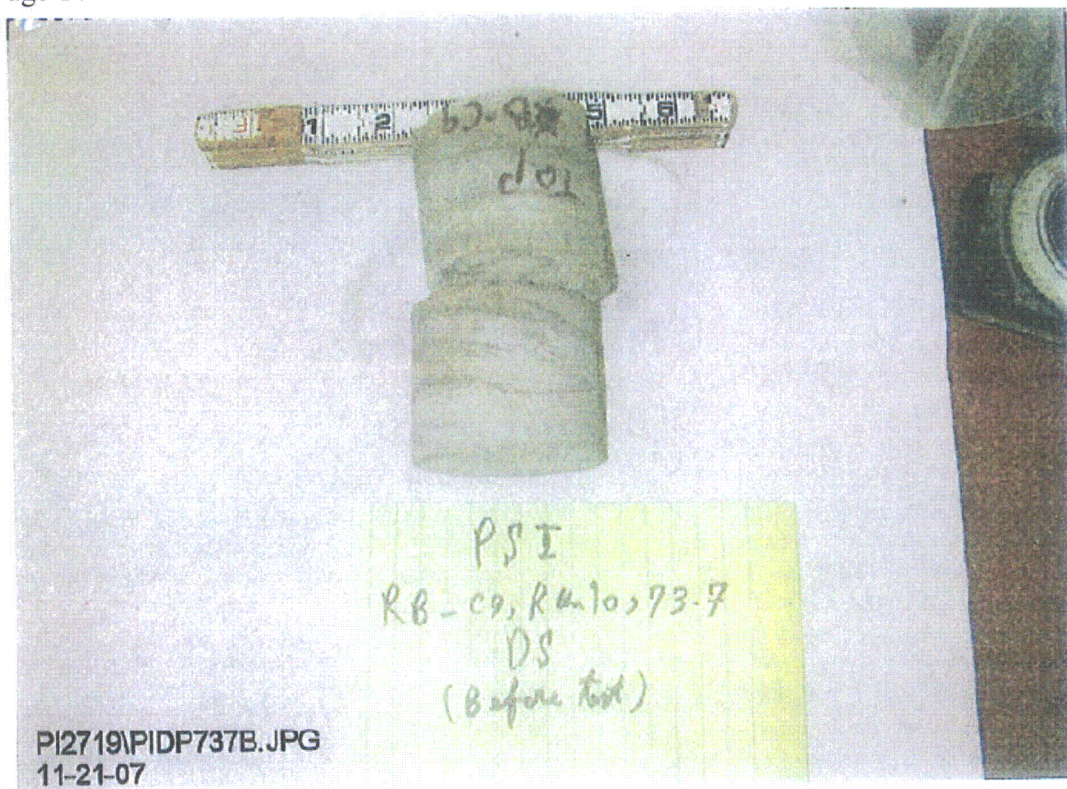


Figure 11A
Photo of discontinuity at approximately 73.3 feet in Boring RB-C9 taken prior to laboratory testing.

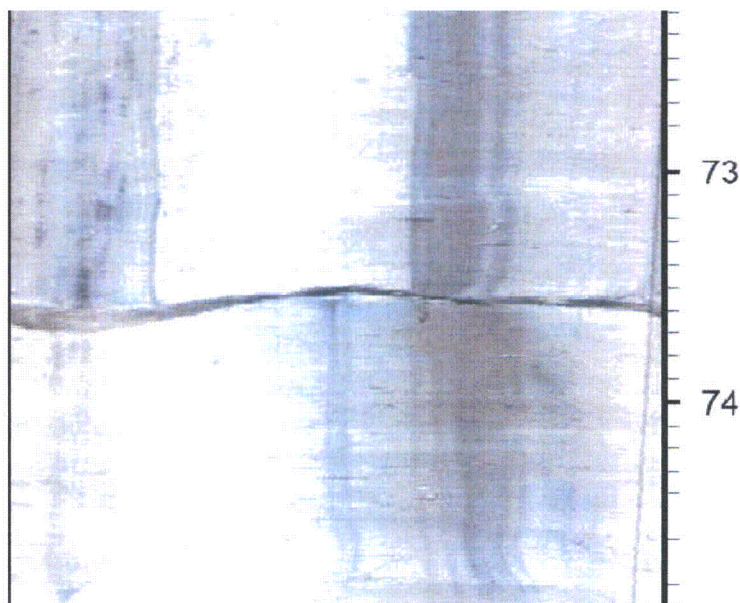


Figure 11B
Optical Televiewer Log in Boring RB-C9 from 72.3 to 74.9 feet.

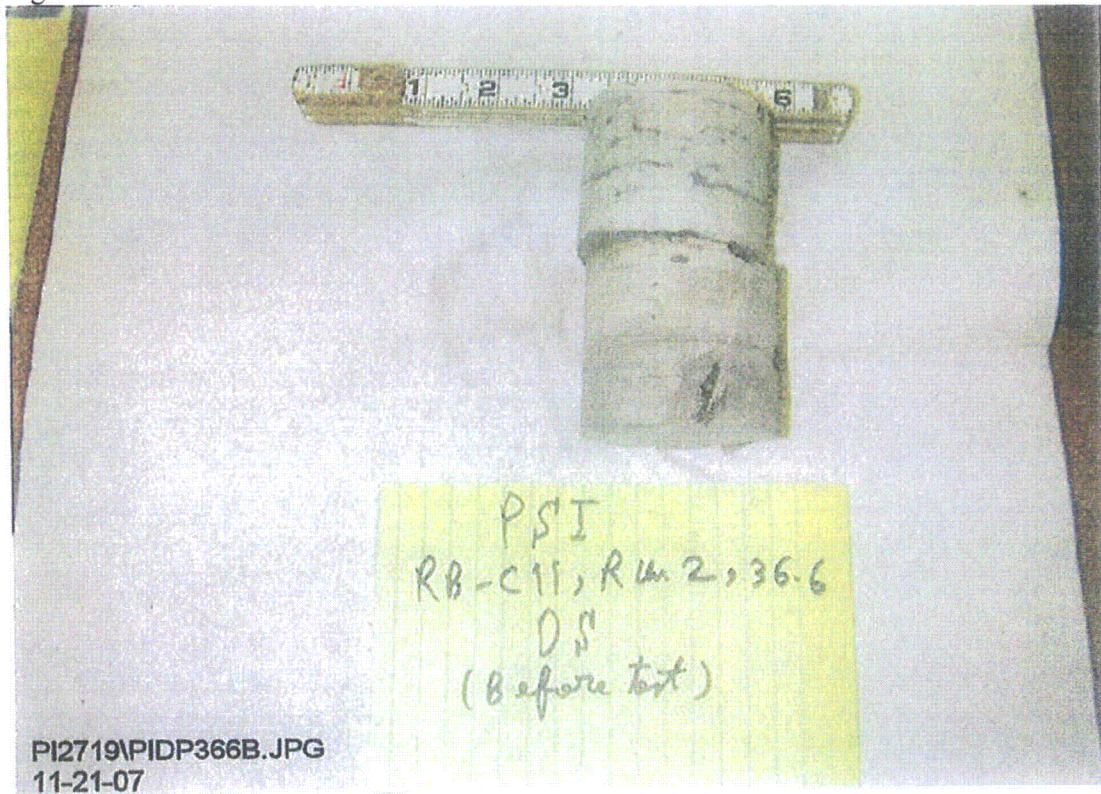


Figure 12A
Photo of discontinuity at approximately 36.6 feet in Boring RB-C11 taken prior to laboratory testing.

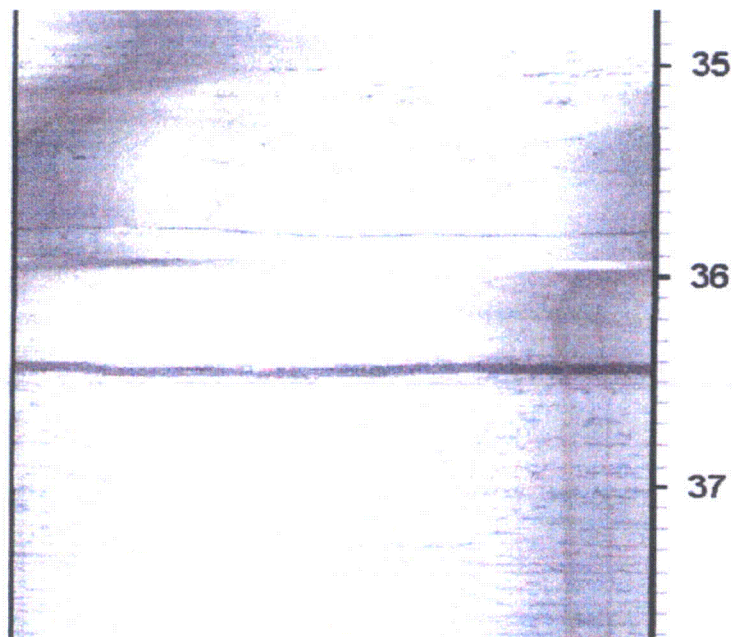


Figure 12B
Optical Televiewer Log in Boring RB-C11 from 34.7 to 37.7 feet.

Proposed COLA Revision

None.

**Attachment 11
NRC3-09-0051**

**Response to RAI Letter No. 16
(eRAI Tracking No. 3936)**

RAI Question No. 02.05.04-3

RAI 02.05.04-3

FSAR Section 2.5.4.2.1.2 provides for Bass Islands Group, Salina Group Units F, E, C, and B, the characterized parameter values of the following material properties often in terms of upper bound, mean, and lower bound values, or minimum, maximum, median, mean, and standard deviation values. Said parameters are specified in terms of a single number associated for the entire bedrock unit or provided for each borehole.

- a. Please provide additional information on why it is appropriate to provide single value of each parameter for the entire bedrock group rather than to provide inferred spatial variation of these parameter values reflecting some spatial gradients or to reflect the potential for these parameters varying with depth or over horizontal directions.*
- b. Please provide the reason and justification for using the Hoek-Brown criterion for each of these bedrock groups including descriptions of each bedrock unit as applied in specifying the Hoek-Brown parameters. For example, what was the relationship between the residual friction angle values associated with discontinuities in the Bass Islands Group and the parameters in the Hoek-Brown criterion for that material? How were the effects of Oolitic Dolomite (FSAR Figures 2.5.4-202 and 2.5.4-203) reflected in the Hoek-Brown criterion for the Bass Islands Group?*
- c. It is assumed that the Hoek-Brown criteria were converted to "equivalent" Mohr-Coulomb values because of the limitation of the programs used in analysis. Please provide the effective confining pressure ranges and the rationale for the selected effective confining pressure ranges used to convert Hoek-Brown criterion into the equivalent Mohr-Coulomb values.*

Response

- a) Please provide additional information on why it is appropriate to provide single value of each parameter for the entire bedrock group rather than to provide inferred spatial variation of these parameter values reflecting some spatial gradients or to reflect the potential for these parameters varying with depth or over horizontal directions.*

FSAR, Figures 2.5.4-220 through 2.5.4-223, show that the shear and compression wave velocities are relatively uniform within each bedrock unit. FSAR Figures 2.5.4-215 and 2.5.4-216 compare the shear and compression wave velocity profiles at four different locations throughout the site, and show that the compression and shear wave velocities are consistent across the site. The relatively consistent shear and compression wave velocities measured indicate uniformity of each bedrock unit across the site; therefore, it is appropriate to provide a single value of each parameter for each entire bedrock unit.

b) Please provide the reason and justification for using the Hoek-Brown criterion for each of these bedrock groups including descriptions of each bedrock unit as applied in specifying the Hoek-Brown parameters. For example, what was the relationship between the residual friction angle values associated with discontinuities in the Bass Islands Group and the parameters in the Hoek-Brown criterion for that material? How were the effects of Oolitic Dolomite (FSAR Figures 2.5.4-202 and 2.5.4-203) reflected in the Hoek-Brown criterion for the Bass Islands Group?

The Hoek-Brown criterion is used to estimate the strength of jointed bedrock masses, which is consistent with the bedrock encountered during the Fermi 3 subsurface investigation. The Hoek-Brown criterion is based on an assessment of interlocking rock blocks and the condition of the surfaces between these blocks. The criterion provides an estimate of equivalent angles of friction and cohesive strengths, which were needed for the bearing capacity analysis using the Terzaghi's approach as discussed in FSAR, Section 2.5.4.10.1.

The descriptions for each bedrock unit as applied in specifying the Hoek-Brown parameters presented in Fermi 3 FSAR, Revision 1, Table 2.5.4-205, are based on information obtained from exploratory borings at the location of proposed Fermi 3. FSAR, Section 2.5.1.2.3.1.1 discusses the Paleozoic Stratigraphy of the Site Area as shown below:

“Unit B was the deepest unit encountered.....The unit is a brown, pale brown, gray, and dark greenish gray dolomite.....The percent recoveries for Unit B recorded during the Fermi 3 subsurface investigation range from 96 to 100 percent. The Rock Quality Designation (RQD) values range from 80 to 100 with an average of 97.1.”

“Unit C was encountered.....The unit is a dark greenish-gray to black claystone and dolomite with interbeds of anhydrite.....The percent recoveries for Unit C recorded during the Fermi 3 subsurface investigation range from 94 to 100 percent. The RQD values range from 80 to 100 with an average of 97.2.”

“Unit E was encountered...The unit is comprised of pale brown, grayish-brown, gray, and bluish gray dolomite and argillaceous dolomite with thin shales and claystones.....The percent recoveries for Unit E recorded during the Fermi 3 subsurface investigation range from 30 to 100 percent with an average of 93.6 percent. The RQD values range from 0 to 100 with an average of 71.6.”

“Unit F contains a wide variety of materials.....The unit contains dolomite, limestone, claystone, shale, breccia, sandstone, and poorly indurated clastic sediments..... The percent recoveries for Unit F recorded during the Fermi 3 subsurface investigation range from 0 to 100 percent with an average of 59.3 percent. The RQD values range from 0 to 100 with an average of 13.4.”

“...The Bass Islands Group encountered during the Fermi 3 subsurface investigation is dominantly a light gray, light brownish gray, to dark gray micritic dolomite.....The

dolomite can be massive, banded, or mottled..... The percent recoveries for Bass Islands Group recorded during the Fermi 3 subsurface investigation range from 0 to 100 percent with an average of 94.0 percent. The RQD values range from 0 to 100 with an average of 53.7.”

Section 2.5.4.2.1.2 states that:

“The strength and deformation characteristics of bedrock units were also estimated using Hoek-Brown criterion (Reference 2.5.4-201), which uses the following five input parameters to estimate rock mass strength:

1. q_u of intact rock core samples.
2. Material index (m_i) related to rock mineralogy, cementation, and origin.
3. Geological strength index (GSI) that factors the intensity and surface characteristics of rock mass discontinuities.
4. Disturbance factor (D) related to the level of the rock mass disturbance due to construction excavation and blasting.
5. Laboratory measured E of the intact rock core samples.

The input parameters, for each bedrock unit, used to estimate rock mass strength based on Hoek-Brown criterion are summarized in Table 2.5.4-205.”

The parameters, q_u and E , were obtained based on the measured mean values from laboratory unconfined compression tests, in accordance to ASTM D7012. The mean q_u and E for each bedrock unit are presented in FSAR, Tables 2.5.4-206, 2.5.4-210, 2.5.4-212, 2.5.4-214, and 2.5.4-216.

The dominant rock type for each bedrock unit in Table 2.5.4-205 was selected based on bedrock descriptions and classification as presented in FSAR, Section 2.5.1.2.3.1.1 as shown above. Then, the material index (m_i) of each bedrock unit was obtained from attached Table 3 from FSAR, Reference 2.5.4-201.

The geological strength index (GSI) values were estimated using attached Table 5 from the FSAR, Reference 2.5.4-201. The structure of each bedrock unit in FSAR Table 2.5.4-205 was based on interpretation of bedrock descriptions and classification as presented in FSAR, Section 2.5.1.2.3.1.1 as shown above.

The disturbance factor (D) depends upon the degree of disturbance due to blast damage and stress relaxation. It varies from 0 for undisturbed in situ rock masses to 1 for very disturbed rock masses. Attached Table 7 from FSAR, Reference 2.5.4-201 provides guidelines for estimating the disturbance factor (D). Since only the Bass Islands Group dolomite will be excavated either by mechanical excavation or blasting, the disturbance factor (D) for this unit was conservatively selected as 1. The disturbance factor (D) for other bedrock units were selected as 0.

Table 3 from Fermi 3 FSAR, Revision 1, Reference 2.5.4-201

Rock mass properties

Table 3: Values of the constant m_i for intact rock, by rock group. Note that values in parenthesis are estimates.

Rock type	Class	Group	Texture			
			Coarse	Medium	Fine	Very fine
SEDIMENTARY	Clastic		Conglomerates* (21 ± 3) Breccias (19 ± 5)	Sandstones 17 ± 4	Siltstones 7 ± 2 Greywackes (18 ± 3)	Claystones 4 ± 2 Shales (6 ± 2) Marls (7 ± 2)
		Non-Clastic	Carbonates	Crystalline Limestone (12 ± 3)	Sparitic Limestones (10 ± 2)	Micritic Limestones (9 ± 2)
	Evaporites			Gypsum 8 ± 2	Anhydrite 12 ± 2	
	Organic					Chalk 7 ± 2
METAMORPHIC	Non Foliated		Marble 9 ± 3	Hornfels (19 ± 4) Metasandstone (19 ± 3)	Quartzites 20 ± 3	
	Slightly foliated		Migmatite (29 ± 3)	Amphibolites 26 ± 6		
	Foliated**		Gneiss 28 ± 5	Schists 12 ± 3	Phyllites (7 ± 3)	Slates 7 ± 4
IGNEOUS	Plutonic	Light	Granite 32 ± 3 Granodiorite (29 ± 3)	Diorite 25 ± 5		
		Dark	Gabbro 27 ± 3 Norite 20 ± 5	Dolerite (16 ± 5)		
	Hypabyssal		Porphyries (20 ± 5)		Diabase (15 ± 5)	Peridotite (25 ± 5)
	Volcanic	Lava		Rhyolite (25 ± 5) Andesite 25 ± 5	Dacite (25 ± 3) Basalt (25 ± 5)	Obsidian (19 ± 3)
		Pyroclastic	Agglomerate (19 ± 3)	Breccia (19 ± 5)	Tuff (13 ± 5)	

* Conglomerates and breccias may present a wide range of m_i values depending on the nature of the cementing material and the degree of cementation, so they may range from values similar to sandstone to values used for fine grained sediments.

** These values are for intact rock specimens tested normal to bedding or foliation. The value of m_i will be significantly different if failure occurs along a weakness plane.

Table 7 from Fermi 3 FSAR, Revision 1, Reference 2.5.4-
Rock mass properties

Table 7: Guidelines for estimating disturbance factor D

Appearance of rock mass	Description of rock mass	Suggested value of D
	Excellent quality controlled blasting or excavation by Tunnel Boring Machine results in minimal disturbance to the confined rock mass surrounding a tunnel.	D = 0
	Mechanical or hand excavation in poor quality rock masses (no blasting) results in minimal disturbance to the surrounding rock mass. Where squeezing problems result in significant floor heave, disturbance can be severe unless a temporary invert, as shown in the photograph, is placed.	D = 0 D = 0.5 No invert
	Very poor quality blasting in a hard rock tunnel results in severe local damage, extending 2 or 3 m, in the surrounding rock mass.	D = 0.8
	Small scale blasting in civil engineering slopes results in modest rock mass damage, particularly if controlled blasting is used as shown on the left hand side of the photograph. However, stress relief results in some disturbance.	D = 0.7 Good blasting D = 1.0 Poor blasting
	Very large open pit mine slopes suffer significant disturbance due to heavy production blasting and also due to stress relief from overburden removal. In some softer rocks excavation can be carried out by ripping and dozing and the degree of damage to the slopes is less.	D = 1.0 Production blasting D = 0.7 Mechanical excavation

The shear strength along the discontinuities is not one of the input parameters used in the Hoek-Brown criterion methodology; therefore, they were not used in the Hoek-Brown evaluation.

Unconfined compression tests were performed on the following oolitic dolomite samples:

- i. Boring RB-C1, run 6, at depths between 62.1 and 63.2 feet
- ii. Boring RB-C5, run 6 at depths between 57.0 and 58.3 feet,
- iii. Boring RW-C1, run 9 at depths between 68.0 and 69.0 feet.

The compressive strength and the elastic modulus of the oolitic dolomite are presented in Fermi 3 FSAR, Revision 1, Table 2.5.4-222 and are repeated in Table 1 here:

Table 1 Summary of Oolitic Dolomite Parameters						
Boring	Core Run No.	Depth (feet)	Unconfined Compression Strength		Elastic Modulus	
			(psi)	(ksf)	(psi)	(ksf)
RB-C1	6	62.1 to 63.2	10,830	1,560	7,300,000	1,051,200
RB-C5	6	57.0 to 58.3	14,360	2,070	7,400,000	1,065,600
RW-C1	9	68.0 to 69.0	10,370	1,490	5,600,000	806,400
Notes: psi = pounds per square inch ksf = kips per square foot						

The compressive strength and the elastic modulus of the oolitic dolomite are comparable to the average compressive strength (1,650 ksf) and the elastic modulus (842,400 ksf) of the remainder of the Bass Islands Group dolomite, and are therefore included in the overall averages of strength and modulus for the Bass Islands Group. In addition, the physical descriptions of the oolitic dolomite are similar to the descriptions of the dolomite within the Bass Islands Group as shown in Fermi 3 boring logs in Appendix 2.5DD of the Fermi 3 FSAR. Therefore, the shear strength parameters obtained using the Hoek-Brown criterion for the Bass Islands Group are considered applicable to the oolitic dolomite layer.

- c) *It is assumed that the Hoek-Brown criteria were converted to "equivalent" Mohr-Coulomb values because of the limitation of the programs used in analysis. Please provide the effective confining pressure ranges and the rationale for the selected effective confining pressure ranges used to convert Hoek-Brown criterion into the equivalent Mohr-Coulomb values.*

The effective confining pressure ranges used to convert the Hoek-Brown criterion to Mohr-Coulomb parameters are presented in Table 2.

Table 2
Range of Confining Pressures Used to Estimate Mohr-Coulomb Parameters

Bedrock Unit	Upper Bound Mohr-Coulomb Parameters		Mean Mohr-Coulomb Parameters		Lower Bound Mohr-Coulomb Parameters		
	Lower Limit of Confining Pressure, σ_t	Upper Limit of Confining Pressure, σ'_{3max}	Lower Limit of Confining Pressure, σ_t	Upper Limit of Confining Pressure, σ'_{3max}	Lower Limit of Confining Pressure, σ_t	Upper Limit of Confining Pressure, σ'_{3max}	
	(ksf)	(ksf)	(ksf)	(ksf)	(ksf)	(ksf)	
Bass Islands Group	-3.46	9.35	-2.86	9.08	-2.67	8.76	
Salina Unit	F	-0.55	8.46	-0.56	8.17	-0.77	7.74
	E	-15.25	10.17	-13.95	9.95	-14.35	9.69
	C	-34.16	10.19	-31.25	9.96	-32.15	9.71
	B	-28.43	10.31	-26.00	10.08	-26.75	9.83

FSAR, Section 2.5.4.2.1.2 states:

“The strength and deformation characteristics of bedrock units were also estimated using Hoek-Brown criterion (Reference 2.5.4-201), which uses the following five input parameters to estimate rock mass strength:

1. q_u of intact rock core samples.
2. Material index (mi) related to rock mineralogy, cementation, and origin.
3. Geological strength index (GSI) that factors the intensity and surface characteristics of rock mass discontinuities.
4. Disturbance factor (D) related to the level of the rock mass disturbance due to construction excavation and blasting.
5. Laboratory measured E of the intact rock core samples.

The input parameters, for each bedrock unit, used to estimate rock mass strength based on Hoek-Brown criterion are summarized in Table 2.5.4-205.”

The minor principal effective stress range selected is $\sigma_t < \sigma'_3 < \sigma'_{3max}$, where σ_t is the tensile strength of rock mass and σ'_{3max} is the upper limit of confining stress over which the relationship between the Hoek-Brown criteria and the Mohr-Coulomb criteria is considered (FSAR

Reference 2.5.4-201). Guidelines are discussed in the FSAR Reference 2.5.4-201 for determination of $\sigma'_{3\max}$ for slopes and for shallow and deep tunnels. For Fermi 3, the equation of $\sigma'_{3\max}$ developed for slopes was selected.

The σ_t and $\sigma'_{3\max}$ are defined in the following equations.

$$\sigma_t = \frac{s\sigma_{ci}}{m_b} \quad [1]$$

where, m_b is the value of the Hoek-Brown constant m for the rock mass, s is a constant which depends upon the rock mass characteristics and, σ_{ci} is the uniaxial compression strength of the intact rock. The value m_b is a function of material index (m_i), geological strength index (GSI) and disturbance factor (D). The value s is a function of geological strength index (GSI) and disturbance factor (D). The equations for m_b and s are shown in the FSAR Reference 2.5.4-201. The σ_{ci} was the mean compression strength of each bedrock unit based on laboratory testing.

$$\frac{\sigma'_{3\max}}{\sigma'_{cm}} = 0.72 \left(\frac{\sigma'_{cm}}{\gamma H} \right)^{-0.91} \quad [2]$$

where σ'_{cm} is the rock mass strength, σ is the unit weight, and H is the height of the slope. The σ'_{cm} is a function of σ_{ci} , m_b , and a , where a is a function of GSI. The equation for σ'_{cm} and a is shown in the FSAR Reference 2.5.4-201. For the Fermi 3 case, H was set equal to the depth of excavation for the Reactor/Fuel Building which is 65 feet.

The rock mass properties and Mohr-Coulomb parameters obtained, based on the Hoek-Brown criterion for each bedrock unit are presented in Tables 2.5.4-207 and 2.5.4-208 of the Fermi 3 FSAR, Revision 1, respectively.

Proposed COLA Revision

None.

NRC3-09-0012
RAI Question RAI 02.05.04-3

Enclosure 1

- Figure 2.5.1-235, Site Exploration Plan**
- Figure 2.5.1-236, Enlargement of Site Exploration Plan**
- Figure 2.5.1-237, Geological Cross Section A-A'**
- Figure 2.5.1-238, Geological Cross Section B-B'**
- Figure 2.5.1-239, Geological Cross Section C-C'**
- Figure 2.5.1-240, Geological Cross Section D-D'**
- Figure 2.5.4-202, Excavation Cross Section D-D'**
- Figure 2.5.4-203, Excavation Cross Section C-C'**
- Figure 2.5.4-204, Excavation Cross Section B-B'**

(following 9 pages)

**Attachment 12
NRC3-09-0051**

**Response to RAI Letter No. 16
(eRAI Tracking No. 3936)**

RAI Question No. 02.05.04-5

RAI 02.05.04-5

FSAR Section 2.5.4.2.2.1.7 provides a list of chemical tests for groundwater and surface water. However, no test result is presented and no discussion is provided for any of the tests performed. Since the foundation and/or sub-foundation concrete may be exposed to the groundwater, please address whether the chemical in groundwater is aggressive or not. Please provide some discussions on these results.

Response

The results of the chemical tests are presented in the attached Table 2.3-43 for the surface water, and attached Tables 2.3-63 through 2.3-66 for the groundwater in the Fermi 3 Environmental Report (ER). The corresponding monitoring well number for each sample ID number presented in Tables 2.3-63 through 2.3-66 is provided in Table 1.

Table 1 Monitoring Well Numbers Corresponding to Sample ID Number Used in the Attached ER Tables for the Groundwater Sample Analytical Results.	
Sample ID Number in ER Table	Monitoring Well Number
DQH0079-01	MW-393S
DQH0146-01	MW-387D
DQH0150-01	MW-387S
DQH0150-02	MW-390S
DQH0227-01	MW-395D
DQH0227-02	MW-395S
DQH0227-03	MW-391D
DQH0227-04	MW-391S
DQH0538-01	MW-381D
DQH0538-02	MW-383S
DQH0538-03	MW-383D
DQH0566-01	MW-386D
DQH0662-01	MW-386S
DQH0662-02 ⁽¹⁾	MW-386S
DQH0662-03	MW-384S
DQH0662-04 ⁽¹⁾	MW-384S
DQH0662-05	MW-384D
DQH0662-06 ⁽¹⁾	MW-384D
DQH0662-07 ⁽²⁾	RB-1-09Aug2007
DQH0785-01	MW-393D

Notes:
 (1) Duplicate samples.
 (2) Results for quality control rinsate blank (RB) sample.

The concentrations of sulfate (SO₄) and chloride in groundwater are summarized in Table 2.

At MW-386S, MW-386D, MW-387D and MW-387S located in the immediate vicinity of Fermi 3, the concentration of sulfate (SO₄) in groundwater ranges from 336 to 1,630 milligram per liter (mg/l), (equivalent to parts per million, ppm) with an average of 1,044 mg/l. Attached American Concrete Institute, ACI 349 Table 4.3.1 indicates the sulfate exposure ranges from “moderate” to “severe”. The highest concentration of sulfate (SO₄) in groundwater was 2,410 mg/l at MW-393S (located at western Fermi site boundary in the overburden groundwater), which corresponds to “severe” sulfate exposure. The SO₄ concentration would then be used in conjunction with ACI 349, shown below, or other applicable industry standard(s) to determine the appropriate cement to use for concrete exposed to it.

At MW-386S, MW-386D, MW-387D and MW-387S, the concentration of chloride in groundwater ranges from 23 to 128 mg/l with an average of 62 mg/l. The highest concentration of chloride in groundwater was 145 mg/l at MW-393S.

Table 2 Groundwater Sulfate and Chloride Concentrations			
Sample ID Number	Monitoring Well Number	Sulfate, SO ₄ Concentration (mg/l)	Chloride Concentration (mg/l)
DQH0538-01	MW-381D	366	79
DQH0538-03	MW-383D	574	28
DQH0538-02	MW-383S	413	78
DQH0662-05	MW-384D	1,480	61
DQH0662-06	MW-384D	1,620	47
DQH0662-03	MW-384S	1,710	35
DQH0662-04	MW-384S	1,720	36
DQH0566-01	MW-386D ⁽¹⁾	1,080	128
DQH0662-01	MW-386S ⁽¹⁾	1,530	39
DQH0662-02	MW-386S ⁽¹⁾	1,630	38
DQH0146-01	MW-387D ⁽¹⁾	336	23
DQH0150-01	MW-387S ⁽¹⁾	644	83
DQH0150-02	MW-390S	240	47
DQH0227-03	MW-391D	1,150	26
DQH0227-04	MW-391S	189	34
DQH0785-01	MW-393D	933	45
DQH0079-01	MW-393S	2,410	145
DQH0227-01	MW-395D	266	11
DQH0227-02	MW-395S	248	24

Notes:
 (1) Monitoring wells located in the immediate vicinity of the Fermi 3.

Table 4.2.3—Requirements for concrete exposed to deicing chemicals

Cementitious materials	Maximum percent of total cementitious materials by weight*
Fly ash or other pozzolans conforming to ASTM C 618	25
Slag conforming to ASTM C 989	50
Silica fume conforming to ASTM C 1240	10
Total of fly ash or other pozzolans, slag, and silica fume	50 [†]
Total of fly ash or other pozzolans and silica fume	35 [†]

*The total cementitious material also includes ASTM C 150, C 595, C 845, and C 1157 cement. The maximum percentages shall include: a) fly ash and other pozzolans present in Type IP or I(PM) blended cement (ASTM C 595 or C 1157); b) slag used in the manufacture of an IS or I(SM) blended cement (ASTM C 595 or C 1157); and c) silica fume (ASTM C 1240) present in a blended cement.
[†]Fly ash or other pozzolans and silica fume shall constitute no more than 25 or 10%, respectively, of the total weight of the cementitious materials.

Table 4.3.1—Requirements for concrete exposed to sulfate-containing solutions

Sulfate exposure	Water-soluble sulfate (SO ₄) in soil, % by weight	Sulfate (SO ₄) in water, ppm	Cement type	Maximum w/cm, by weight, normal weight concrete	Minimum f' _c , normal weight concrete, psi [†]
Negligible	0.00 ≤ SO ₄ < 0.10	0 ≤ SO ₄ < 150	—	—	—
Moderate [†]	0.10 ≤ SO ₄ < 0.20	150 ≤ SO ₄ < 1500	II, IP(MS), IS(MS), P(MS), I(PM)(MS), I(SM)(MS)	0.50	4000
Severe	0.20 ≤ SO ₄ < 2.00	1500 ≤ SO ₄ < 10,000	V	0.45	4500
Very severe	SO ₄ > 2.00	SO ₄ > 10,000	V plus pozzolan [‡]	0.45	4500

*When both Tables 4.3.1 and 4.2.2 are considered, the lowest applicable maximum water-cementitious material ratio and highest applicable minimum f'_c shall be used.
[†]Seawater.
[‡]Pozzolan that has been determined by test or service record to improve sulfate resistance when used in concrete containing Type V cement.

Table 4.4.1—Maximum chloride ion content for corrosion protection of reinforcement

Type of member	Maximum water-soluble chloride ion (Cl ⁻) in concrete, percent by weight of cement
Prestressed concrete	0.06
Reinforced concrete	0.15

concrete made with a cement that provides sulfate resistance and that has a maximum water-cementitious material ratio and minimum f'_c from Table 4.3.1.

4.3.2 Calcium chloride as an admixture shall not be used in concrete to be exposed to severe or very severe sulfate-containing solutions, as defined in Table 4.3.1.

4.4—Corrosion protection of reinforcement

4.4.1 For corrosion protection of reinforcement in concrete, maximum water-soluble chloride ion concentrations in hardened concrete at ages from 28 to 42 days contributed from the ingredients including water, aggregates, cementitious materials, and admixtures shall not exceed the limits of

Table 4.4.1. When testing is performed to determine water-soluble chloride ion content, test procedures shall conform to ASTM C 1218.

4.4.2 When reinforced concrete will be exposed to deicing chemicals, salt, brackish water, seawater, or spray from these sources, requirements of Table 4.2.2 for maximum water-cementitious material ratio and minimum f'_c, and the minimum concrete cover requirements of 7.7 shall be satisfied. See 18.16 for unbonded tendons.

CHAPTER 5—CONCRETE QUALITY, MIXING, AND PLACING

5.1—General

5.1.1 Concrete shall be proportioned to provide an average compressive strength f'_{cr}, as prescribed in 5.3.2, and shall satisfy the durability criteria of Chapter 4. Concrete shall be produced to minimize the frequency of strength tests below f'_c, as prescribed in 5.6.3.3. For concrete designed and constructed in accordance with the Code, f'_c shall not be less than 2500 psi.

5.1.2 Requirements for f'_c shall be based on tests of cylinders made and tested as prescribed in 5.6.3.

5.1.3 Unless otherwise specified, f'_c shall be based on 28-day tests. If other than 28 days, test age for f'_c shall be as indicated in design drawings or specifications.

5.1.4 Splitting tensile strength tests shall not be used as a basis for field acceptance of concrete.

5.1.5 Design drawings shall show specified compressive strength of concrete f'_c for which each part of the structure is designed.

5.2—Selection of concrete proportions

5.2.1 Proportions of materials for concrete shall be established to provide:

- (a) Workability and consistency to permit concrete to be worked readily into forms and around reinforcement under conditions of placement to be employed, without segregation or excessive bleeding;
- (b) Resistance to special exposures as required by Chapter 4;
- (c) Conformance with strength test requirements of 5.6.

5.2.2 Where different materials are to be used for different portions of proposed work, each combination shall be evaluated.

5.2.3 Concrete proportions shall be established in accordance with 5.3 or, alternatively, 5.4, and shall meet applicable requirements of Chapter 4.

5.3—Proportioning on the basis of field experience or trial mixtures, or both

5.3.1 Sample standard deviation

5.3.1.1 Where a concrete production facility has test records, a sample standard deviation s_s shall be established. Test records from which s_s is calculated:

- (a) Shall represent materials, quality control procedures, and conditions similar to those expected and changes in materials and proportions within the test records shall not have been more restrictive than those for proposed work;
- (b) Shall represent concrete produced to meet a specified concrete strength or strengths within 1000 psi of f'_c;

Proposed COLA Revision
None

**Attachment 13
NRC3-09-0051**

**Response to RAI Letter No. 16
(eRAI Tracking No. 3936)**

RAI Question No. 02.05.04-6

RAI 02.05.04-6

FSAR Sections 2.5.4.2.2.2 and 2.5.4.3 refer to figures and tables showing the locations of explorations and various geologic cross-sections including those through the Seismic Category I structures.

- a. The scale of FSAR Figures 2.5.1-235 and 2.5.1-236 is such that it is difficult to locate various borings or geophysical and other test results with respect to the buildings and other site features. Please provide the aforementioned figures at "large enough scale" with adequately detailed information to be helpful in locating and evaluating various results from the field investigation with respect to various proposed buildings and other features at the site.*
- b. Please provide key figures referenced in FSAR Section 2.5.4.3 at scales and with adequately detailed information that would facilitate various evaluations. For example, such figures might make it easier to evaluate potential effects of various buildings and their proximity and their relationships to foundation materials and boring logs and other subsurface information without addressing different figures (and tables) often at rather small scales.*

Response

- a) FSAR Figures 2.5.1-235 through 2.5.1-240 are provided at full size in the enclosure to this response.
- b) FSAR Figures 2.5.4-202 through 2.5.4-204 are provided at full size size in the enclosure to with this response.

FSAR Figure 2.5.1-235 shows the overall Fermi site with all the subsurface exploration locations provided. The subsurface investigation in the Fermi 3 power block area along with the site arrangement is shown on FSAR Figure 2.5.1-236. The locations, dimensions, and proximity of the structures in the power block area are based on the ESBWR DCD.

The location of north-south Geologic Cross Section A-A', which extends across much of the Fermi site, is shown on FSAR Figure 2.5.1-235, with Geologic Cross Section A-A' provided on FSAR Figure 2.5.1-237.

The locations of three additional Geologic Cross Sections, B-B', C-C' and D-D', in the immediate power block area are shown on FSAR Figure 2.5.1-236. Geologic Cross Sections B-B', C-C' and D-D' are provided on FSAR Figures 2.5.1-238, 2.5.1-239 and 2.5.1-240, respectively.

Fermi 3 FSAR, Revision 1, Section 2.5.4.3 states:

“Figure 2.5.4-202 through Figure 2.5.4-204 show geologic cross-sections through the Seismic Category I structures showing the detailed relationship of the foundations of all Seismic Category I structures to the subsurface materials.”

“Table 2.5.4-224 provides the foundation elevations of the major structures in the Power Block area. The key dimensions of the foundations for the R/FB, CB, and the FWSC are provided in the DCD Table 3.8-13. The finished ground level grade (finish grade) of elevation 179.6 m (589.3 ft) NAVD 88 was obtained from Subsection 2.4.1.”

FSAR Figure 2.5.4-202 through Figure 2.5.4-204 also show the relationship of the Seismic Category I structures to the exploratory boring used to develop the geologic cross sections. Note that FSAR Figures 2.5.4-202 through 2.5.4-204 were generated from FSAR Figures 2.5.1-238 and 2.5.1-240 by adding features associated with the excavation and structures. Table 1 provides the correlations between corresponding geologic cross section figures in FSAR Sections 2.5.1 and 2.5.4.

Table 1 Corresponding Geologic Cross Section Figure Numbers Between FSAR Section 2.5.1 and 2.5.4		
Section 2.5.1	Section 2.5.4	Cross-Section on Figure 2.5.1- 236
Figure 2.5.1-238	Figure 2.5.4-204	B-B'
Figure 2.5.1-239	Figure 2.5.4-203	C-C'
Figure 2.5.1-240	Figure 2.5.4-202	D-D'

In summary, FSAR Figures 2.5.1-235 through 2.5.1-240, and Figures 2.5.4-202 through 2.5.4-204 are provided at full size as supplemental attachments with this response. These figures provide information to evaluate potential effects of various buildings and their proximity and their relationships to foundation materials and boring logs and other subsurface information.

Proposed COLA Revision

None

**Attachment 14
NRC3-09-0051**

**Response to RAI Letter No. 16
(eRAI Tracking No. 3936)**

RAI Question No. 02.05.04-8

RAI 02.05.04-8

FSAR Section 2.5.4.2.2.5.2 states that "the selection of Eur from last cycle as an estimate of the in-situ modulus is reasonable because the condition of the bedrock at the highest pressure level is probably closer to the in-situ undisturbed bedrock than at the lower pressure levels and previous unload/reload cycles." It also states that the "material being tested was a very complex geological unit consisting of interbedded limestone/dolomite/claystone/siltstone/shale and breccias with varying degrees of induration." Given that an applicable strain range and applied unload/reload cycles may be affecting the values of Eur and possible effects of macrofeatures may not be present within the influence zone of the pressuremeter test, please provide additional information regarding why the Eur from the last cycle (2nd or 3rd cycle) is an appropriate representation of the modulus of in-situ undisturbed bedrock. Please describe how the results were used and identify the calculations where these pressuremeter test values were used.

Response

The ideal pressure vs. displacement plot for a pressuremeter test is illustrated in Figure 1. The membrane was expanded by controlling the flow of compressed nitrogen into the pressuremeter and increasing the pressure in small steps until the membrane started to expand against the borehole wall. The pressure is relatively constant or increases slowly with increasing displacements before the membrane reaches the borehole wall. After the membrane encounters the borehole wall, the pressure increases rapidly with increasing displacements. In general, there is a smooth transition before and after the membrane encounters the borehole wall as shown in Figure 1. In intact materials the pressure-displacement curve will initially curve upwards then tend to a linear form with increasing displacements. As the pressure increases, eventually, the curve will exhibit concave behavior as shown in Figure 1 at higher pressure ranges. If the pressures are high enough, relative to the shear strength of the material, a limiting pressure will be reached. This limit pressure is a function of the shear strength of the material. For intact materials, the generic shape of the pressure-displacement curve will be the same for all material that fails under shear. For strong materials such as hard rocks, the limit pressure may not be reached as the pressure required would be beyond the pressure that the pressuremeter can apply.

Additional information can be obtained from pressuremeter tests that can be used to help characterize the behavior of the material being tested (i.e. the slopes of the unload-reload loops). Figure 2 shows typical unload-reload loops performed at different pressure ranges. The total pressure is lowered to no more than 40 percent of the maximum pressure reached at any stage during the pressuremeter testing. The purpose is to keep the material in the elastic range and not allow the material to fail plastically inwards on the membrane. For homogeneous materials which contain no fractures, the successive unload-reload loops performed at different pressure ranges will be relatively parallel. The slope of the unload-reload loop will be a measure of the shear modulus commonly identified by the letter G. The Young's modulus, E, can be determined from the unload-reload slope by assuming a Poisson's ratio. The Pressuremeter modulus, E_m , is

determined from the slope of the linear section of the pressure-strain curve. This is not an elastic parameter since the slope includes a combination of elastic and plastic strains.

If, however, the material is naturally fractured or mechanically fractured during the drilling process, then the slope of the unload-reload loops increases for each successive unload-reload cycles performed at higher pressures as illustrated in Figure 2. For materials that are fractured during the drilling process, the slope of the unload-reload loops increases until all the joints are close up; and beyond this point the slope of the unload-reload loops becomes, relatively, parallel. For materials which are naturally fractured, the slope of the unload-reload loops will not become parallel. The slope of the unload-reload loops continues to increase as the joints are being closed up. The strain sensors may reach a limit before the joints are fully close up. Hence the slope of successive unload-reload loops can be used to give a qualitative indication of the fractured nature of the material. The modulus measured from the slope of the final unload-reload loop will be a conservative estimate of the in-situ shear modulus.

Figure 3 shows the typical pressure-displacement behavior for material tested in the Salina Unit F. It is shown that the slopes of the three unload-reload loops get progressively steeper with increasing strain, which is an indication of fractured material, as observed during drilling. As explained above, the slope of the unload-reload loops continues to increase as the joints are being closed up. Therefore, the E_{ur} from the last cycle is an appropriate representation of the modulus of in-situ undisturbed bedrock for the Salina Unit F.

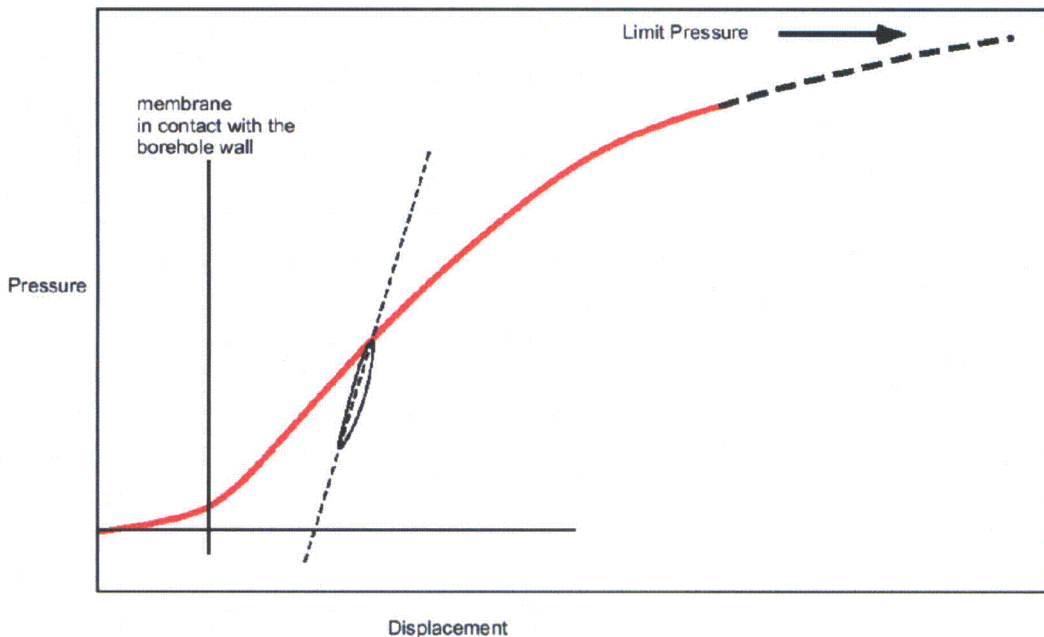


Figure 1 – Ideal Pressure-Displacement Curve For A Pressuremeter Test.

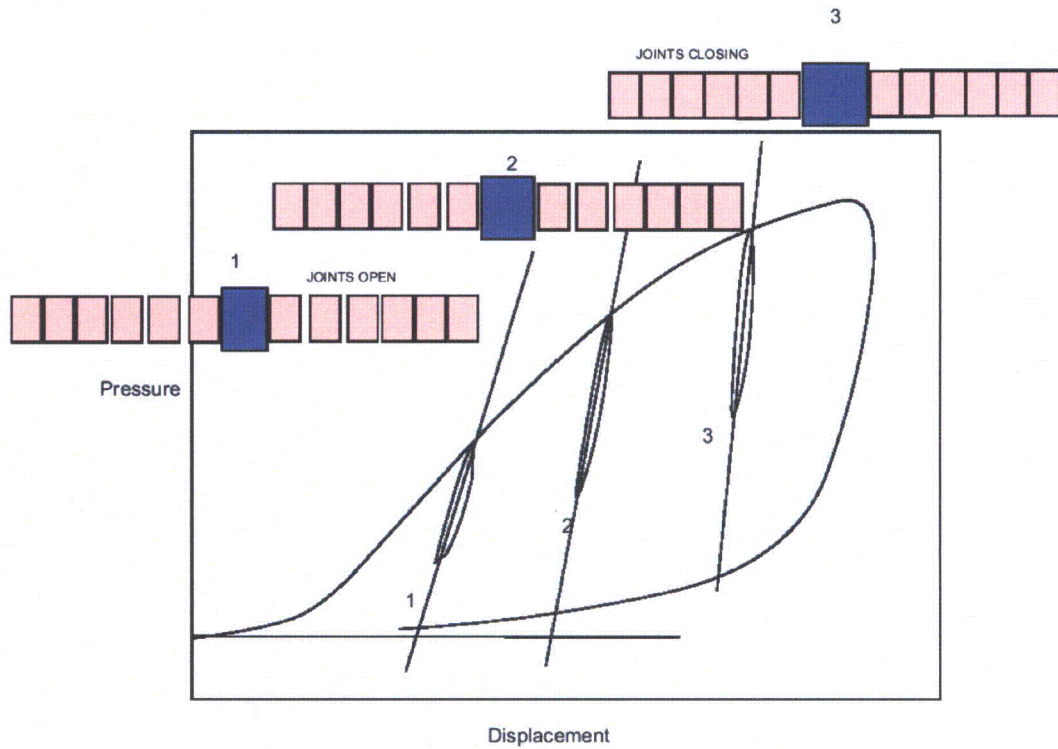


Figure 2 – Ideal Pressuremeter Test With Several Unload/Reload Loops.

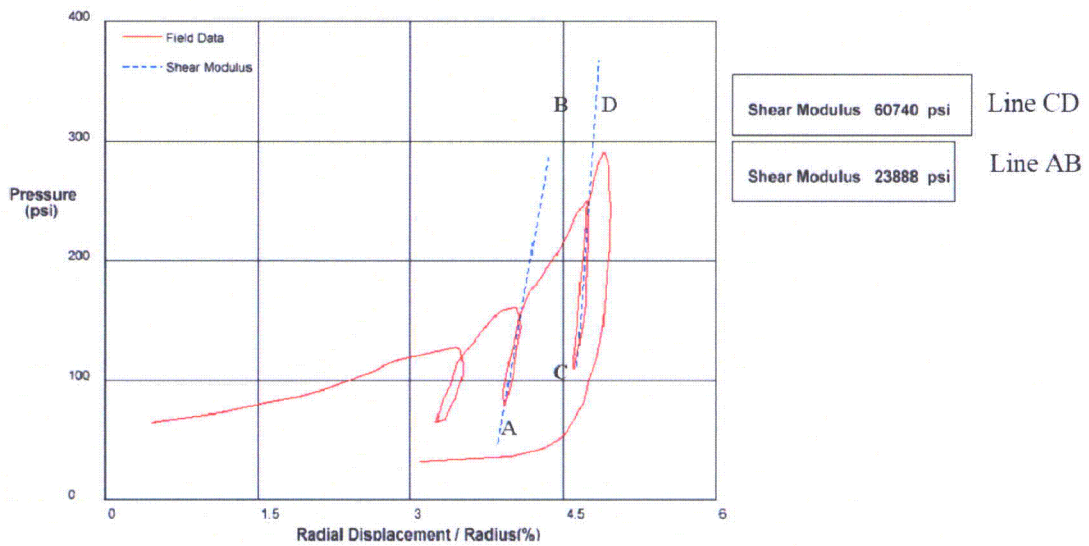


Figure 3 – Typical Pressure-Displacement Behavior in Salina Unit F.

The elastic modulus, E, obtained from the pressuremeter testing was compared to the E obtained based on Hoek-Brown criterion as discussed in FSAR, Section 2.5.4.10.2:

“...The average E, based on the pressuremeter tests in Salina Group Unit F, falls within the upper and lower bound E based on Hoek-Brown criterion.”

Since the lower bound E based on Hoek-Brown criterion is lower than the measured E, it was selected for settlement analysis as discussed in FSAR, Section 2.5.4.10.2:

“For analysis of settlements, the lower bound E based on the Hoek-Brown criterion for each bedrock unit were selected. It is believed that the average E of the bedrock units will be greater than the lower bound E from the Hoek-Brown criterion; therefore, estimated settlement will represent upper limit estimates. These lower bound E values are used for settlement analysis.”

It is concluded that the E_{ur} from the last cycle is an appropriate representation of the modulus of in-situ undisturbed bedrock for the Salina Unit F as discussed above. It is shown that the E obtained from the pressuremeter testing was higher than the E obtained based on Hoek-Brown criterion. Therefore, to provide a bounding estimate of settlement and rebound of Seismic Category I foundations; the E obtained based on Hoek-Brown criterion was used.

Proposed COLA Revision

None.

Attachment 15
NRC3-09-0051

Response to RAI Letter No. 16
(eRAI Tracking No. 3936)

RAI Question No. 02.05.04-10

RAI 02.05.04-10

FSAR Section 2.5.4.3 together with FSAR Figure 2.5.4-202 indicates that two types of low strength lean concrete and structural backfill of granular soil material will be used. One type of lean concrete is to follow the DCD criteria and the other type is unspecified.

- a. Please indicate whether the concrete will conform to industry standards such as the American Concrete Institute (ACI 349) for safety-related nuclear plants specification with the required compressive strength.*
- b. Please provide assurance that the structural backfill material will be obtained from a source with specified minimum acceptance criteria, compacted to specific American Society of Testing and Materials criteria.*

Response

- a. Fermi 3 FSAR, Revision 1, Section 2.5.4.5.4.2 states:

“Lean concrete used as fill under the FWSC will be proportioned, tested and the placement controlled in accordance with Regulatory Guide 1.142. The lean concrete fill will have a mean 28-day compressive strength of equal to or greater than 2000 psi with a mean shear wave velocity of equal to or greater than 3600 ft/s.”

Regulatory Guide 1.142, “Safety-Related Concrete Structures For Nuclear Power Plants (Other Than Reactor Vessels And Containments)”, endorses American Concrete Institute (ACI) 349 Code Requirements for Nuclear Safety Related Concrete Structures and Commentary. ACI 349 addresses concrete quality, mixing and placing. Therefore, for Fermi 3 the quality, mixing and placing of lean concrete will conform to an industry standard.

- b. The structural (or engineered) backfill material will be obtained from a source with specified minimum acceptance criteria in the ESBWR DCD, Revision 6. The engineered backfill will be tested in accordance ASTM standard as discussed in the FSAR, Section 2.5.4.5.1:

“Once the imported source material is identified, the material(s) are sampled and tested to verify adherence to the required specifications for engineered granular backfill. Laboratory tests including moisture content per ASTM D2216 (Reference 2.5.4-213), sieve analysis per ASTM D422, (Reference 2.5.4-216), standard Proctor per ASTM D698 (Reference 2.5.4-234), modified Proctor tests per ASTM D1557 (Reference 2.5.4-235), Relative Density test per ASTM D 4253

and 4254 (Reference 2.5.4-236, Reference 2.5.4-237) and Direct Shear Test per ASTM

D3080 (Reference 2.5.4-223) are performed to verify design requirement compliance for engineered granular backfill. The soundness of aggregate is confirmed using sulfate soundness per ASTM C88 (Reference 2.5.4-238) and Los Angeles abrasion tests per ASTM C131 and ASTM C535 (Reference 2.5.4-239, Reference 2.5.4-240).”

The FSAR text will be updated to reflect additional backfill requirements addressed in the DCD, Revision 6.

Proposed COLA Revision

Propose revision for FSAR Section 2.5.4.5.4.2 and FSAR Table 2.0-201 are shown in the attached markup.

Markup of Detroit Edison COLA
(following 3 pages)

The following markup represents how Detroit Edison intends to reflect this RAI response in the next appropriate update of the Fermi 3 COLA. However, the same COLA content may be impacted by revisions to the ESBWR DCD, responses to other COLA RAIs, other COLA changes, plant design changes, editorial or typographical corrections, etc. As a result, the final COLA content that appears in a future submittal may be different than presented here.

2.5.4.5.3.3 **Foundation Bedrock Grouting**

A foundation bedrock grouting program was completed for the Fermi 2 excavation and was successful in reducing groundwater flow through the rock mass into the excavation during construction (Reference 2.5.4-241). A similar approach to the foundation bedrock grouting program used for Fermi 2 may be used for Fermi 3 as part of the excavation support and seepage control system.

2.5.4.5.4 **Compaction Specifications and Quality Control**

This section describes the methods and procedures used for verification and quality control of foundation materials.

2.5.4.5.4.1 **Foundation Bedrock**

Properties of foundation materials are discussed in Subsection 2.5.4.2. This section describes methods and procedures used for verification and quality control of foundation materials.

Visual inspection of the final bedrock excavation surface is performed to confirm material is in general conformance with the expected foundation materials based on boring logs. Visual inspection is performed of exposed bedrock foundation subgrade to confirm that cleaning and surface preparations are properly completed. Concrete fill may be used to create a level, uniform surface for installation of concrete foundation slab.

Geologic mapping of the final exposed excavated bedrock surface is performed before placement of concrete fill and foundation concrete. The geologic mapping program includes photographic documentation of the exposed surface and documentation for significant geologic features.

The details of the quality control and quality assurance programs for foundation bedrock are addressed in the design specifications prepared during the detailed design phase of the project.

2.5.4.5.4.2 **Backfill Materials and Quality Control**

Backfill for the Fermi 3 may consist of concrete fill or a sound, well graded granular backfill. Concrete backfill as required per the Referenced DCD is used to backfill the gap between the foundation mat of R/FB and CB and bedrock. Engineered granular backfill to be used will have a ϕ' equal to or greater than 30 degrees when properly placed and compacted. The anticipated extent of lean concrete fill and granular

35

Insert 1

In addition, the engineered backfill is required to meet the following criteria:

- i. Product of peak ground acceleration α (in g), Poisson's ratio ν and density γ
 $\alpha(0.95\nu + 0.65)\gamma$: 1220 kg/m³ (76 lbf/ft³) maximum
- ii. Product of at-rest pressure coefficient k_0 and density:
 $k_0\gamma$: 750 kg/m³ (47 lbf/ft³) minimum
- iii. At-rest pressure coefficient:
 k_0 : 0.36 minimum
- iv. Soil density
 γ : 1900 kg/m³ (119 lbf/ft³) minimum

backfill is shown on Figure 2.5.4-202, Figure 2.5.4-203, and Figure 2.5.4-204.

Concrete fill mix designs are addressed in a design specification prepared during the detailed design phase of the project. Field observation is performed to verify that approved mixes are used and test specimens are obtained that verify that specified design parameters are reached. The foundation bedrock and concrete fill provide adequately high factors of safety against bearing capacity failure under both static and seismic structural loading. Quality Control testing requirements for bedrock include visual inspection and geologic mapping.

Engineered granular backfill sources are identified and tested for engineering properties, in accordance with recommendations from Subsection 2.5.4.5.1 and other testing as required by design specifications.

Engineered granular backfill is compacted to achieve density that results in the backfill having a minimum ϕ' of ~~25~~ degrees. Based on correlations of strength characteristics for granular soils (Reference 2.5.4-242), the ϕ' of compacted granular soils can achieve 35 degree. Engineered granular backfill materials are placed in controlled lifts and compacted. Within confined areas or close to foundation walls, smaller compactors are used to prevent excessive lateral pressures against the walls from stress caused by heavy compactors.

Evaluation and discussion of liquefaction issues related to soil backfill materials is provided in Subsection 2.5.4.8. Lateral pressures applied against foundation walls are evaluated and discussed in Subsection 2.5.4.10.

A quality control sampling and testing program is developed to verify that concrete fill and granular backfill material properties conform to the specified design parameters. Sufficient laboratory compaction and grain size distribution tests are performed to account for variations in fill material. A test fill program may be included for the purposes of determining an optimum size of compaction equipment, number of passes, lift thickness, and other relevant data for achievement of the specified compaction.

Lean concrete used as fill under the FWSC will be proportioned, tested and the placement controlled in accordance with Regulatory Guide 1.142. The lean concrete fill will have a mean 28-day compressive

**Attachment 16
NRC3-09-0051**

**Response to RAI Letter No. 16
(eRAI Tracking No. 3936)**

RAI Question No. 02.05.04-11

RAI 02.05.04-11

FSAR Section 2.5.4.4.1, under “Geophysical Surveys for Dynamic Characteristics of Subsurface Materials”, states that the dynamic characteristics of soil and bedrock were measured using downhole P-S suspension logging, downhole seismic testing, and SASW logging. It concludes in FSAR Section 2.5.4.4.1.1, under “P-S Suspension Logging and Downhole Seismic Testing in Bedrock Units”, that from Figure 2.5.4-216 “the downhole Vs values in general agree with Vs obtained using P-S suspension logging.” It also concludes in FSAR Section 2.5.4.4.1.2, under “P-S Suspension Logging and Spectral Analysis of Surface Wave in Soil Layers”, that “the results are considered acceptable, because soil shear wave velocities measured using the P-S Suspension method agree with those measured using SASW method.”

For downhole seismic testing, and SASW logging, please provide test data for shear wave velocity and compressive wave velocity in addition to average values. Additionally, please discuss how these data may be varying (or not varying) with the depth, and provide information on whether these variability observed from downhole seismic testing and SASW logging may need to be considered in the characterization of those soil and bedrock units.

Response

The detailed results of the compression and shear wave velocity measurements performed at Fermi 3 are provided in the FSAR, Reference 2.5.4-248, which will be available for review by NRC staff and their contractors at several Detroit Edison locations.

The compression and shear wave velocities measured using the downhole seismic method were plotted along with P-S suspension results on FSAR, Figures 2.5.4-221 through 2.5.4-223 for locations RB-C8, CB-C3, and RB-C4. The measured compression and shear wave velocities for all locations are combined on FSAR Figures 2.5.4-215 and 2.5.4-216.

Within the Bass Islands Group dolomite FSAR, Figures 2.5.4-221 through 2.5.4-223 show the measured shear and compression wave velocities were constant throughout the unit depth at a given boring location. FSAR Figure 2.5.4-216 shows the downhole shear wave velocity measured at RB-C8 is lower than measured at CB-C3. The low downhole shear wave velocity measurement and adjustment for RB-C8 was explained in the FSAR, Section 2.5.4.4.1.1 as partially repeated here:

“Figure 2.5.4-216 shows all measured Vs using P-S suspension and downhole seismic methods in one plot. Although the arrival of shear waves for the downhole seismic method are difficult to interpret due to poor quality shear wave forms, the downhole Vs values in general agree with Vs obtained using P-S suspension logging....At Boring RB-C8, the Vs obtained, from approximately El. 167.6 to 143.3 m (550 to 470 ft) (in Bass Islands Group), using downhole seismic method is close to the lower bound of the measured Vs using P-S suspension logger....”

“Since good quality compression wave forms are obtained from the downhole seismic method, the V_s in Boring RB-C8, from El. 167.6 to 143.3 m (550 to 470 ft), can be calculated using.....The calculated V_s at RB-C8 using V_p obtained from downhole seismic method and a Poisson’s ratio of 0.33 is 1,859 m/s (6,100 fps) which agrees with the P-S suspension data.”

Additionally, the calculated V_s at RB-C8 within the Bass Islands Group dolomite agrees (within 15 percent) with the measured V_s at CB-C3 using the downhole seismic method.

For Salina Unit F, only limited compression and shear wave velocity measurements using the downhole seismic method were performed between depths of approximately 110 and 205 feet as stated in FSAR, Section 2.5.4.4.1.1:

“Repeated collapse of the boreholes in the 33.5 to 62.5 m (110 to 205 ft) depth range (Salina Group Unit F) was experienced and resulted in oversized borehole and irregular borehole shapes.....”

“.....Limited measurements were performed in Salina Group Unit F in any of the borings due to oversized holes and irregular hole shapes. However, arrival time of shear and compression waves above and below the interval of the oversized zones could be measured using the downhole seismic method; therefore, average V_s and V_p across the oversized zone were measured.....”

Below a depth of approximately 205 feet, to the limit of the downhole seismic data collected, FSAR, Figures 2.5.4-221 through 2.5.4-223 for locations RB-C8, CB-C3, and RB-C4 show the measured shear and compression wave velocities were constant over a given interval at a given boring location

The shear wave velocities in the overburden were measured using SASW and P-S suspension logging. The variability of the shear wave velocity using SASW logging within the overburden is discussed in the FSAR, Section 2.5.4.4.1.2 and is repeated in part here:

“The measured V_s using the SASW method for Boring RB-C4, RW-C1, MW-381, and MW-393 is shown on Figure 2.5.4-219. In the fill, V_s in the Fermi 3 power block area generally decreases with depth from ground surface to approximate 4.6 m (15 ft) below the ground surface, then V_s increases when glacial till layer is encountered. The V_s near MW-381, increases with increasing depth. The V_s near MW-393 decreases from ground surface to approximately 1.8 m (6 ft) below ground and then increases to approximately 320 m/s (1050 fps) below 1.8 m (6 ft). The measured V_s ranges from approximately 244 to 351 m/s (800 to 1150 fps) for glacial till. Below 0.9 m (3 ft), V_s in the fill is approximately 244 m/s (800 fps).”

The shear wave velocity measurements using SASW logging were used to establish the shear wave velocity of only the glacial till as discussed in the FSAR, Section 2.5.4.2.1.1.3. No SASW logging was performed in the bedrock units.

The P-S suspension logging results were used to establish the bedrock V_s and V_p values for analysis, while the downhole results were used to validate the P-S suspension results. FSAR, Figures 2.5.4-215 and 2.5.4-216 show that the compression and shear wave velocities measured using the downhole method fall within the variability of the compression and shear wave velocities measured using the P-S suspension method. Use of P-S suspension logging to establish the bedrock V_s and V_p values for analysis is address in the response to RAI 2.5.4-12.

Proposed COLA Revision

Proposed text revision for FSAR Section 2.5.4.2.1.1.3 is shown in the attached markup.

Markup of Detroit Edison COLA
(following 1 page)

The following markup represents how Detroit Edison intends to reflect this RAI response in the next appropriate update of the Fermi 3 COLA. However, the same COLA content may be impacted by revisions to the ESBWR DCD, responses to other COLA RAIs, other COLA changes, plant design changes, editorial or typographical corrections, etc. As a result, the final COLA content that appears in a future submittal may be different than presented here.

The average S_U measured from three UC and two UU tests is 124.5 and 76.6 kPa (2.6 and 1.6 ksf), respectively. In addition, the average S_U measured from three \overline{CU} tests, isotropically consolidated to their in-situ vertical effective stress, is 167.6 kPa (3.5 ksf). Based on the above three methods, an average S_U of 129.3 kPa (2.7 ksf) was chosen for design.

Twelve \overline{CU} tests were performed on the glacial till. The ϕ' and c' values, based on the maximum principal stress difference criteria, are 30.6 degrees and 0, respectively. The ϕ' and c' values, based on the peak principal stress ratio failure criterion, are 31.3 degrees and 14.4 kPa (0.30 ksf), respectively. In addition to the \overline{CU} tests, a set of three direct shear tests was performed. The results indicated a ϕ' of 37 degrees and c' of approximately 0 for glacial till. Conservative estimates of the Mohr-Coulomb parameters, with $\phi' = 31^\circ$ and $c' = 0$ are used for glacial till. Based on the pore pressure response of glacial till from \overline{CU} tests, the till is considered as heavily overconsolidated soil.

Unit weight and moisture content were measured in the laboratory for glacial till. Average dry unit weight of the till is approximately 17.9 kN/m³ (114 pcf), with an average natural moisture content of 15 percent.

E was computed from plots of axial stress versus axial strain based on UU and \overline{CU} laboratory tests results. The average calculated E is approximately 28.7 MN/m² (600 ksf).

The glacial till will be removed from under Seismic Category I structures. However, based on the characteristic of glacial till, it may be used to support Non-Seismic Category I structures.

The static engineering properties of glacial till presented herein are suitable for stability analysis and design of temporary excavation support systems and slopes, and foundation support, where applicable.

based on SASW
method

Subsection 2.5.4.4.1 discusses the techniques used to measure shear wave velocity (V_s) and compression wave velocity (V_p) and the results of the testing. The measured V_s ranges from 244 to 351 m/s (800 to 1,150 fps). The measured V_s is used to calculate the low-strain shear modulus of glacial till. Subsection 2.5.4.7 discusses the shear modulus behavior at larger strain levels.

Based on static and dynamic engineering properties presented above, glacial till is considered as the upper most competent material at Fermi 3. The dynamic engineering properties of the till are suitable for ground motion response analysis for Fermi 3.

Attachment 17
NRC3-09-0051

Response to RAI Letter No. 16
(eRAI Tracking No. 3936)

RAI Question No. 02.05.04-12

RAI 02.05.04-12

FSAR Section 2.5.4.4.1 concludes that overall results obtained from P-S Suspension logging are acceptable for all analysis purposes. However, the staff noted that shear wave velocities obtained from P-S suspension method are generally greater than those from downhole method and SASW method; this is also evidenced by RB-C8 downhole values for Bass Islands, and SASW method for glacial till. Please provide justification exclusive use of P-S logging results rather using average results of downhole, SASW and P-S logging.

Response

FSAR, Figures 2.5.4-215 and 2.5.4-216 show that the compression and shear wave velocities in the bedrock units measured using the downhole seismic method fall within the variability of the compression and shear wave velocities measured using the P-S suspension method, except for the shear wave velocity measured in RB-C8.

The low downhole shear wave velocity measurement and adjustment for RB-C8 was explained in the Fermi 3 FSAR, Revision 1; Section 2.5.4.4.1.1 as partially repeated here:

“Figure 2.5.4-216 shows all measured Vs using P-S suspension and downhole seismic methods in one plot. Although the arrival of shear waves for the downhole seismic method are difficult to interpret due to poor quality shear wave forms, the downhole Vs values in general agree with Vs obtained using P-S suspension logging....At Boring RB-C8, the Vs obtained, from approximately El. 167.6 to 143.3 m (550 to 470 ft) (in Bass Islands Group), using downhole seismic method is close to the lower bound of the measured Vs using P-S suspension logger....”

“Since good quality compression wave forms are obtained from the downhole seismic method, the Vs in Boring RB-C8, from El. 167.6 to 143.3 m (550 to 470 ft), can be calculated using.....The calculated Vs at RB-C8 using Vp obtained from downhole seismic method and a Poisson’s ratio of 0.33 is 1,859 m/s (6,100 fps) which agrees with the P-S suspension data.”

Results of evaluations conducted to understand the variability of the compression and shear wave velocities measured using the P-S suspension method were discussed in FSAR, Section 2.5.4.4.1.1. The discussions and is partially repeated here:

“Analyses were performed to compare Vs and Vp measurements obtained with other subsurface information such as RQD, caliper, natural gamma, and optical televiewer logs. The study was mainly focused on the Bass Islands Group and Salina Group Unit F where RQD was low. The purpose of the analysis was to understand if the measured Vs and Vp were representative of the actual subsurface conditions. In addition, the analyses provided

insight regarding why waveforms were highly variable between 9.1 and 36.6 m (30 and 120 ft) (in Bass Islands Group) in all boreholes.”

“Irregular readings were obtained in the Bass Islands Group between the depths of 9.1 and 36.6 m (30 and 120 ft). The waveforms were difficult to interpret in this depth range in most boreholes. The variability observed in the measured V_p and V_s from P-S Suspension logs in the Bass Islands Group can be better explained based on optical televiewer logs. Figure 2.5.4-209 through Figure 2.5.4-212 compare the optical televiewer logs and the measured velocities in Borings TB-C5, RB-C8, CB-C3 and RB-C4, respectively. These figures indicate that the variability in the measured V_p and V_s within the Bass Islands Group is mainly caused by geologic features such as fractures, bedding planes, brecciation, oolitic rock, and pitting of the bedrock. At these features, the velocities tend to be lower.”

“For the P-S suspension instrumentation, the separation of R1–R2 is 1 m (3.3 ft) and the separation of S–R1 is 1.9 m (6.3 ft). The inconsistency between receiver to receiver (R1–R2) and source to receiver (S–R1) profiles in the Bass Islands Group was because the volume of bedrock sampled from near to far receivers (R1–R2) is less than the volume of bedrock sampled from the source to near receiver (S–R1); therefore, R1–R2 velocity will show greater variability due to the nature of discontinuities in Bass Islands Group (Subsection 2.5.1.2.4.3) as compared to the S–R1 velocity.”

“Understanding the variability observed in the measured V_p and V_s in the Salina Group Unit F can be aided using natural gamma logs. Figure 2.5.4-213 and Figure 2.5.4-214 show the comparison of the natural gamma logs and the measured velocities in Borings TB-C5 and CB-C3, respectively. Figure 2.5.4-213 and Figure 2.5.4-214 show that the variability in the measured V_p and V_s within the Salina Group Unit F correlates with the variability in the natural gamma value in Boring TB-C5 and CB-C3, respectively. The higher gamma value indicates the presence of shale or claystone and the lower gamma value indicates dolomite or limestone. The measured V_p and V_s increase in the areas where dolomite and/or limestone are present.”

“Based on the above observations, it is concluded that the variability of the measured V_s and V_p from P-S Suspension logs in the Bass Islands Group and Salina Group Unit F can be correlated directly with observed geologic features; therefore, the measured V_s and V_p are considered representative of the actual ground conditions.”

“The measured V_p for the bedrock at Fermi 3 was compared to the measured V_p at Fermi 2. The measured V_p using the seismic refraction surveys at Fermi 2 site for Bass Islands Group, Salina Group Unit F and Salina Group Unit E are within the range of the measured V_p at Fermi 3. The measured V_p at Fermi 2 for the Salina Group Unit C and B were lower than the range of measured V_p at Fermi 3; the difference is less than 15 percent and 5 percent for Unit C and Unit B, respectively.”

In summary the P-S suspension Vs data were considered to be more reliable than the Vs downhole seismic data for the following reasons:

- The clarity of the Vs wave forms was better for the P-S suspension data than for the downhole seismic data.
- The variability of the P-S suspension Vs and Vp data could be correlated well with physical features observed in the bedrock.
- Greater confidence interpreting P-S suspension Vs data.

Therefore, The P-S suspension logging results were used to establish the bedrock Vs and Vp values for analysis, while the downhole results were used to validate the P-S suspension results. This is stated in FSAR, Section 2.5.4.4.1.1 as repeated here:

“Both the P-S suspension logger and downhole seismic testing procedures were used to obtain Vs and Vp of bedrock units at Fermi 3. The P-S Suspension method was considered as the primary method for obtaining the Vs and Vp profile, while the Downhole Seismic method was used to validate the results measured using P-S Suspension logging.”

The design shear wave velocity range for glacial till presented in the FSAR, Section 2.5.4.2.1.1.3, is based on the SASW method. No SASW logging was performed in the bedrock units.

Proposed COLA Revision

None

Attachment 18
NRC3-09-0051

Response to RAI Letter No. 16
(eRAI Tracking No. 3936)

RAI Question No. 02.05.04-23

RAI 02.05.04-23

FSAR Section 2.5.4.10.1 states that the two methods, Terzaghi approach and Uniform Building Code were used in evaluating bearing capacity. Please provide information on why these two methods (particularly the second method) are adequate and appropriate for the bearing capacity at the Fermi 3 site, considering apparently weaker Salina Group Unit F beneath the Bass Islands Group.

Response

The Terzaghi approach takes into consideration the effect of the weaker zone below the Bass Islands Group based on general bearing capacity failure behavior. To account for the influence of Salina Unit F, the design Mohr-Coulomb parameters c and ϕ used in the bearing capacity analysis were established as the weighted average of the individual Mohr-Coulomb parameters for the Bass Islands Group and Salina Unit F. The weighting of the Bass Islands Group and of the Salina Unit F was based on the influence depth of one times the foundation width below the bottom of the foundation. The weighted average was developed independently for c and ϕ .

The allowable bearing pressure approach of the Uniform Building Code considers the allowable contact pressure on unweathered bedrock under a uniaxial loading condition to assure that the foundation bedrock has sufficient capacity against rupture. To account for the influence of Salina Unit F, the unconfined compression strength used in the Uniform Building Code analysis was a weighted average of the unconfined compression strength of Bass Islands Group and Salina Unit F. The weighting of the Bass Islands Group and of the Salina Unit F was based on the influence depth of one times the foundation width below the bottom of the foundation.

The allowable bearing pressure from the Uniform Building Code is greater than or equal to the Terzaghi method; therefore the static bearing pressure demand was compared to the allowable bearing pressure based on the Terzaghi's approach.

Proposed COLA Revision

None

**THIS PAGE IS AN
OVERSIZED DRAWING OR
FIGURE,
THAT CAN BE VIEWED
AT THE RECORD TITLED:**

**“Figure 2.5.1-235,
Site Exploration Plan”**

**WITHIN THIS PACKAGE... OR
BY SEARCHING USING THE
DOCUMENT/REPORT NO.**

D-01

**THIS PAGE IS AN
OVERSIZED DRAWING OR
FIGURE,
THAT CAN BE VIEWED AT THE
RECORD TITLED:**

**“FIGURE 2.5.1-236,
Enlargement of Site
Exploration Plan”**

**WITHIN THIS PACKAGE... OR
BY SEARCHING USING THE
DOCUMENT/REPORT NO.**

D-02

**THIS PAGE IS AN
OVERSIZED DRAWING OR
FIGURE,
THAT CAN BE VIEWED AT THE
RECORD TITLED:**

**“FIGURE 2.5.1-237,
Geologic Cross
Section A-A”**

**WITHIN THIS PACKAGE... OR
BY SEARCHING USING THE
DOCUMENT/REPORT NO.**

D-03

**THIS PAGE IS AN
OVERSIZED DRAWING OR
FIGURE,
THAT CAN BE VIEWED AT THE
RECORD TITLED:**

**“Figure 2.5.1-238,
Geologic Cross
Section B-B”**

**WITHIN THIS PACKAGE... OR
BY SEARCHING USING THE
DOCUMENT/REPORT NO.**

D-04

**THIS PAGE IS AN
OVERSIZED DRAWING OR
FIGURE,
THAT CAN BE VIEWED AT THE
RECORD TITLED:**

**“Figure 2.5.1-239
Geologic Cross
Section C-C”**

**WITHIN THIS PACKAGE... OR
BY SEARCHING USING THE
DOCUMENT/REPORT NO.**

D-05

**THIS PAGE IS AN
OVERSIZED DRAWING OR
FIGURE,
THAT CAN BE VIEWED AT THE
RECORD TITLED:**

**“Figure 2.5.1-240,
Geologic Cross
Section D-D”**

**WITHIN THIS PACKAGE... OR
BY SEARCHING USING THE
DOCUMENT/REPORT NO.**

D-06

**THIS PAGE IS AN
OVERSIZED DRAWING OR
FIGURE,
THAT CAN BE VIEWED AT THE
RECORD TITLED:**

**“Figure 2.5.4-202,
Excavation Cross
Section D-D”**

**WITH IN THIS PACKAGE... OR
BY SEARCHING USING THE
DOCUMENT/REPORT NO.**

D-07

**THIS PAGE IS AN
OVERSIZED DRAWING OR
FIGURE,
THAT CAN BE VIEWED AT THE
RECORD TITLED:**

**“Figure 2.5.4-203,
Excavation Cross
Section C-C”**

**WITHIN THIS PACKAGE... OR
BY SEARCHING USING THE
DOCUMENT/REPORT NO.**

D-08

**THIS PAGE IS AN
OVERSIZED DRAWING OR
FIGURE,
THAT CAN BE VIEWED AT THE
RECORD TITLED:**

**“Figure 2.5.4-204,
Excavation Cross
Section B-B”**

**WITHIN THIS PACKAGE... OR
BY SEARCHING USING THE
DOCUMENT/REPORT NO.**

D-09X